Global Thermohaline Circulation and Ocean-Atmosphere Coupling

by

Xiaoli Wang

B.S., Nanjing University, China
(1987)

Submitted to Department of Earth, Atmosphere, and Planetary Sciences
in partial fulfillment of the requirements for the degree of

Doctor of Philosophy in Global Change Science

at

MASSACHUSETTS INSTITUTE OF TECHNOLOGY

April 1997

Author .....
Department of Earth, Atmosphere, and Planetary Sciences
April, 1997

Certified by .....
Peter H. Stone
Professor of Meteorology
Thesis Supervisor

Certified by .....
Jochem Marotzke
Assistant Professor of Physical Oceanography
Thesis Supervisor

Accepted by .....
Thomas H. Jordan
Chairman, Department of Earth, Atmospheric, and Planetary Sciences

Global Thermohaline Circulation and Ocean-Atmosphere Coupling

by

Xiaoli Wang

Submitted to the Department of Earth, Atmosphere, and Planetary Sciences
on April, 1997, in partial fulfillment of the
requirements for the degree of
Doctor of Philosophy in Global Change Science

Abstract

A global ocean general circulation model (GCM) with idealized geometry (two basins of equal size, Marotzke and Willebrand, 1991) is coupled to an energy balance atmospheric model with nonlinear parameterizations of meridional atmospheric transports of heat and moisture.

With the coupled model that prescribes the atmospheric heat and moisture transports, the North Atlantic meridional mass overturning rates at equilibrium increases as the global hydrological cycle strength increases. Furthermore, the equilibrium overturning rate is primarily controlled by the hydrological cycle of the Southern Hemisphere, whereas the Northern Hemispheric hydrological cycle has little impact.

The transition of the thermohaline circulation from the conveyor belt to the southern sinking state is controlled by two factors, the hydrological cycle in Northern Hemisphere, and the ratio of hydrological cycle strengths between the Northern Hemisphere and the Southern Hemisphere. Increasing either of them destabilizes the thermohaline circulation .

The large-scale dynamics of the North Atlantic overturning is mainly interhemispheric, with the bulk of the overturning rising in the Southern Hemisphere. Multiple intermediate states exist that are only quantitatively different, under very small salinity perturbations.

The coupled feedbacks between the thermohaline circulation and the atmospheric heat and moisture transports are demonstrated to exist in the coupled model, and all of them are positive. In addition, it is identified that the coupled feedbacks associated with the atmospheric transports in the Southern Hemisphere are also positive.

Two different flux adjustments are used in the coupled model, with one adjusting the atmospheric transports efficiencies, the other adjusting the surface fluxes. Different flux adjustments influence the coupled feedback intensities, and hence the

stability of the thermohaline circulation.

Thesis Supervisor: Peter H. Stone
Title: Professor of Meteorology

Thesis Supervisor: Jochem Marotzke
Title: Assistant Professor of Physical Oceanography

Acknowledgments

Completion of this thesis is a synergistic product of many minds. First and foremost, I feel a deep sense of gratitude to Prof. Peter Stone and Prof. Jochem Marotzke, who jointly provided a harmonious and inspiring mentorship towards this interdisciplinary venture. I have been most fortunate to have worked closely with such two great minds, to have engaged numerous late-afternoon discussions with them. Their vision and wisdom are abundant in this work.

I extend my sincere thanks to all the faculty of CMPO, for providing me an excellent education chance. Among them, special thanks are to Prof. Kerry Emanuel and Prof. John Marshall, for their serving as the thesis committee.

I'm also grateful for Pacanowski, Dixon, and Rosati of GFDL, for providing us Modular Ocean Model (MOM 1) codes. I wish to thank Yin and Sarachik of University of Washington for supplying us their convection scheme. Special thanks are to Moto Nakamura for helping use his coupled model codes, and to Yong Zhu for teaching me NCAR graphics.

I benefit greatly from schooling with many fellow students of Meteorology, Physical Oceanography, and the Joint Program on Science and Policy of Global Change, particularly Dan Davidoff, Maria Bister, Xinyu Zheng, Lars Schade, Jean A. Fitzmaurice, Mort Webster, Alicia Lavin, Alison Macdonald. I especially wish to thank my long-term officemate, Amy Solomon, for her kindness and moral support for every turn of the graduate life. I'd also like to express my sincere gratitude to my working buddy, Jeff Scott, for his valuable scientific discussions, and his unflagging enthusiasm to the work.

Jane McNabb, Tracey Stanelun, Joel Sloman, and Stacey Frangos are most helpful in guiding me through the unfamiliar grounds of bureaucrazy. Linda Meinke solved any computer failure with a fashion.

Last, but not least, I give my deepest thanks to my family, to my parents and parents-in-law, for their unconditional love; to my husband, Lee, for his constant supports, insights, and good sense of humor; to my little angel, Charles, for his demonstrations of growth and pure potentiality.

I dedicate this thesis to the happy memory of my grandma, whose love gave me the eyes to see grace.

This research was supported jointly by the Northeast Regional Center of the National Institute for Global Environmental Change, by the Program for Computer Hardware, Applied Mathematics, and Model Physics (both with funding from the U.S Department of Energy), and by the MIT Joint Program on Science and Policy of Global Change.

.

Contents

List of Figures

List of Tables

Chapter 1

Introduction

1.1 Thermohaline circulation in the climate system

Over the last billion years, in spite of cosmic disturbances and the volcanic and tectonic activities of the earth's interior, the climate of the earth has remained sufficiently hospitable to permit the continuous evolution of advanced forms of life. The stability of the earth's climate system is largely due to the presence of a vast volume of water, covering more than 70% of the earth's surface. This mobile reservoir, i.e, the global oceans, with a large capacity for heat and chemical constituents, acts as a stabilizer against chemical and climatic variations.

While the stabilizing buffer effect of the oceans can easily be appreciated, the role of the oceans in the climate system is not limited only to that. Another significant role of the oceans invokes ocean circulation, and its transport mechanisms of heat and chemical components. The poleward oceanic heat transport is comparable to that of the atmosphere (Fig.1-1), and can have an important impact on the climate

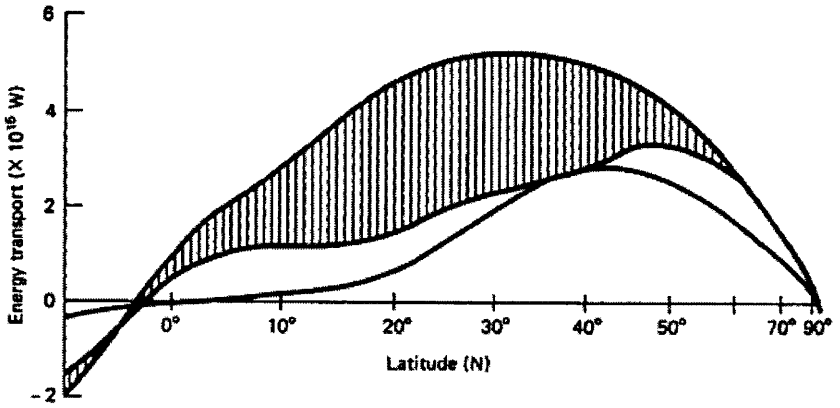

Figure 1-1: The northward transport of energy as a function of latitude. The outer curve is the net transport deduced from radiation measurements. The blank area is the part transported by the atmosphere and the shaded area the part transported by the ocean. The lower curve denotes the part of the atmospheric transport due to transient eddies (from Vonder Haar and Oort, 1973).

variability and sensitivity.

The ocean circulation is composed of two different modes, the fast, shallow circulation driven by wind stress, and the slow, deep circulation driven by air-sea surface fluxes of heat and freshwater. The latter is called the thermohaline circulation . The thermohaline circulation has multiple equilibria, and the cause of climate changes in the geologic past has been suggested to be associated with the transitions between different states of the thermohaline circulation .

Palaooceanographic data suggest that deep water formation in the North Atlantic around Greenland was shut down during the last glacial maximum about 18,000 years B.P.(before present), and again during Younger Dryas period (between about 11,000 and 10,000 years B.P.) (e.g, Broecker et al. 1985; Dansgaard, et al. 1993; Taylor, et al. 1993). These interpretations are supported by observational evidence from deep-sea sediment cores which suggest that deep water production was significantly reduced during the last glacial maximum (e.g, Boyle and Keigwin,1987; Sarnthein et

al. 1994).

In this thesis, the goal is to study the role of the thermohaline circulation in climate change. The focus will be on the fundamental dynamics of the thermohaline circulation , and the large-scale interaction processes between the atmospheric dynamics and the thermohaline circulation . This thesis is aiming not for the state-of-the-art simulation of the thermohaline circulation , but for understanding of the processes. To this end, we choose simplicity over realism in the model set-up. As a result, we are able to explore the sensitivity of the thermohaline circulation over a wide range of parameters, and therefore, to identify the processes that are important in climate change. Such knowledge will guide us to improve realistic climate models.

The thermohaline circulation can be depicted in a highly simplified schematic picture, frequently referred to as *conveyor belt* (Fig.1-2). In the Atlantic Ocean, it starts with deep convection processes in high latitudes (mostly in the Greenland, Norwegian, and Labrador Seas), which lead to the formation of North Atlantic Deep Water (NADW). The NADW flows southward through the Atlantic, effectively mixed into the Indian and Pacific Oceans by the Antarctic Circumpolar Current (ACC). A shallow warm current then returns to the North Atlantic to close the conveyor belt circulation (Gordon, 1986). Even though the detailed paths of the circulation are highly turbulent (Macdonald and Wunsch, 1996), the gross features of the thermohaline circulation are believed to be quite robust.

One climate impact is the substantial amount of heat transported by the thermohaline circulation . The oceanic heat transport across 24° N of the North Atlantic is estimated as 1.2 ± 0.3PW (1PW=10^{15}W) (e.g, Bryden et al, 1991; Roemmich and Wunsch, 1985). The maximum contribution from the wind-driven circulation can only account for less than 30% of the observed value (Wang et al., 1995; Boning et

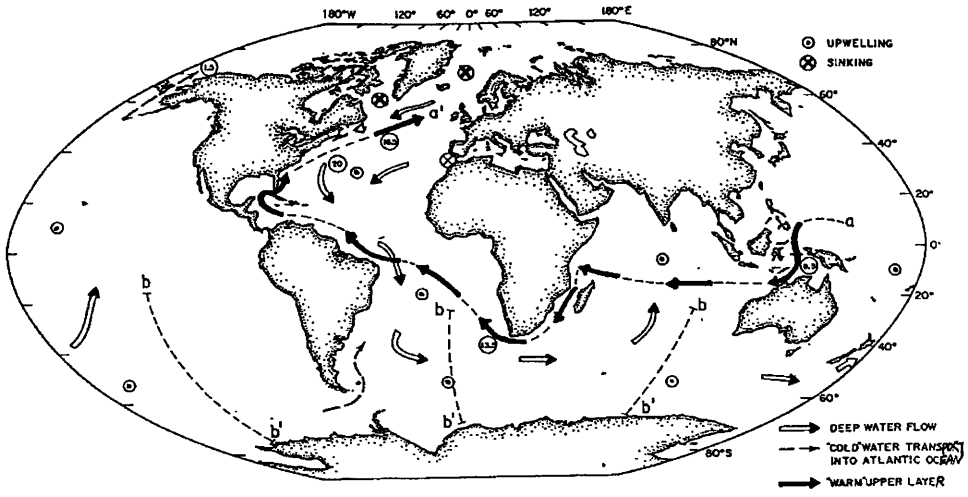

Figure 1-2: Global structure of the thermohaline circulation associated with NADW production. The warm water route, shown by the solid arrows, marks the proposed path for return of upper layer water to the northern North Atlantic as is required to maintain continuity with the formation and export of NADW. The circled values are volume flux in $10^6 m^3 s^{-1}$ which are expected for uniform upwelling of NADW with a production rate of $20 \times 10^6 m^3 s^{-1}$. These values assume that the return within the cold water route, via the Drake Passage, is of minor significance (from Gordon, 1986).

al., 1996). Therefore, the thermohaline circulation has to be the dominant transport mechanism in the North Atlantic.

The transport mechanism of the thermohaline circulation has also been hypothesized in studies of the biogeochemical cycles in the ocean. Significant interhemispheric transport of carbon in the ocean has been proposed by Broecker and Peng (1992), in order to reconcile observed air-sea carbon fluxes (Tans et al., 1990). Changes of the thermohaline circulation intensity could effectively influence the oceanic uptake of CO_2, and therefore the atmospheric CO_2 concentration. The latter is believed to be able to cause global climate changes, as demonstrated in many climate models.

Modeling the thermohaline circulation has proved challenging, for the dynamics spans small scale convection processes and global scale oceanic motions. As a result, we now have a wide spectrum of models in use, from box models, to two-dimensional models, to coarse 3D GCMs, to eddy resolving 3D models which can be run only for simulated times of order decades. Another challenging aspect of the thermohaline circulation arises from its boundary layer. The thermohaline circulation is driven by fluxes of heat and freshwater through the sea surface. Since the surface fluxes depend on the evolution of both atmosphere and ocean, any model of the thermohaline circulation must include an atmospheric model. The atmosphere-ocean coupling processes have not yet been well understood. So far, the so called *mixed boundary conditions* have been widely used, which refer to a restoring of sea surface temperature (SST) and a prescribed surface freshwater flux. It crudely represents the different coupling processes for surface temperature and salinity.

Under the mixed boundary conditions, multiple equilibria of thermohaline circulation have been found to be robust in every level of model complexity, from box models (Stommel, 1961), to 2D models (Marotzke et al. 1988; Stocker and Wright,

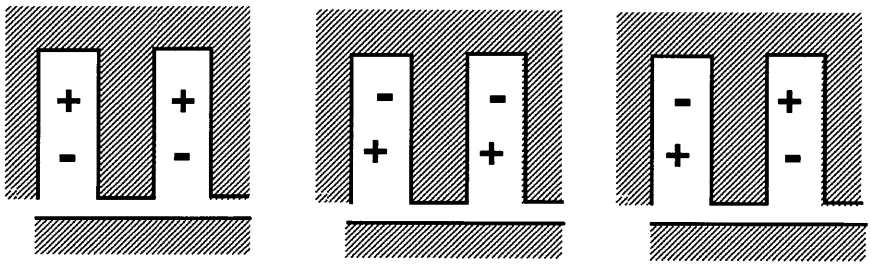

Figure 1-3: Scheme of the three essentially different steady states of the global ocean GCM. + denotes sinking and deep water formation in the respective hemisphere, - the absence of it. The third equilibrium, corresponds to the present circulation (taken from Marotzke and Willebrand, 1991).

1991), to 3D GCMs (e.g, Bryan, 1986; Marotzke and Willebrand, 1991; Hughes and Weaver, 1994). Marotzke and Willebrand (1991) (hereafter MW91) have attempted to investigate the full range of possible equilibria of the global ocean in an idealized geometry GCM. Four steady states were found, three of which are essentially different (Fig.1-3). One of the equilibria corresponds to the observed global thermohaline circulation pattern: The production of deep water in one basin, and none in the other.

1.2 How stable is the thermohaline circulation?

There exist a number of fundamental questions that remain unsolved. For example, how stable is the present thermohaline circulation ? What causes the transition from one state to another? Which processes are most important in the interaction between the atmosphere and the ocean? These are among the most interesting questions to be addressed by climate dynamists, and have been investigated in numerous previous studies.

A series of reviews (e.g, Weaver and Hughes, 1992; Willebrand, 1993; Marotzke, 1994; Marotzke, 1996; Rahmstorf et al. 1996), have extensively addressed the most up-to-date progresses on the thermohaline circulation topic. Here I'll only concentrate on the coupled models studies.

The coupled models can be categorized into three classes, highly parameterized coupled box models, fully coupled GCMs, and hybrid coupled models. Powerful as they are in demonstrating the important processes of the thermohaline circulation (e.g, Birchfield, 1989; Nakamura et al. 1994; Marotzke and Stone, 1995), the difficulty with the coupled box models is their crude representation of 3-D ocean dynamics. They are usually decoupled from the process of convection which is the most important connection with deep water formation. Due to the absence of rotation, they are unable to model the fundamental dynamical balance, geostrophy. The coupled box models also lack of wind-driven circulation which is an essential mechanism for heat and salinity advection. Therefore, their direct applicability to the real climate system may be very limited.

The objection against the fully coupled GCMs is that an artificial flux adjustment is needed in order to prevent the model from drifting away from the current thermohaline circulation (Sausen et al., 1988; Manabe and Stouffer, 1988; Murphy, 1995). The need for flux adjustment implies that the atmosphere-ocean coupling processes are not well understood. The source of the errors in the coupled GCMs is hard to pinpoint, since both the atmospheric and oceanic components have major errors in their simulations of heat transport. The atmospheric GCMs typically overestimate the poleward heat transport in the atmosphere by 1 to 2 PW (Stone and Risbey, 1990; Gleckler et al. 1995). The ocean GCMs tend to underestimate the poleward heat transport in the ocean, sometimes by more than 50% (e.g, Manabe and Stouffer,

1988). Another difficulty with the coupled GCMs is that it is hard to separate the individual contribution of a given process, and thus it is difficult to identify what is essential and what is of secondary importance. (Also computation with the coupled GCMs is very expensive).

The goal of this study has been to find the simplest coupled model which captures the salient features of the thermohaline circulation , while at the same time, specifying as little as possible. As will be seen, the model developed for this thesis is a hybrid coupled atmosphere-ocean model. There already have been a series of such simplified coupled models (e.g, Stocker et al. 1992; Saravanan and McWilliams, 1995; Rahmstorf and Willebrand, 1995; Lohmann et al. 1996). Saravanan and McWilliams (1995) have coupled an eddy-resolving two-level global primitive equation model of the atmosphere to a zonally-averaged sector Boussinesq equation model of the ocean. The sector 2-D ocean model did not include wind-driven gyres and convective adjustment process.

Rahmstorf and Willebrand (1995) developed a hybrid coupled model, with a global idealized 3-D ocean GCM coupled to an energy balance atmospheric model. As to the oceanic component, ours is, in most aspects, identical to their model. However, the hydrological cycle in their model was fixed to the diagnosed freshwater flux from the spin-up run, and did not interact with the model equilibrium state changes. In contrast, our model will allow a self-consistent representation of the coupling between the atmospheric hydrological cycle and the thermohaline circulation .

On the other hand, the coupled model developed by Lohmann et al.(1996) included an interactive hydrological cycle in their zonally averaged energy balance model for the atmosphere. But their ocean GCM has a simpler two hemisphere sector configuration, while ours will be a two-basin global geometry. Also their coupled model involved sea ice system, but ours is ice-free.

Overall, what distinguishes our hybrid coupled model from these previous models are essentially two aspects, the handling of the atmospheric hydrological cycle, and the global scope of the thermohaline circulation .

The handling of the atmospheric hydrological cycle was inspired by the work of Nakamura et al. (1994, hereafter NSM94). We are going to incorporate a similar coupling strategy, but within the framework of a 3-D global ocean GCM. The ocean GCM configuration is, in most aspects, identical to the one used in MW91, with an idealized global geometry.

There are basically two sets of questions that have not been explored before. First, how the global thermohaline circulation responds to hydrological cycle changes has never been investigated systematically. Actually, we don't even know how realistic the modeled thermohaline circulation will be, if the surface forcing is derived from observations. Here, we explore the sensitivities of the thermohaline circulation to changes of the surface forcing, in hopes that the dynamics that controls the global thermohaline circulation will be disclosed. Winton and Sarachik (1993) have found a series of self-sustaining oscillations of the thermohaline circulation as the surface salinity flux increased. Their model was limited to a one hemisphere sector configuration. It is interesting to examine the thermohaline circulation in a global configuration.

The second set of questions is associated with the interaction between the atmospheric transport processes and the thermohaline circulation . NSM94 identified a destablizing feedback mechanism between the atmospheric moisture transport and the thermohaline circulation , named EMT feedback. While the thermohaline circulation represented in NSM94 is merely a three box model, an important question is whether the same feedback acts in the complex model, as well as whether there is any new feedback emerging from the complex model.

The approach in building the coupled model has been to develop and test the component models independently, and then to combine them. While the oceanic component is a 3-D GCM with an idealized geometry, the atmospheric model is an energy and moisture balance model with nonlinear parameterizations of the atmospheric transports. The hope is that with such an intermediate level coupled model, it may be easier to elucidate the coupled feedbacks between the thermohaline circulation and the atmospheric eddy transports.

The thesis is organized as following. In Chapter 2, the component models of atmosphere and ocean are presented , together with the coupling procedure. In Chapter 3, the oceanic model is tested, forced with observed meridional atmospheric transports. A series of sensitivity experiments are presented and discussed for various hydrological cycles. A mechanistic box model is used to help understand the dynamics underlying the model behavior. Chapter 4 deals with perturbation experiments of the oceanic model to elucidate the interhemispheric dynamics of the thermohaline circulation . Chapter 5 presents the coupled model calculations, and a series of feedback mechanisms are identified in the perturbation experiments. Finally, Chapter 6 summarizes the results, and discusses the successes and failures of the model.

Chapter 2

Model Description

2.1 Introduction

In this chapter, the two component models will be presented individually, then the coupling procedure between the two models will be described. Note that the atmosphere and ocean models are on two different levels of complexity. While the oceanic model is a three-dimensional primitive equation model, the atmospheric model is a highly parameterized transport model. Therefore, the coupled model is hybrid. The justification for such a hybrid coupled model comes from our interest in the thermohaline circulation on time scales of hundreds to thousands of years. On these time scales, the atmosphere is assumed to be in statistical equilibrium with the underlying ocean.

Since the atmospheric process model is not a standard model, but developed from scratch, the model physics and parameterizations will be discussed in detail. On the other hand, the oceanic model follows, in most aspects, the standard development of a widely-used publicly available model (Cox, 1984; Pacanowski et al., 1990; Pacanowski, 1995). Thus, the description of the oceanic model will be brief.

2.2 Oceanic model

The oceanic model is an oceanic general circulation model (GCM), provided to us by GFDL. We use the version of the GCM developed by Pacanowski et al. (1990), known as the Modular Ocean Model (hereafter MOM1). The MOM1 version is based on the earlier Cox version (1984), but has major coding improvements. One such improvement stems from its logical organization of the code with "hooks" readily available for adding new physics to the model. This facilitates our coupling of a new atmospheric model. Another improvement is that its modules do not interact with each other, but interact with the main program in only a few places. This interfacing strategy tends to localize code modifications, thereby keeping the code structure simple, and easily modified.

Weaver et al. (1993) has compared two different GCM model configurations of Weaver and Sarachik (1991) and Marotzke and Willebrand (1991). From several experiments performed with various horizontal resolutions (e.g, $2° \times 2°$ vs. $4° \times 4°$), it was concluded that, within the context of coarse-resolution modeling, the exact nature of the coarse resolution is not important in determining the stability and variability properties of the thermohaline circulation . However, this conclusion cannot be immediately extended to fine-resolution, eddy-resolving studies (Weaver et al., 1993).

Here, we choose a coarse-resolution model configuration, and the model set-up is, in most aspects, identical to that of MW91 (Fig.2-1). The horizontal resolutions are 3.75° in longitude and 4° in latitude. There are 15 levels in the vertical, with intervals varying from 50 m near the surface to 500 m near the bottom. The bottom is taken to be flat, and has uniform depth of 4500m. The model consists of two identical basins of 60° width each. The ocean domain extends from 64° N to 64° S. A channel

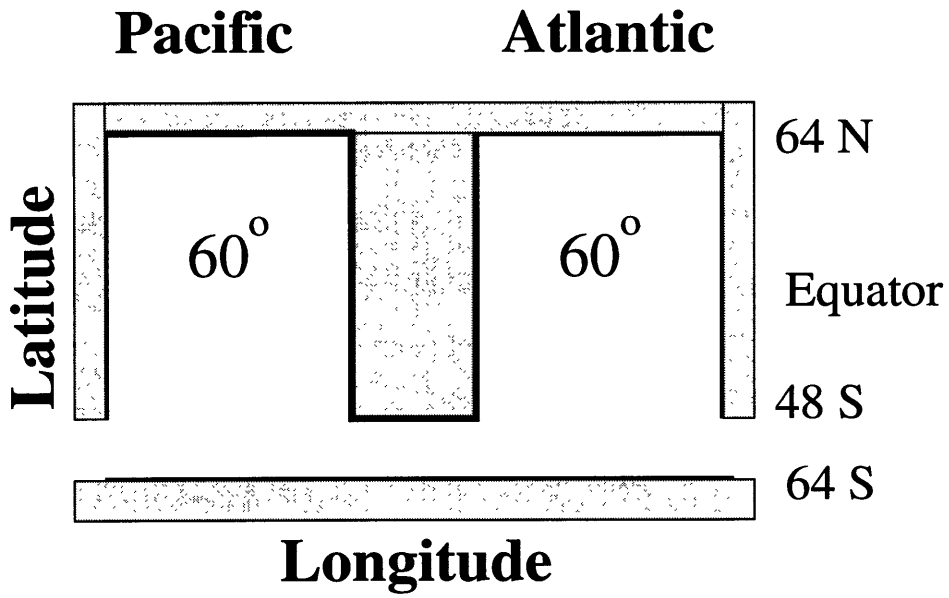

Figure 2-1: Geometry of the global model.

representing the Antarctic Circumpolar Current (ACC) connects the two basins from 48° S to 64° S. A cyclic boundary condition is applied for the ACC region.

The mass transport in the ACC is difficult to represent in a coarse resolution model with flat bottom. Following MW91, the ACC transport is thus prescribed, and a value of 140 Sv is used. The dynamics of the ACC is not important here, it is only important that the ACC provides a connection between the two basins. The two basins are identical in geometry, and can arbitrarily be referred to as Pacific or Atlantic.

Constant mixing coefficients are used. To ensure numerical stability, the horizontal viscosity A_H must be large enough to allow the viscous western boundary layer to be resolved (Bryan et al. 1975), and is taken as $2.5 \times 10^5 m^2/sec$, the same value as MW91. The diffusivities follow MW91, with horizontal and vertical diffusivities of $K_H = 10^3 m^2/sec$, and $K_v = 5 \times 10^{-5} m^2/sec$. The only exception is the vertical viscosity A_v. We choose A_v, $10^{-2} m^2/sec$, two orders of magnitude higher than MW91,

in order to suppress inertial instability near the equator (Weaver and Sarachik, 1990).

It must be borne in mind, however, that the large-scale motions produced in an OGCM can be sensitive to the particular choice of diffusion parameters. An example concerning this sensitivity question is the study by Bryan (1987), which explicitly set out to examine the sensitivity of the thermocline structure, meridional overturning, and meridional heat flux to the choices of vertical diffusion. The numerical experiment results demonstrate that the meridional mass transport increased as the vertical diffusivity (K_v) increased, exhibiting a 1/3 power dependence. In this study, the vertical diffusivity is in the middle of the range explored by Bryan (1987), and has been used as his standard.

Since the evolution of momentum is much faster than that of tracers (temperature and salinity), Bryan (1984) suggested that the timesteps for momentum and tracers can be split, to accelerate the integration to equilibrium, a technique called asynchronous integration. The asynchronous integration is used during all the experiments, with timestep of 2 hours for momentum, and 2 to 6 days for tracers. To prevent leap frog time splitting, there is mixing between timesteps every 17 timesteps.

The convection scheme was provided to us by Yin and Sarachik (1994). The scheme is the best of its kind. According to our trial runs, it not only completely removes all static instability at each time step, but also proves to be the fastest complete convection scheme.

The rigid lid ($w = 0$, at $z = 0$) approximation is used for the surface boundary, and a free slip ($\frac{\partial \vec{V}}{\partial z} = 0$) at the bottom, and no slip ($\vec{V} = 0$) at the lateral walls.

There is no heat nor salt flux at the bottom and the lateral walls. At the surface, the wind stress, taken from MW91 (Fig.2-2), is zonal and prescribed as a simple function of latitude only, reflecting the major features of the observed distribution.

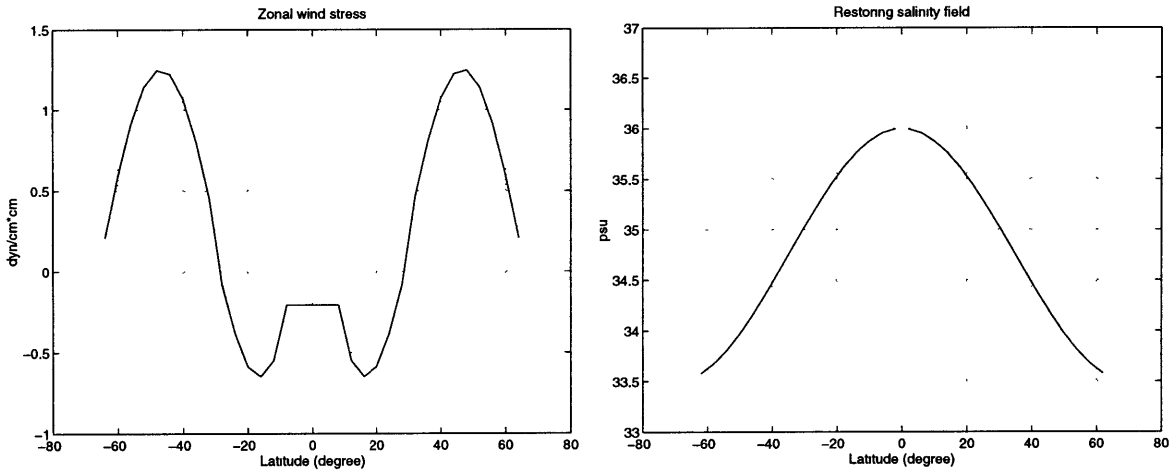

Figure 2-2: Forcing fields of the OGCM: Zonal wind stress τ_x in dyn/cm^2 (left), and restoring salinity field in psu (right), as functions of latitude.

The prescribed salinity profile, when a restoring condition is used, is from MW91 (Fig.2-2, no ITCZ). The model spins up from a motionless state with horizontally uniform temperature and salinity distributions. The initial temperature is taken from the observed globally averaged vertical profile (Levitus, 1982), and the initial salinity is set to 34.2ppt at all levels. The spin-up is speed up if the deep ocean is fresh (Bryan, 1986). The surface condition for the tracers involves the coupling between atmosphere and ocean, and thus will be deferred to Section 2.4.

2.3 Atmospheric model

The atmospheric model developed here is based on the atmospheric component in the coupled box-model by NSM. Their two-box atmospheric model has been expanded into a 1-D (in latitude only), basin-dependent model in this study (fig.2-3). Meanwhile, the physical elements of the 1-D model are similar to that of the box model.

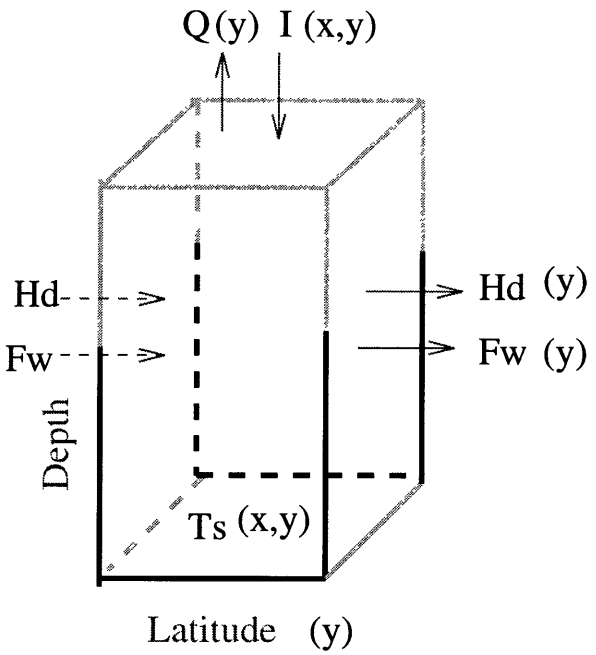

Figure 2-3: Illustration of the atmospheric model

The development of the model is guided by three primary principles. First, the model is highly parameterized, and the parameters are constrained by observations of the annual mean states. Second, no atmospheric source of asymmetric forcing is allowed. The atmosphere is assumed symmetric regarding to the two basins, or the northern/southern hemispheres. The second assumption echoes the same hypothesis underlying the ocean model set-up. MW91 tried to examine the asymmetry of the thermohaline circulation that is purely internal. The possible attributions from external asymmetries, e.g, the basin geometry, or the inter-basin freshwater transport were excluded. The third principle is that the model should reflect the box model approach (NSM) as closely as possible, thus the knowledge from the box model can be related directly to this study.

The first physical element of the model is the radiative parameterization. The net radiative forcing at the top of the atmosphere is defined as,

$$R = Q(1 - \alpha) - I \tag{2.1}$$

where Q is the incoming solar radiation, α is the planetary albedo, and I is the outgoing longwave radiation. Following North (1975), Q is approximated as,

$$Q(y) = \frac{Q_0}{4}[1 + \frac{Q_2}{2}(3y^2 - 1)] \tag{2.2}$$

where $y = sin\phi$, $Q_0 = 1365 Wm^{-2}$, and $Q_2 = -0.482$.

The planetary albedo α, based on observations (Stephens et al., 1981), was fitted by Legendre polynomials (Miller, unpublished, 1990)(Fig.2-4). To remove the asymmetric source, we average it between two hemispheres, and use a form symmetric about the equator,

$$\alpha(y) = 0.322 + \frac{0.231}{2}(3y^2 - 1) + \frac{0.086}{8}(35y^4 - 30y^2 + 3) \tag{2.3}$$

Note that the albedo α is held fixed during this study, therefore any feedback associated with the albedo(e.g, ice-albedo feedback) is excluded.

The outgoing longwave radiation is estimated using the empirical relation of Budyko (1969),

$$I = F_0 + \frac{dF_t}{dT_s} Ts \tag{2.4}$$

where Ts is the surface temperature (in units of degree Celsius). ERBE longwave radiation data (Trenberth and Solomon, 1994) and the observed SST (Levitus, 1982)

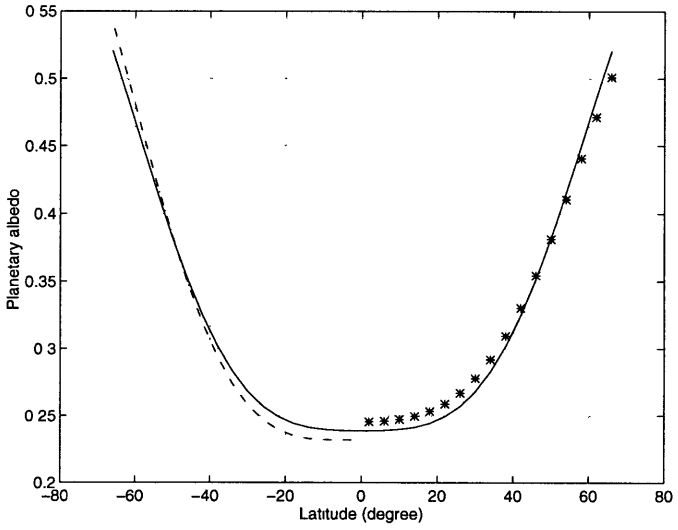

Figure 2-4: Observed zonally averaged planetary albedo, Southern Hemisphere (dot-dashed), Northern Hemisphere (starred), and the one used in this study (solid).

are used to determine the coefficients F_0 and $\frac{dF_t}{dT_s}$,

$$F_0 = 195 W m^{-2}; \tag{2.5}$$

$$\frac{dF_t}{dT_s} = 2.78 W m^{-2} (^{\circ}C)^{-1}. \tag{2.6}$$

The longwave parameterization is one of the important 'hooks' between the atmosphere and the ocean. The coefficient $\frac{dF_t}{dT_s}$, as will be seen in next Chapter, determines the Newtonian damping time scale of the SST in the ocean model.

The second physical element of the model is the atmospheric meridional heat/moisture transport parameterization. The meridional transport mechanisms are different for low and high latitudes. In low latitudes, the Hadley circulation is the dominant mechanism of poleward transports, whereas in high latitudes, eddies transport most of the energy poleward (Fig.1-1, the lower curve). The eddy transport parameterizations are the foci of this work, because the thermohaline circulation is mainly a high-latitude

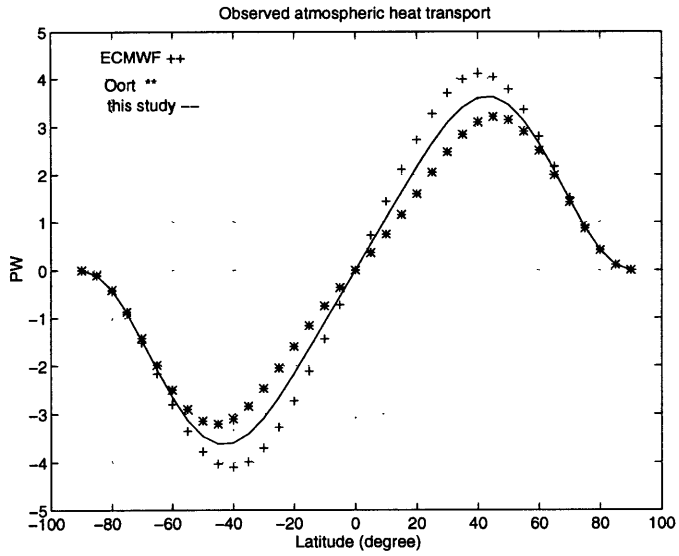

Figure 2-5: Observed zonally averaged atmospheric heat transport

phenomena. The thermohaline circulation is sensitive to the atmospheric moisture transport in high latitudes (e.g, Manabe and Stouffer, 1994). On the other hand, the moisture transport in low latitude has been shown to be of little importance to both the existence and the strength of the thermohaline circulation (Zaucker et al., 1994). As a result, the transport mechanisms in low latitudes are not explicitly represented.

The latitudinal profile of atmospheric heat transport is prescribed based on observations. Two data sets are used, one from rawinsonde data (Oort,1983), the other from ECMWF operational analysis products (Keith, 1995). We average the two analyses, and modify the profile to be antisymmetric about the equator (Fig.2-5). Furthermore, the profile is fitted by Legendre polynomial functions,

$$H_d(y) = 3.866y - \frac{2.851}{2}(5y^3 - 3y) - \frac{1.016}{8}(63y^5 - 70y^3 + 15y); \qquad (2.7)$$

where $y = sin\phi$.

The moisture transport is taken from Baumgartner and Reichel (1975), modified in

two ways. First, in order to close the water budget over the oceanic model domain, all the freshwater flux beyond 64N/S is assumed to concentrate in the northern/southern boundary region. The second modification is to average between the two hemispheres, and to achieve a profile antisymmetric about the equator (Fig.2.3). Consequently, the freshwater is also conserved within each hemisphere, and no moisture transport crosses the equator. As with the heat transport profile, we fit the moisture transport profile by Legendre polynomial functions,

$$F_w = 2.092y \pm 5.796P2 + 8.472P3 \pm 7.728P4 + 2.362P5; (SH : +; NH : -) \quad (2.8)$$

where $P1 = y$, $P2 = \frac{1}{2}(3y^2 - 1)$, and $P3 = \frac{1}{2}(5y^3 - 3y)$,

$$P4 = \frac{1}{8}(35y^4 - 30y^2 + 3), P5 = \frac{1}{8}(63y^5 - 70y^3 + 15y) \quad (2.9)$$

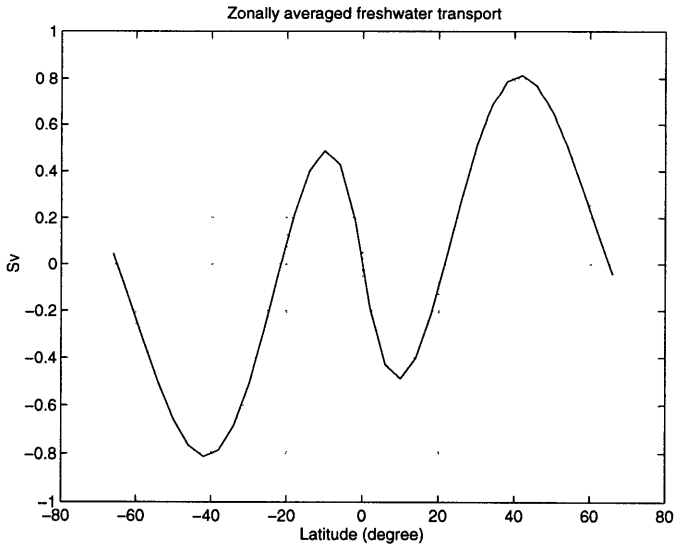

Figure 2-6: Observed zonally averaged atmospheric freshwater transport

2.4 Coupling procedure

To mimic the atmospheric box model of NSM as closely as possible, the latitudinal profiles of the atmospheric transports remain fixed during this study. However, the amplitude of each profile is determined by parameterizations of eddy transports at 35° N/S respectively. We assume that the transports by the mean circulation at 35° N/S are negligible, compared to transports by eddy activity (e.g, Fig.1-1). The eddy transport of heat is defined as,

$$H_d(35°) = 2\pi cos\phi \int_0^\infty [\rho_a(L_v\overline{v'q'} + C_p\overline{v'T'})]dz \tag{2.10}$$

where ρ_a is the atmospheric density, L_v is the latent heat of condensation, C_p is the specific heat of dry air at constant pressure, q is the specific humidity or mixing ratio, and v and T represent the meridional velocity and the potential temperature, respectively.

The eddy sensible heat transport is parameterized based on baroclinic stability theory (Held, 1978; Stone and Miller, 1980),

$$\overline{v'T'} = A(\frac{\partial T}{\partial y})^n; \tag{2.11}$$

While the eddy moisture transport is parameterized (Leovy, 1973; Stone and Yao, 1990) as,

$$\overline{v'q'} = r_h(\frac{\partial q_s}{\partial T})\overline{v'T'} \tag{2.12}$$

$$q_s \approx 0.622\frac{2.53 \times 10^{11}}{P}e^{-(5420/T)} \tag{2.13}$$

where q_s is the saturated mixing ratio, r_h is the relative humidity. The overbar denotes

a zonal and temporal mean. The prime of a quantity denotes the deviation from the quantity's zonal and temporal mean. The power law of the meridional transports depends on both latitude and vertical stability (Branscome, 1983; Stone and Yao, 1990). Empirically, n is found to vary with latitude in the range from 1.6 to 4 (Stone and Miller, 1980). Here, we choose a value appropriate for 35° N, n=2.5.

Combining the constants together, we can rearrange the parameterizations as,

$$H_d(35°) = (C_S + C_L e^{(-5420/T)})(\frac{\partial T}{\partial y})^{2.5} \tag{2.14}$$

$$Fw(35°) = C_F e^{(-5420/T)}(\frac{\partial T}{\partial y})^{2.5} \tag{2.15}$$

The coefficient C_S represents the eddy sensible heat transport. The eddy latent heat transport, thus the moisture transport, is given by the coefficient C_L. Both the transports of sensible and latent heat depend on a power of the temperature meridional gradient at 35° N/S, but the latent heat transport (also the moisture transport) is also affected by the temperature itself at 35° N/S, as defined by the Clausius-Claperon equation (Eq.2.13). The parameterization is another important 'hook' between the atmosphere and the ocean.

The coupling procedure between the atmosphere and the ocean is illustrated by Figure 2.4. We assume that the atmospheric heat capacity is negligible, so that the divergence of the atmospheric heat transport, plus the net radiation at the top of the atmosphere must be balanced by the surface heat flux. Similarly, the moisture conservation of the atmosphere requires that the divergence of the moisture transport

equals the surface freshwater flux.

$$Flx_{heat} = Q(1-\alpha) - I + \frac{1}{2\pi a^2}\frac{\partial Hd}{\partial y} \tag{2.16}$$

$$Flx_{frsh} = \frac{1}{2\pi a^2}\frac{\partial Fw}{\partial y} \tag{2.17}$$

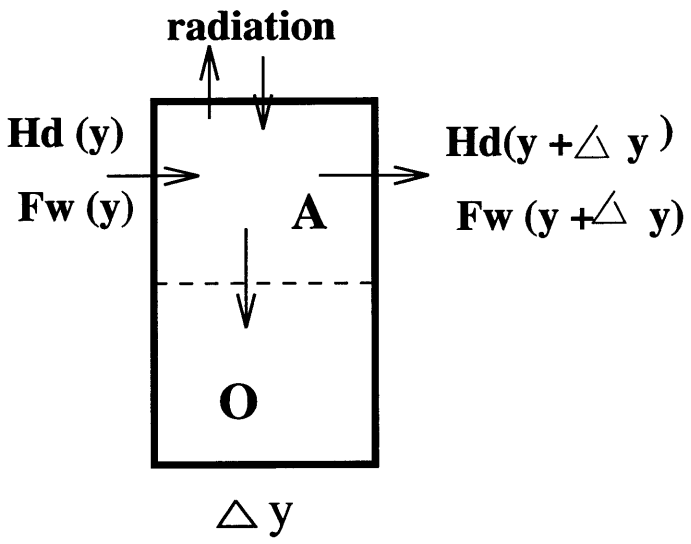

Figure 2-7: Schematic illustration of the coupling between atmosphere and ocean

To estimate the oceanic surface fluxes of heat and freshwater, land has to be considered. Land is treated in a simplified fashion here, because its dynamics is not easily captured. The important point is that the land serves as a possible source/sink for surface fluxes. The heat capacity of land is assumed negligible, therefore, the surface heat flux over land is assumed zero. The land surface temperature is assumed to be zonally uniform and equal to the zonally-averaged SST. Since the area ratio between ocean and land is $\frac{1}{2}$ at each latitude (except the ACC), a factor of 3 is introduced in Eq. 2.16. Note however that the longwave radiation term I is allowed to differ for the two ocean basins, if they have different temperatures, according to

Eq. 2.4.

The freshwater flux into the ocean depends on run-off from land. We assume that the freshwater flux into the ocean is multiplied by a factor that varies from a maximum of 3., to a minimum of 0.5, with 1.5 and 1. between. The multiple factor is conceptually close to that used in the coupled box model (NMS; Marotzke, 1996). In the four cases, we assume that there is no zonal transport of moisture between basins, and each basin receives identical freshwater flux that is zonally uniform. Again, this approach is consistent with our principle of no atmospheric source of asymmetric forcing. Through the multiplicative factor, the hydrological cycle over the ocean can be varied in a systematical way. The thermohaline circulation forced by these different hydrological cycles will be presented in Chapter 3.

The ocean influences the atmosphere by affecting the temperature gradient, and therefore the transports at 35°N/S. In the eddy transport formulae(Eq.2.14 and 2.17), we use an atmospheric temperature profile determined by the SST field in the oceanic model. The atmospheric temperature profile is assumed to have the form,

$$T(y) = T_0 + \frac{T_2}{2}(3y^2 - 1) \tag{2.18}$$

The polynomial function coefficients (T_0 and T_2) are determined by assuming that the area-weighted SST over two latitude ranges (0°-35°, 35°-64°) are equal to the same averaged atmospheric temperature. The reason for such an area-weighted average approach is that the typical meridional scales of eddies that transport heat is 20° to 30° (Stone, 1984), and the transport should not respond only to smaller scale structure in SST. It also is in close accordance to NSM's box model structure.

The coupling procedure can be summarized as following,

changing the thermohaline circulation $\longrightarrow$ changing the SST field $\longrightarrow$ changes the atmospheric temperature and its meridional gradient at 35° N/s $\longrightarrow$ changes the atmospheric heat/moisture transports $\longrightarrow$ changes the surface heat/freshwater flux $\longrightarrow$ further changes the thermohaline circulation .

Chapter 3

Thermohaline Circulation Driven by Observed Atmospheric Transports

3.1 Introduction

As the two component models and their coupling procedure have been described in the previous chapter, here we will first test the oceanic component model with the surface forcings derived from observed atmospheric heat and freshwater transports. The starting point of this chapter is based on the work of MW91 and Marotzke (1996).

MW91 investigated the full range of possible equilibria of the thermohaline circulation . In their spin-up process, the surface temperature and surface salinity were restored to prescribed profiles with a 30 day relaxation time scale. At the end of the spin-up, the freshwater flux was diagnosed from the model's steady state. The model was then put through a series of perturbation experiments using the fixed diagnosed

freshwater flux, but still the same restoring of temperature. This combination of surface temperature and salinity boundary conditions is known as " mixed boundary conditions".

Under the mixed boundary conditions, depending on the initial state, the thermohaline circulation can reach an equilibrium state corresponding to the observed current thermohaline circulation pattern: In one basin (the "Atlantic"), North Atlantic Deep Water is formed, and no deep water is formed in the other basin (the "Pacific").

The surface heat and freshwater fluxes in the MW91 are actually what the ocean model demanded, in order to obtain a realistic SST and SSS simulation. The surface forcings are not directly related to atmospheric observations. If the surface forcings in the ocean model differ from what an observation-based atmospheric model provides, the coupled model will have to artificially adjust the discrepancy to prevent a drifting away from the current climate.

Here, the OGCM is spun up with the surface forcings derived from the observed atmospheric transports. While the atmospheric transports are prescribed from observations, the longwave radiation is still interactive with the local SST. Such coupled box model were studied by Marotzke (1996). It is worth finding out how realistic the thermohaline circulation will be in the OGCM. The hope is that if the OGCM with observed atmospheric transports reaches a realistic conveyor belt circulation, we may avoid artificial flux adjustments in later coupled models.

The experimental procedure is addressed in Section 3.2. The conveyor belt circulation simulated in the ocean model is described in Section 3.3. Section 3.4 describes the ocean model equilibrium response to changes of the hydrological cycle. The model results are explained by a mechanistic box model in Section 3.5.

3.2 Experimental strategy

In this section, the experiment strategy is discussed. We will first describe how we construct the surface forcings from the observed atmospheric transports. Then the spin-up procedure for setting up the conveyor belt circulation is described.

3.2.1 Boundary condition

The boundary condition derived from the observed atmospheric transports is fundamentally a mixed boundary condition type model. As discussed in Section 2.3, in the model, the freshwater flux is determined from the divergence of the atmospheric moisture transport, on the assumption of atmospheric moisture conservation. Since the atmospheric moisture transport is prescribed to the observation, the freshwater flux for the ocean model is thus fixed.

On the other hand, the surface heat flux in the model is calculated from the net radiative flux and the divergence of the atmospheric heat transport. With fixed observed atmospheric heat transport and interactive longwave radiation term, this is equivalent to restoring the temperature to a prescribed profile (T^*) with longwave radiative timescale.

In this sense, the model here is still similar to MW91 model, though we reform the mixed boundary conditions based on a better physical basis, and directly relate them to the observed atmospheric transports. As Fig.3-1 shows, the freshwater flux from the model has stronger freshening in the high latitudes than that from the MW91 model. It is worth mentioning that the multiplicative factor reflecting the runoff is chosen to be 1.5 (hereafter 1.5Fw) for our control run. The justification for such choice will be deferred to Section 3.4.

The prescribed temperature profile T^* in the model is defined as the temperature

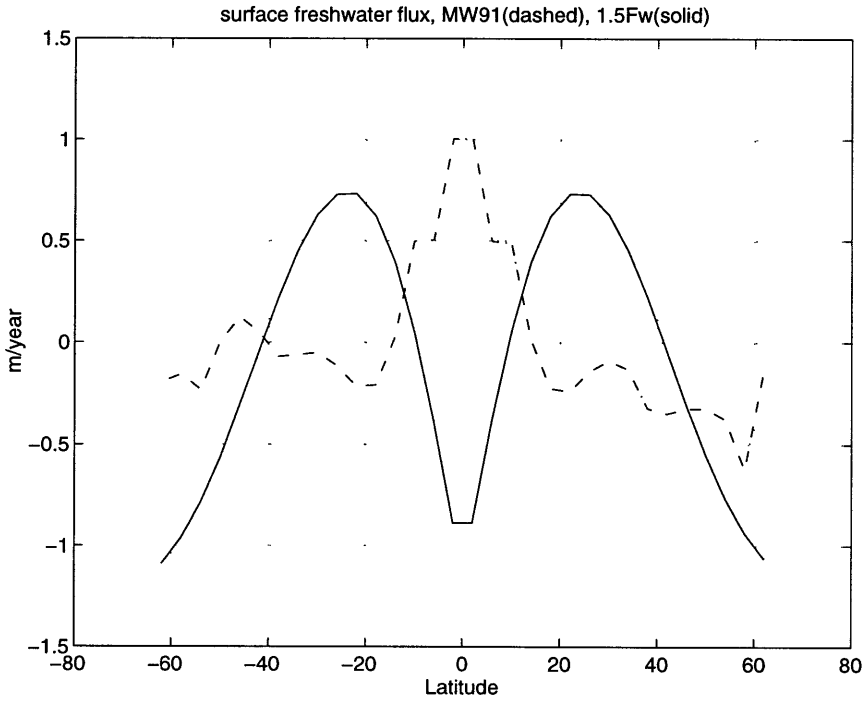

Figure 3-1: Comparison of two distributions of the ocean model's surface freshwater fluxes, the one used in MW91 (dashed), and the one in the model with multiplicative factor of 1.5 (solid).

that ocean is forced towards (Bretherton, 1982). It is the equilibrium temperature that the ocean would reach in the absence of ocean currents (i.e, when there is no oceanic heat transport). T^* is calculated in the model using the observed atmospheric heat transport and the net radiative forcing parameterization, while setting oceanic heat transport to zero. Figure 3-2 plots T^* as a function of latitude. In comparison, the observed SST is also plotted. T^* exhibits a much steeper meridional gradient.

The time scale for restoring to T^* arises naturally from the model. It is solely determined by the longwave radiative coefficient $\frac{dF_t}{dT_s}$ (as $2.78 W m^{-2} (^\circ C)^{-1}$). It gives a time scale of 288 days for a top ocean layer 50m thick, representing the time scale to remove the global scale SST anomalies through longwave radiation to space.

On the other hand, the small scale zonal SST anomalies are removed in the model

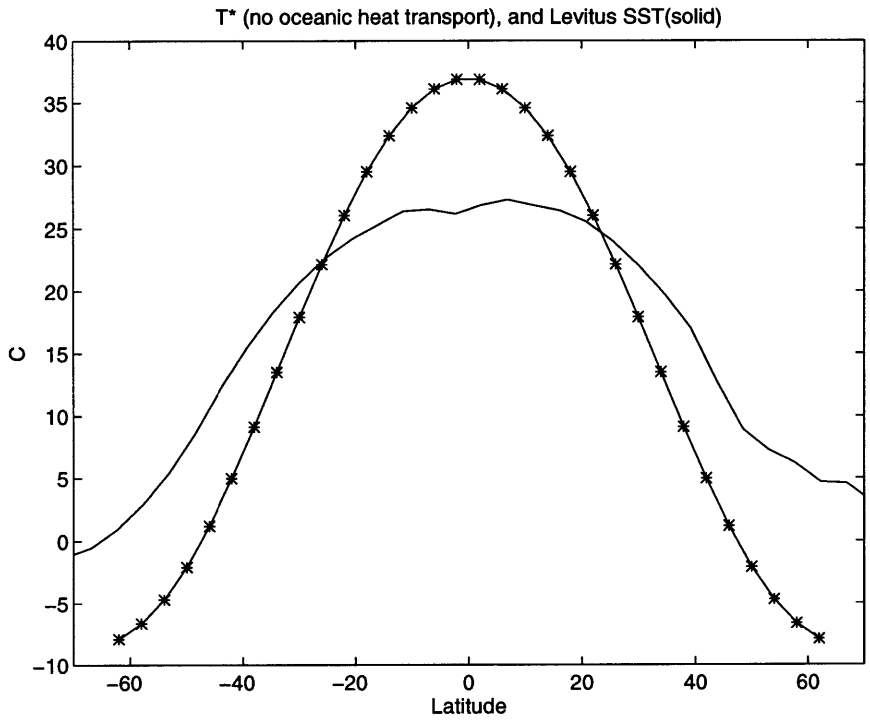

Figure 3-2: The Levitus (1982) zonal mean SST (solid), and the T^* in the model (starred), unit: ° C.

by zonally averaging the SST within each basin at every timestep (2 days). Without this zonal mixing, the location of the North Atlantic Deep Water formation is in the mid-latitudes, rather than near the northern boundary of the model, because the small scale heat flux anomalies in the surface shift the deep convection locations. The experiment results (not shown) indicate that such small scale anomalies will disappear if there is no wind in the model.

While the emphasis of the mixed boundary conditions in MW91 is on a realistic simulation of SST and SSS, the model developed here puts more stresses on a realistic simulation of surface heat and freshwater fluxes. This is crucial to ensure an appropriate coupling between the two components. The coupled model, if the ocean model is perfect, can have an accurate simulation of both SST, SSS, and the surface

fluxes. This is not possible with the normally used mixed boundary condition.

3.2.2 Spin-up procedure

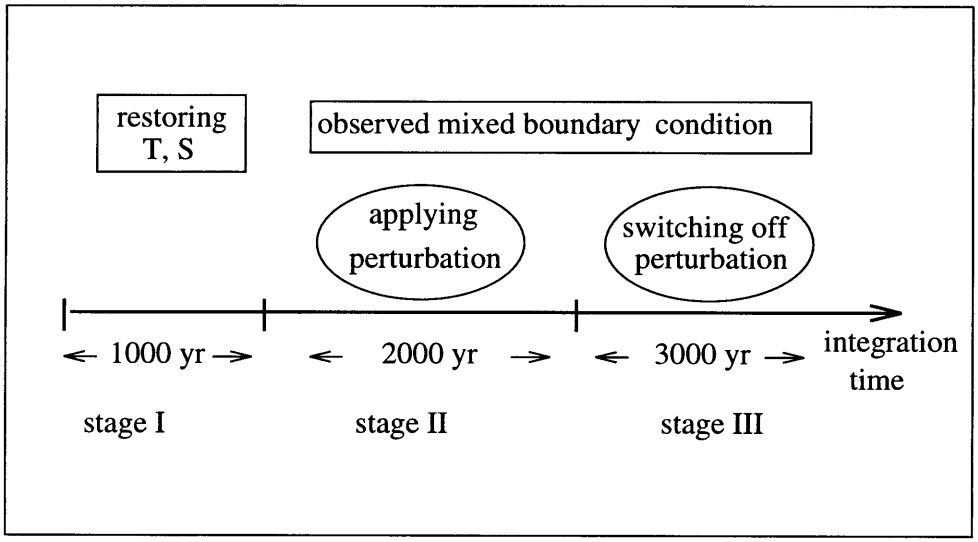

Figure 3-3: Numerical procedure for spin-up

The spin-up procedure to obtain the conveyor belt circulation is, in most aspects, identical to that used in MW91. The model spins up from an initial motionless state with horizontally uniform tracers fields. The wind stress field is fixed and identical to that in MW91(Fig. 2-2). The whole procedure can be divided into three stages, as illustrated in Figure 3-3.

Stage I: For the first 1,000 years of integration, the restoring conditions for surface temperature and salinity are used. The surface temperature, is restored to the T^* profile with a time scale of 288 days, using the observed thermal boundary condition as discussed in Section 3.2.1. The surface salinity is restored to an idealized salinity profile, with time scale of 30 days. The idealized salinity profile is taken from MW91 (Fig. 2-2). This restoring stage ensures that the surface salinity field is spun up

quickly.

Stage II: In this stage, the salinity condition is switched to a fixed freshwater flux derived from the observed atmospheric moisture transport, (i.e 1.5Fw), while the temperature condition remains the same as in Stage I. These mixed boundary conditions are used during the rest of the procedure (Stages II and III).

At the end of Stage I, the deep water forms in the northern oceans of both basins. To reach the state with sinking in the North Atlantic only, the freshwater flux is perturbed by 0.9m/y north of 40N, such that there is a zonal atmospheric freshwater transport from Atlantic to Pacific. Note that the perturbation used here is 4 time larger than that in MW91. The perturbation lasts for 2,000years, until the conveyor belt circulation is fully set up. Then the perturbation is switched off in Stage III.

Stage III: To allow the conveyor belt circulation to reach the equilibrium state, the integration is continued for another 3,000 years after the perturbation is switched off. The time series of the globally averaged surface heat uptake is plotted in Figure 3-4. It shows that the model reaches statistically steady state at the end of the integration.

3.3 Simulation of conveyor belt circulation

The equilibrium state at the end of Stage III has a North Atlantic Deep Water (NADW) formation of 18 ± 1 Sv near 48° N, and there is no deep water formed in the North Pacific (Fig. 3-5). In comparison, the estimated NADW formation based on the observational data is 27 ± 3Sv near 48° N (Macdonald and Wunsch, 1996). Across 25° N, the North Atlantic overturning is estimated to be 17 ± 3 Sv by Macdonald and Wunsch (1996), while the model reaches about 10 Sv. As will be seen in Section 3.4, the NADW formation rate is varied with the multiplicative

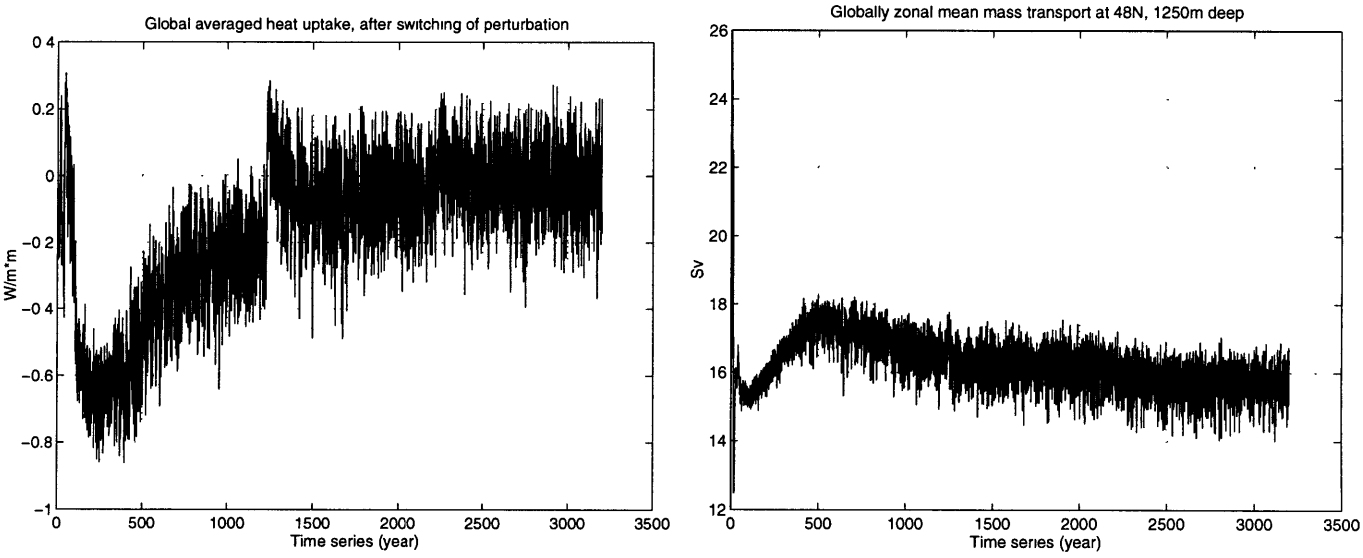

Figure 3-4: Left: the time series of the globally averaged heat uptake (unit: W/m^2) in the model after the perturbation was turned off. Right: the time series of the globally zonal mean mass transport(unit: Sv) at 48° N, 1250m deep, after the perturbation was turned off.

factor used in the freshwater flux calculation. We could tune that factor to achieve a stronger overturning that is close to the observed value (e.g, 3Fw case in Section 3.4). But the stronger overturning is found unstable in a later fully coupled version model. Therefore, the current model with the multiplicative factor of 1.5 is chosen as the control run.

The barotropic mass streamfunction, which is essentially determined by the wind forcing, is shown in Fig.3-6.

Despite its weak overturning strength, the simulated conveyor belt circulation in the model captures some realistic features that are generally missing when the conventional mixed boundary conditions are used. For example, the SST north of 48° N in the Atlantic is up to 9° C warmer than that in the Pacific (Fig.3-7), since the deep water formation in the North Atlantic leads to more warmer water advected from low latitudes. Such an inter-basin SST difference is not captured if the temperature

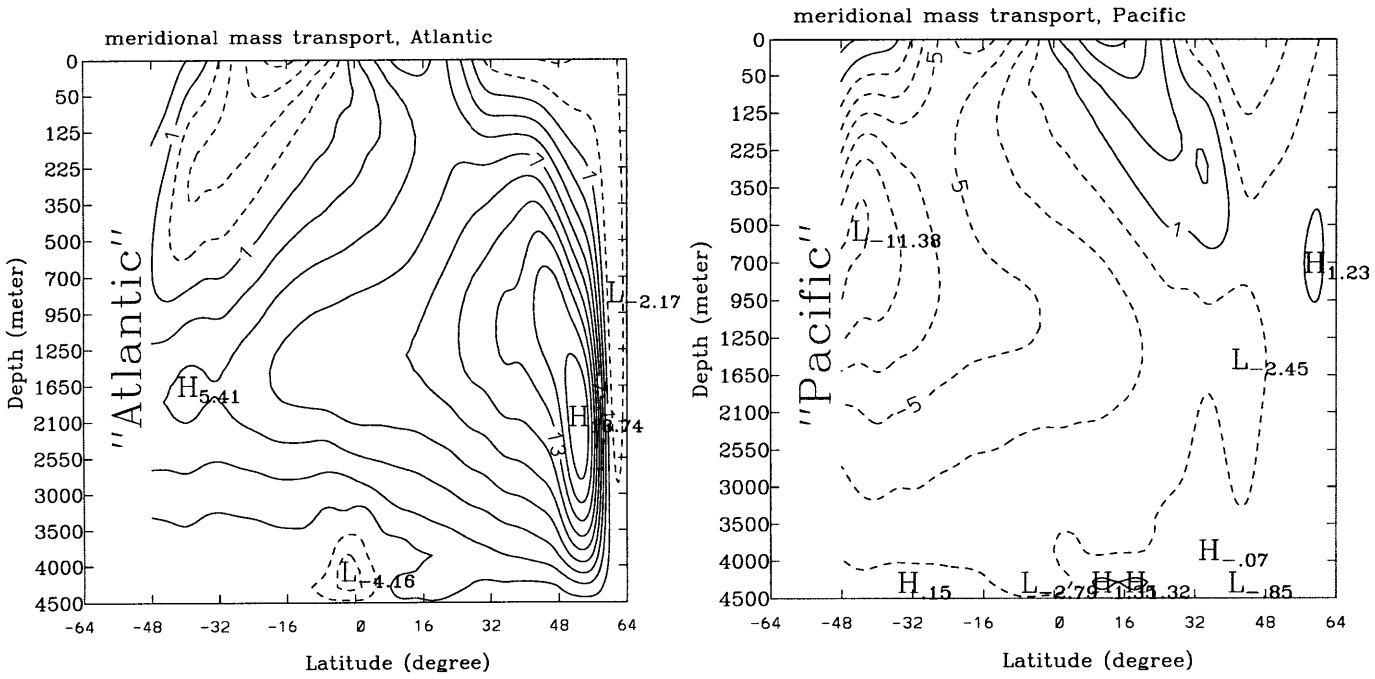

Figure 3-5: The model of 1.5Fw with the observed atmospheric transports: steady zonal mean meridional mass stream function (unit, Sv): Atlantic (left),and Pacific (right).

restoring time is too short (e.g, 30 days used in the conventional mixed boundary conditions).

One feature that fails to improve in the model is the oceanic heat transport. The oceanic heat transport simulated is only about 50% of the observed, with a maximum of 0.6 PW in the North Atlantic (Fig.3-8). The underestimation of the oceanic heat transport can be attributed to several shortcoming of the model. First, the NADW formation rate in the model is low, about 18 Sv, compared to 24 Sv in MW91. As a result, the maximum heat transport in the North Atlantic of MW91 is about 50% higher than of the present model.

Another shortcoming is the coarse resolution of the ocean GCM. So far, two processes were identified that can underestimate the oceanic heat transport when the horizontal resolution of the GCM is not eddy-resolving. The first process is,

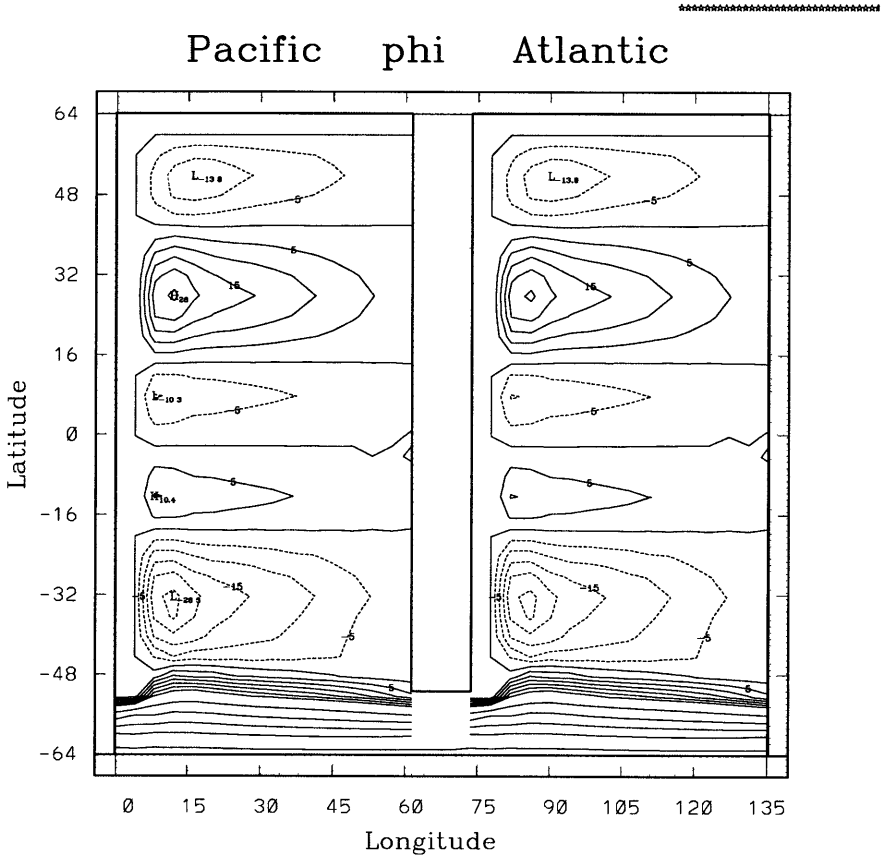

Figure 3-6: The model of 1.5Fw with the observed atmospheric transports: barotropic mass streamfunction, unit: Sv.

as noted by Veronis (1975), the parameterization of eddy mixing by a horizontal diffusivity in coarse resolution oceanic model. In the frontal region near the western boundary, the diapycnal diffusion induces a strong upwelling of cold water, and thus reduces the amount of deep water transported towards lower latitudes and across the equator. This shortcut in the North Atlantic overturning was found to underestimate the oceanic heat transport (Boning et al., 1995). The second process is associated with the horizontal resolution. Wang et al. (1995) found that, due to the weak temperature advection by the western boundary current, the heat transported by the western boundary current can be underestimated by 50% for a coarse horizontal

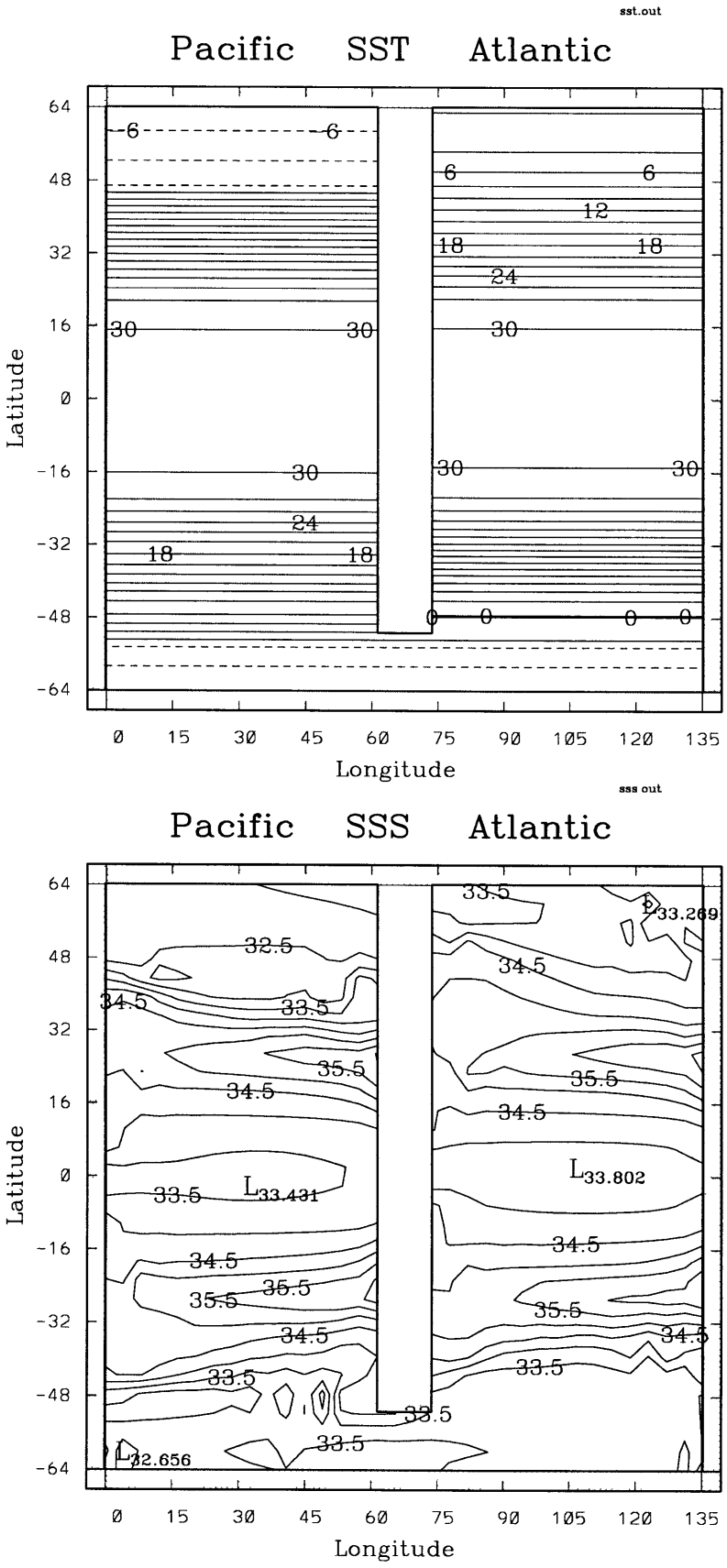

Figure 3-7: The model of 1.5Fw with the observed atmospheric transports: the SST (° C) and SSS (ppt) distributions at the steady state.

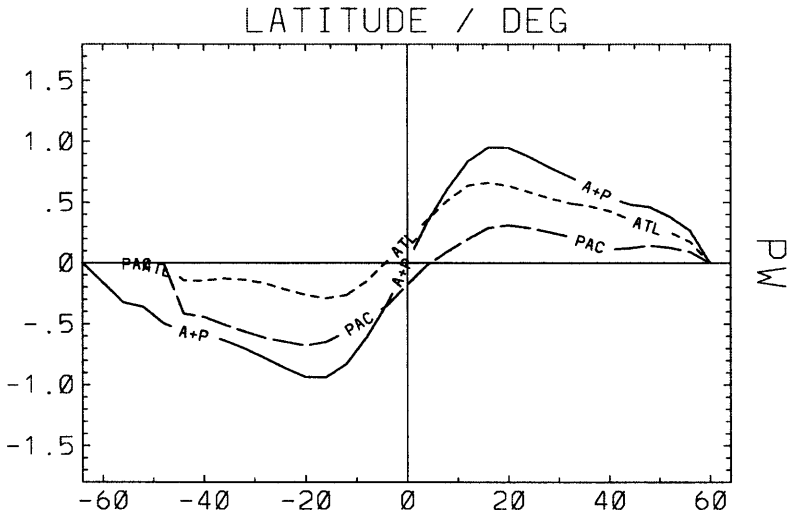

Figure 3-8: The model of 1.5Fw with the observed atmospheric transports: the oceanic heat transport (PW) at the steady state.

resolution ($4° \times 4°$) model.

In the present model, both the atmospheric heat transport and the shortwave radiative forcing are constrained by the observations. If in addition, the longwave radiative forcing was also fixed to the observations, the oceanic heat transport would have been equal to the observed value in the steady state. Since the longwave radiation is parameterized as a linear function of SST, the model can compensate its low oceanic heat transport by obtaining a much stronger equator-to-pole gradient of SST, and hence a stronger differential longwave radiative forcing. As will be seen in Chapter 5, this will cause the fully coupled model to drift away from the observed climate, and a flux adjustment cannot be avoided.

3.3.1 Surface density flux

In this section, we diagnose the terms forcing the circulation. The purpose is to search for dynamical properties that may control the thermohaline circulation intensity.

The thermohaline circulation is driven by the surface heat and freshwater fluxes. In a purely dynamical context, one naturally does not distinguish the two forcing fluxes, but the combination of the two, the density flux. The surface density flux is defined as:

$$F_\rho = -\rho(\alpha F_T - \beta F_S) \tag{3.1}$$

where F_T is surface temperature flux, and F_S is surface salt flux. The surface density flux F_ρ converts water from one density to another. When $F_\rho > 0$, water mass is transformed to higher density, and vice versa. If the ocean is close enough to a statistically steady state, this surface density conversion must be reversed somewhere else within the circulation. In other words, water parcels experience a motion in *density space*, which has to be coordinated with motions in *physical space*. This means that knowledge of the motion in *density space* can be translated into knowledge about the circulation in physical space.

This idea was initiated by Walin (1982), who attempted to use the surface heat flux to infer the thermal circulation in the ocean. Speer and Tziperman(1992) applied the same idea to estimate water mass formations in the North Atlantic, using climatological data for surface heat, and freshwater fluxes, and the surface density of the North Atlantic. The North Atlantic annual average sinking that escapes across the equator was estimated to be about 9 Sv.

Here, we apply the same idea to the ocean model, but with a different intention. We are interested in the latitudinal distribution of the surface density flux, and the relative contribution from the surface heat flux and the surface freshwater flux. Our intention is to identify the large-scale pattern of the density flux, and to relate it to the dynamics of the thermohaline circulation .

The Atlantic surface density flux in the model is plotted in Fig. 3-9, as a function

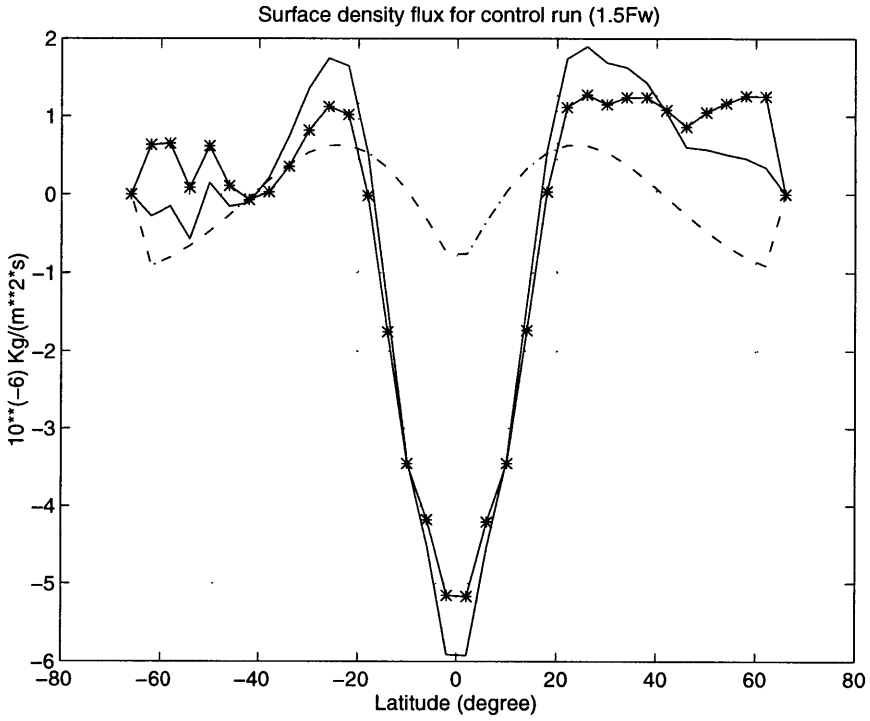

Figure 3-9: The model of 1.5Fw with the observed atmospheric transports: Atlantic surface density flux (solid), thermal component (starred), and haline component (dashed) diagnosed from the steady state. Unit: $10^{-6}Kgm^{-2}s^{-1}$.

of latitude, together with the thermal and haline components. The haline component of the density flux is linearly proportional to the freshwater flux, while the thermal component is nonlinearly related to the heat flux, due to the nonlinear state equation used in the model. The thermal expansion α used is approximated as,

$$\alpha = -0.072 - 0.01 \times T \tag{3.2}$$

Compared to the annual mean surface density flux map based on observations in the North Atlantic (Schmitt et al. 1989), the one from the model has similar large-scale features, with density gain in the middle and high latitudes, and density loss in the low latitudes. But there is significant difference between the observed map

and the model on the separate contributions of heat and salt to the density flux in the high latitude. Schmitt et al.(1989) found that the heat/salt density flux ratio is around 10 near 60° N, while the one in the model is about 1 in that region. The reason for such discrepancy is not clear.

On the other hand, there is no similar observed density flux map for the South Atlantic so far. The density flux diagnosed in the model indicates that, south of 40° S, the water mass is converted towards less dense water. That is, the density loss associated with freshening overcomes the density gain associated with cooling. It implies that the deep water upwells in the high latitude of the South Ocean.

The purpose of diagnosing the surface density flux is to look for large-scale dynamical properties that control the thermohaline circulation intensity. From the above analysis, it appears that in the high latitudes of the North Atlantic, water mass is transformed towards heavy dense water from the surface. At the steady state, this transformed water must be carried away from the sources, by the circulation, and, in other latitudes, has to be converted back to lower density. The analysis shows that there are two regions that have water transformation towards lower density, one is the low latitude region, the other is the high latitude of the South Atlantic. The next section will attempt to pinpoint which of the two is the location of the reversed conversion for the North Atlantic Deep Water in our model.

3.4 Conveyor belt circulation under different hydrological cycles

To study the large-scale dynamics of the thermohaline circulation , we vary the surface freshwater flux systematically to force the thermohaline circulation . A set of surface

freshwater fluxes with different multiplicative factors is displayed in Fig. 3-10. The 1.5Fw case corresponds to the run in last section. The same spin-up procedure in Section 3.2.2 is applied in all runs. All the runs achieve conveyor belt circulation patterns at the end of the integrations.

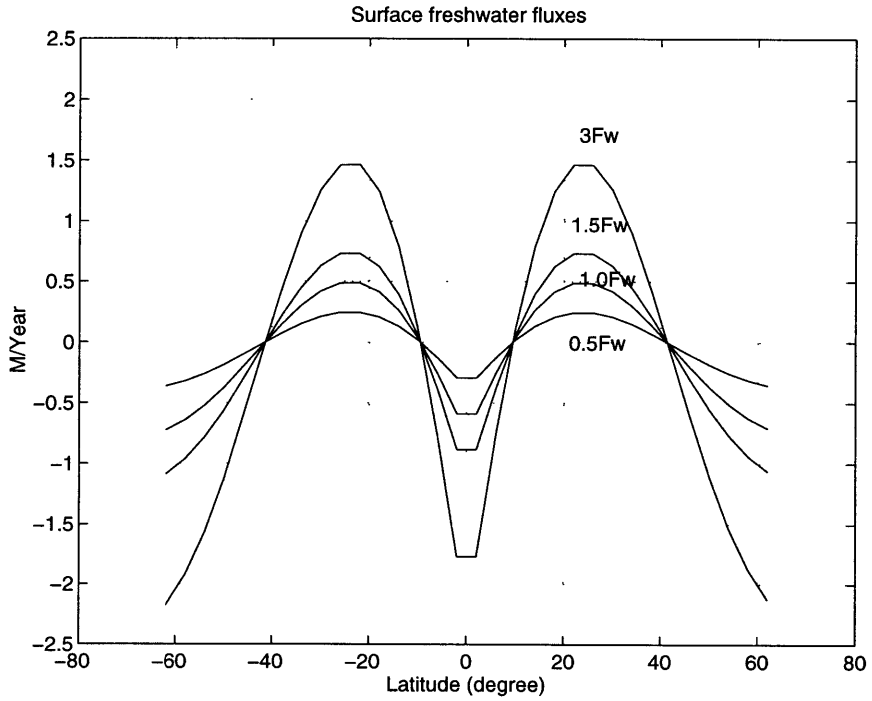

Figure 3-10: The four surface freshwater fluxes (unit, m/year) used in the sensitivity runs.

For all four runs, the conveyor belt circulation intensity increases as Fw increases, as shown in Fig. 3-11. The 3Fw run has the strongest overturning of 28 Sv, whereas the 0.5Fw run has the weakest overturning of 12 Sv. The result that the conveyor belt circulation is stronger under stronger freshwater flux is counter-intuitive. Enhanced freshening in high latitudes of the North Atlantic is expected to reduce the NADW formation, and therefore, to weaken the overturning, as evidenced in the global warming scenario of Manabe and Stouffer (1994, hereafter MS94). MS94 found that, as CO_2 increases, the atmospheric moisture transport gets stronger, and the stronger

freshwater flux causes the North Atlantic overturning to weaken or even disappear.

The apparent contradiction is resolved if we note the existence of multiple equilibria of the thermohaline circulation . What we found is actually the conveyor belt equilibrium under the different freshwater fluxes, while MS94 found a transition to the southern sinking equilibrium. It is also easy to switch to the southern sinking state in our model, by simply changing the initial state of the thermohaline circulation . The switching between different equilibria will be studied in the next chapter.

Note that we compare the thermohaline circulation *equilibrium* responses within the same category (i.e, the conveyor belt type). Under the different freshwater fluxes, the strongest freshwater flux run obtains the warmest SST in the North Atlantic high latitudes, as well as the strongest northward oceanic heat transport (Fig. 3-12).

The latitudinal distributions of the Atlantic surface density flux are compared in Fig. 3-13 for the 3.Fw, 1.5Fw and 1.Fw runs. As it shows, the three surface density fluxes in the North Atlantic north of 50° N are actually very close, even though their haline components are different. Whereas in the South Atlantic south of 50° S, the surface density fluxes differences are mainly caused by the different freshwater fluxes. The strongest freshwater flux case has the maximum density conversion towards lower densities.

The average density transformation is defined as,

$$\frac{\int F_\rho dS}{\int dS} \tag{3.3}$$

where dS is an element of the surface area.

We calculate the average transformation of each hemisphere. The hemispheric difference of the average transformation is defined as the interhemispheric surface density transport. The correlation between the interhemispheric surface density transport

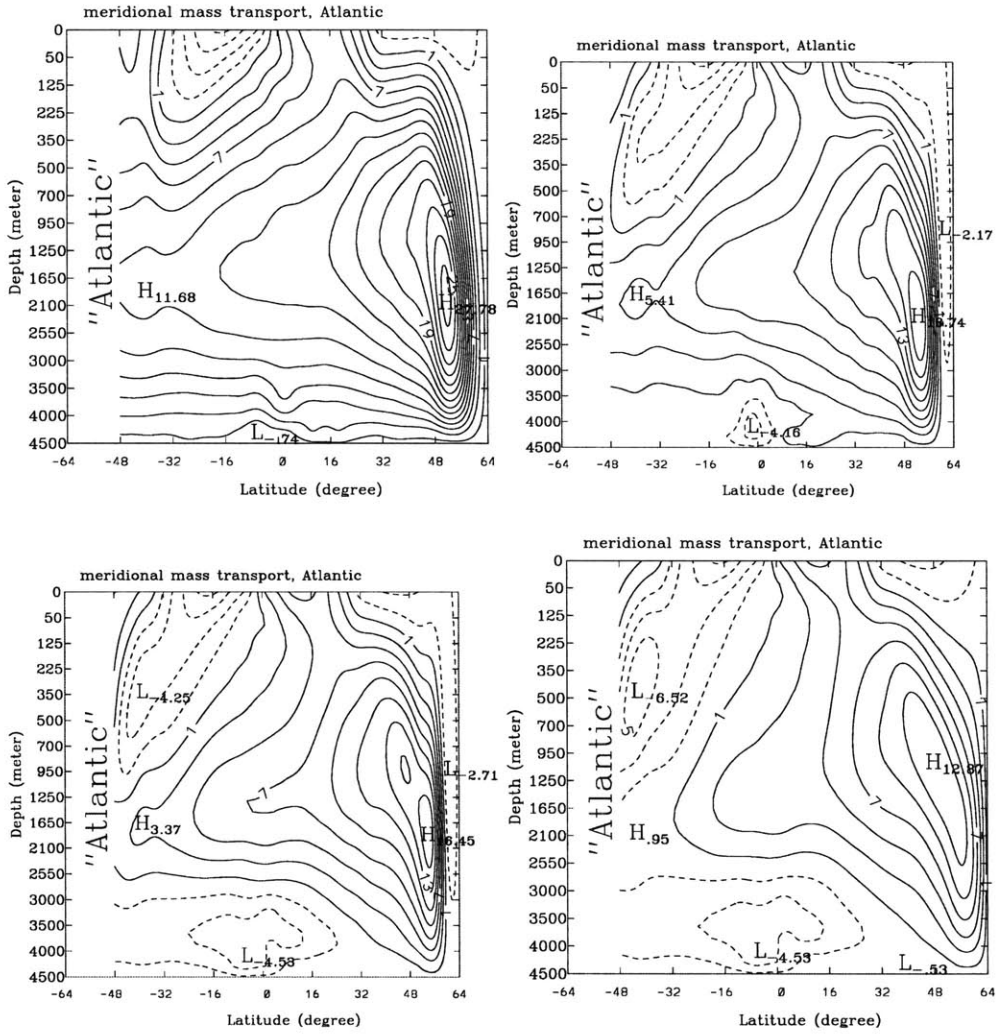

Figure 3-11: The zonal mean mass transport streamfunction in the Atlantic at the steady states: 3Fw run (upper left), 1.5Fw run (upper right), 1.0Fw run (lower left), and 0.5Fw run (lower right). Unit of the streamfunction: Sv.

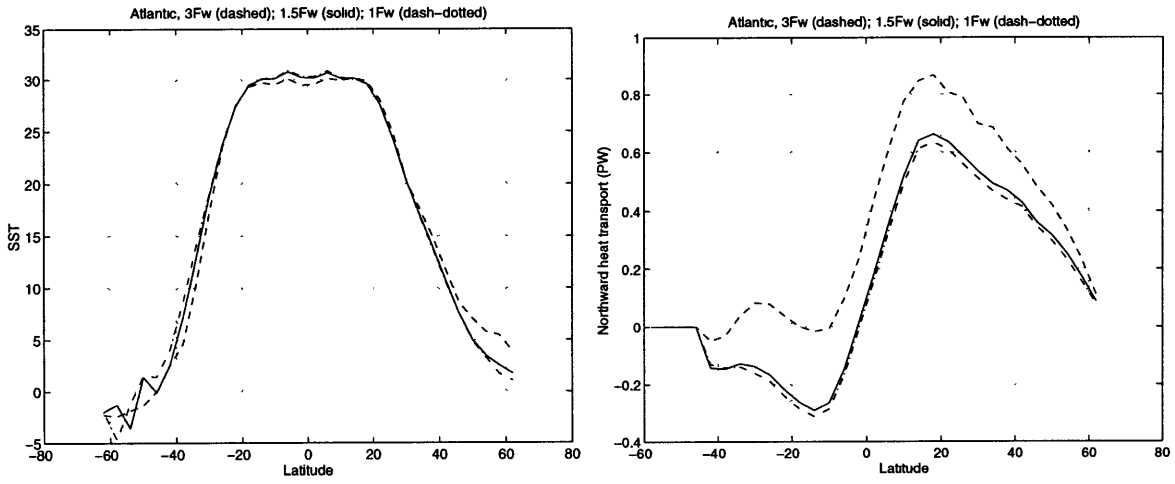

Figure 3-12: The Atlantic latitudinal distributions of SST (left, unit of ° C), and the northward oceanic heat transports (right, unit of PW) for three runs of 3Fw, 1.5Fw and 1Fw.

and the North Atlantic overturning intensities are plotted in Figure 3-14 for the four runs. The overturning intensity is approximately proportional to the interhemispheric surface density transport linearly.

A similar linear relation between the overturning intensity and the gradient of steric height P, has been found by Hughes and Weaver (1994) (Fig.3-15). The steric height P measures the depth-integrated pressure above a reference level. In a vertically stratified model, the dynamical quantity is no longer the surface density, but the steric height P. Taking the mid-depth of the overturning cell as the reference level, Hughes and Weaver demonstrated that the North Atlantic overturning is almost linearly proportional to the meridional difference in zonally-averaged steric height P between the latitude of the maximum zonally-averaged surface density in the north to the boundary of the South Atlantic.

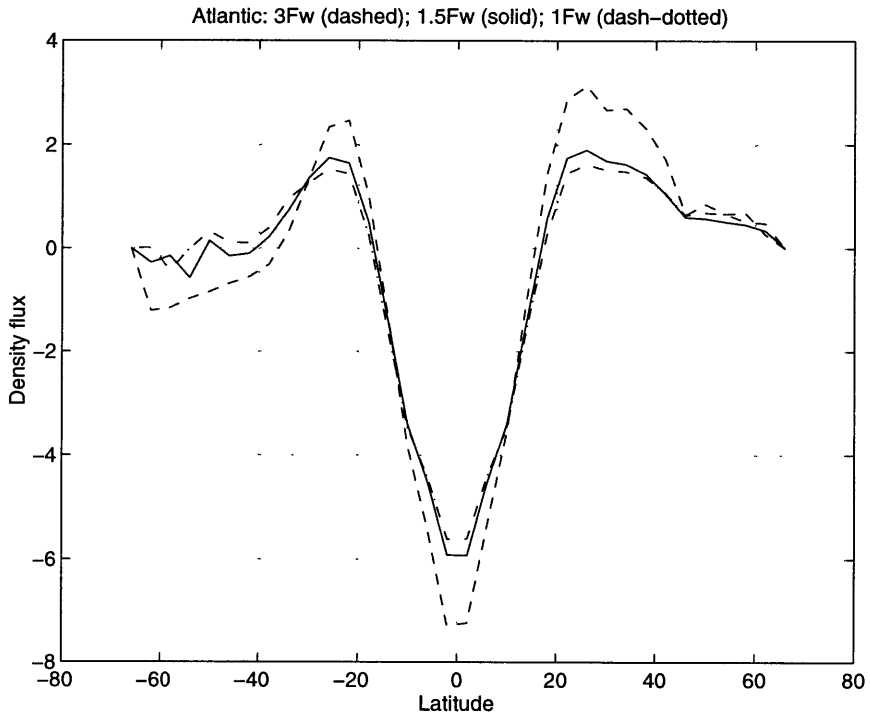

Figure 3-13: The Atlantic latitudinal distributions of the surface density fluxes in the steady states of 3Fw, 1.5Fw and 1Fw runs.

3.5 A mechanistic box model

There are two distinct types of box models, concerning the large-scale dynamics of the thermohaline circulation . One is Stommel's (1961), in which the flow is assumed proportional to the density difference between the high latitude box and the low latitude box (Fig.3-16). The Stommel box model was the first model to predict the existence of multiple equilibria, and has served as the theoretical foundation for many high level models of the thermohaline circulation . But the Stommel box model suggests that as the freshwater flux Fw increases, the flow will decrease, which is opposite to our GCM results in the last section.

The other type of box model was proposed by Rooth (1982). He conceptualized the thermohaline circulation , with a three-box model, as a pole-to-pole deep circulation.

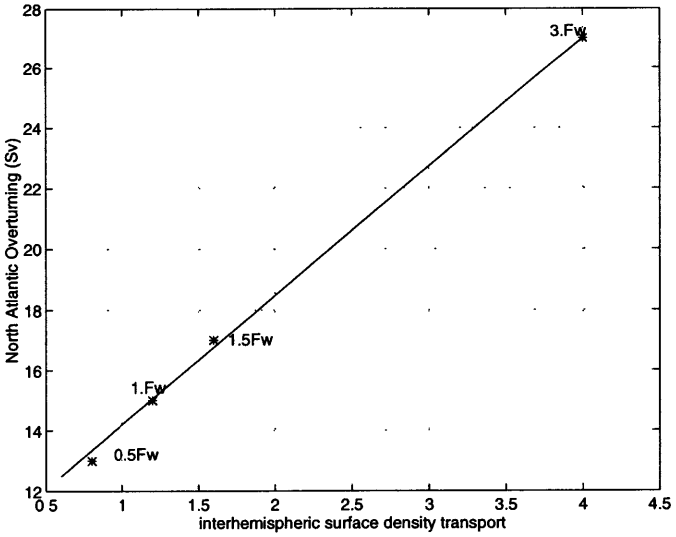

Figure 3-14: The maximum strength of the North Atlantic overturning (unit of Sv) as a function of the interhemispheric surface density transports (southward) for the four runs of 3Fw, 1.5Fw, 1Fw, and 0.5Fw.

In the three-box model, the flow is parameterized as a linear function of the density difference between two polar boxes (Fig.3-17). The Rooth box model is frequently used to illustrate that the thermohaline circulation can have a steady asymmetric pattern about the equator, even though the forcing is symmetric (e.g, Bryan, 1986).

There was one result in Rooth (1982) that has attracted little attention. The result was for how the flow strength varies with the hydrological cycle intensity. It was derived assuming that the temperature was constant and symmetric about the equator. It showed that the flow strength ϕ followed the square root dependence on the hydrological cycle intensity, Fw, i.e,

$$\phi \propto \sqrt{Fw} \tag{3.4}$$

The square root law between ϕ and Fw arises from the asymmetric density changes in the two polar boxes. The density ρ_1 is little influenced by Fw change, because of the

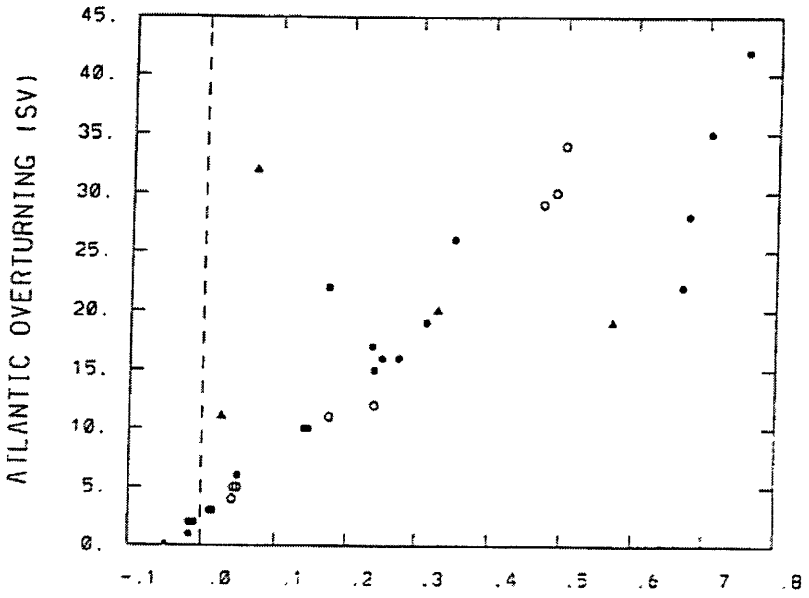

Figure 3-15: North Atlantic overturning (Sv) versus the meridional gradient of zonally-averaged depth-integrated steric height P ($10^{-6}kg/m$) between 47.25° S and the latitude of the maximum zonally-averaged surface density in the North Atlantic (from Hughes and Weaver, 1994).

counterbalancing between the Fw forcing change and the change of advection of salty water from low latitudes. On the other hand, the density ρ_3 is directly influenced by the Fw change, and gets smaller as Fw gets stronger without being counter-balanced by advections from low latitudes. As a result, the steady state flow intensity increases as Fw increases.

The results from the GCM runs are compared to the prediction from the square root law of the Rooth box model (Fig. 3-18). The agreement between the two models results is reasonably good, in the sense that they both increase with Fw. It suggests that the large-scale dynamics in the GCM is overwhelmed by the interhemispheric picture. However, it must be noted that the agreement breaks down as Fw goes to zero. For the extreme case of no freshwater flux, the GCM can not maintain conveyor

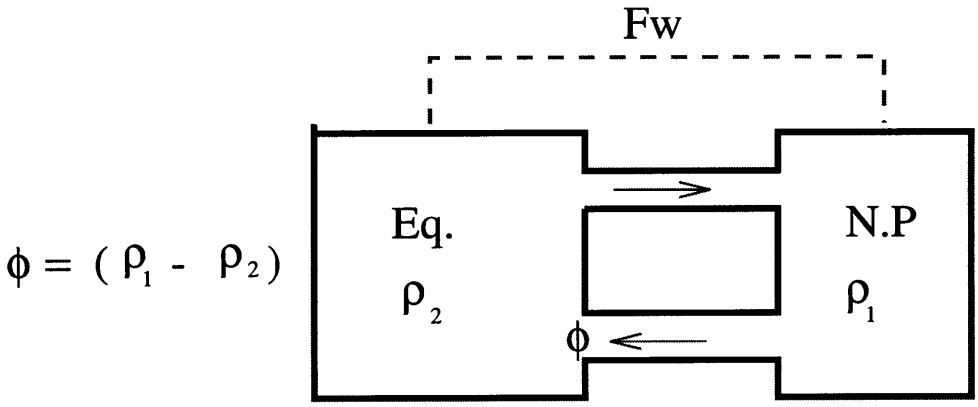

Figure 3-16: The two-box model of Stommel(1961)

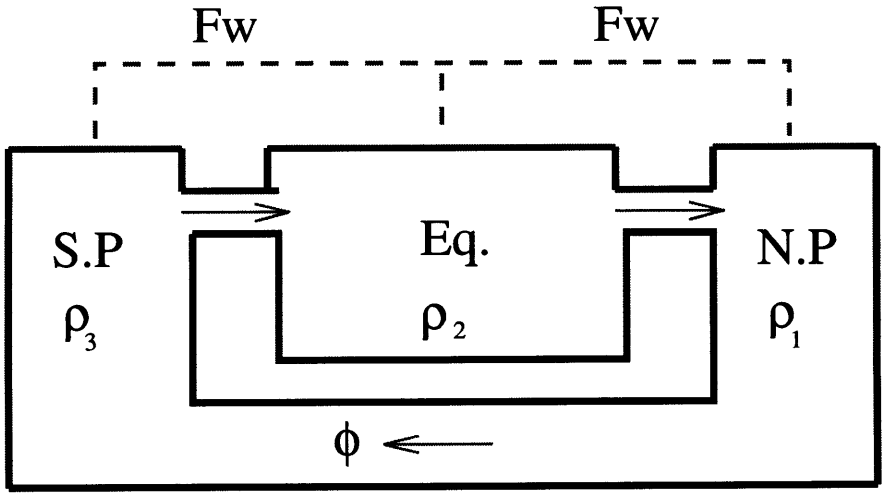

Rooth (1982)

Figure 3-17: The three-box model of Rooth (1982)

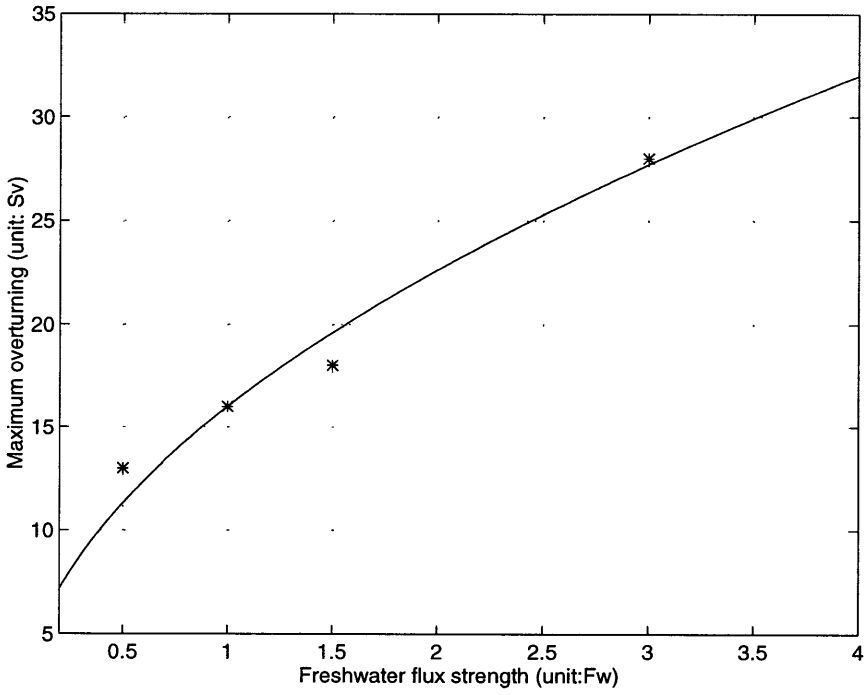

Figure 3-18: North Atlantic overturning strengthes (unit of Sv) versus the global hydrologic cycle strengthes (unit of "Fw"), the square root law prediction (solid), and the GCM results (starred).

belt circulation because there is no salinity gradient to sustain the asymmetry between the two basins. As will be shown in the next chapter, the thermohaline circulation under no freshwater flux will be the state with sinking in both basins, and the strength of the overturning depends on the thermal forcing.

The interhemispheric dynamics analysis in Rooth (1982) was only partial. More extensive analyses have been carried out by Rahmstorf (1996), and Scott et al.(manuscript in preparation, hereafter SMS96). Their work has supplied insightful paradigms for our GCM results.

One result from Rahmstorf (1996) and SMS96 is that, in Eq.3.4, the Fw that appears is actually the freshwater flux in the southern hemisphere (hereafter Fw-S). Rooth assumed the same Fw in both hemispheres, and did not explicitly distinguish

between the two hemispheres. The appearance of Fw-S only in the square root law has the surprising implication that the freshwater flux in the northern hemisphere (hereafter Fw-N) does not control the steady flow intensity at all.

The asymmetric role of the two Fw's on the steady flow identified in the box model, if robust in more complex models, will have important implication on the climate sensitivity. We will carry out perturbation experiments in the next chapter to test how robust the box model's results is in our OGCM.

Chapter 4

Interhemispheric Dynamics of Thermohaline Circulation

4.1 Introduction

In this chapter, the interhemispheric dynamics of the thermohaline circulation is further explored through a series of perturbation experiments. As demonstrated in last chapter, the global ocean GCM agrees reasonably well to the Rooth three-box model on how the steady overturning strength varies with the hydrological cycle strength in the observed range of surface forcings. This indicates that the thermohaline circulation dynamics in the GCM can be as simple as the three-box model, to zero order.

The basic assumption in the three-box model is that the upwelling of the deep circulation is concentrated in the southern high-latitude box, in the contrast to the uniform upwelling assumption in the classic Stommel-Arons deep circulation theory (1960). Warren's (1981) review of the deep circulation shows how many of the key deep western boundary currents have been successfully found, yet there is not a sense

that the basin-wide uniform upwelling has been verified. On the other hand, the tracer distributions suggest that special sites like the Southern Ocean and the Equator contribute a great deal to the upwelling, and that it may be otherwise rather unevenly distributed in space. For example, the distinct patterns of silicate, nutrients and salinity, plus particularly radiocarbon, have all demonstrated that the deep water of the North Pacific rises only to mid-depth (about 2500m), and flows southward toward further rising site in the Southern Ocean (e.g, Fiadeiro, 1983; Toggweiler and Samuels, 1992). Rhines (1993) speculated that the extensive high-latitude outcropping region in the Southern Ocean may be a dominant site for upwelling from great depth, since strong, widespread upward Ekman pumping assists the uplift of the deep water.

The upwelling in the GCM is not evenly distributed in space either. Besides strong upwelling near the western boundary in the mid-latitude, half of the overturning flows across the equator, of that, half upwells in the high-latitude of the South Ocean (see Fig. 3-5). How the hydrological cycles change the upwelling process has not been systematically studied with a GCM. The studies with the box model suggest that the roles of the hydrological cycles in the two hemispheres are highly asymmetric (Rahmstorf, 1996; SMS96).

Here we are going to apply two different kinds of perturbations to the model to study the roles of the hydrological cycles in the two hemispheres. In particular, the emphasis is on the transient responses of the overturning to the changes of the hydrological cycles. The perturbation methods are described in Section 4.2, and the results of the model under the perturbations are presented in Section 4.3 and 4.4.

4.2 Perturbation methods

The two kinds of perturbations applied to the coupled model are both finite amplitude perturbations. One is an internal perturbation, where only the initial fields of some variables are altered. The internal perturbation can make the model shift from one equilibrium state to another, but the equilibrium structure in the phase space will not be altered. Internal perturbations have been widely used to determine the stability of the equilibrium states that are qualitatively different (far apart in the phase space). However, it becomes impractical for a model characterized by many multiple equilibria, some of which are only different quantitatively. As will be shown in Section 4.3, our coupled model has the latter behavior.

The second type is an external perturbation, applied to certain boundary forcing terms. Such perturbations can change the equilibrium structure of the phase space, possibly destablizing existing types of equilibria and creating new types of equilibria. A example of an external perturbation is a scenario where the atmospheric CO_2 concentration doubles over a century or so (e.g, Manabe and Stouffer, 1994). With a fully coupled GCM, the significant effect of doubling CO_2 is global warming, which results in an enhanced atmospheric hydrological cycle. As a rough imitation of the CO_2 increasing scenario, we design an external perturbation on the atmospheric hydrological cycle. We perturb the freshwater flux Fw profile of each hemisphere separately and jointly. The intention is to distinguish the roles of Fw in the two hemispheres. The equilibrium state to which we apply the perturbation is the coupled model(1.5Fw) steady state. The Fw profile of each hemisphere is varied slowly in time, at a constant linear rate of 0.1% per year.

4.3 Random wind perturbations and the overturning predictability

In the perturbation experiments, the zonal wind stress field is also perturbed uniformly in space by random variations, north of 46° N. The random variation has Gaussian distribution, with standard deviation of 1 dyn/cm^2 and zero mean value. The deviation of the variation is based on the ECMWF wind stress data (Stammer, personal communication). The perturbation is applied in every time step (2 days). It mimics the seasonal cycle of the wind in the annual mean coupled model.

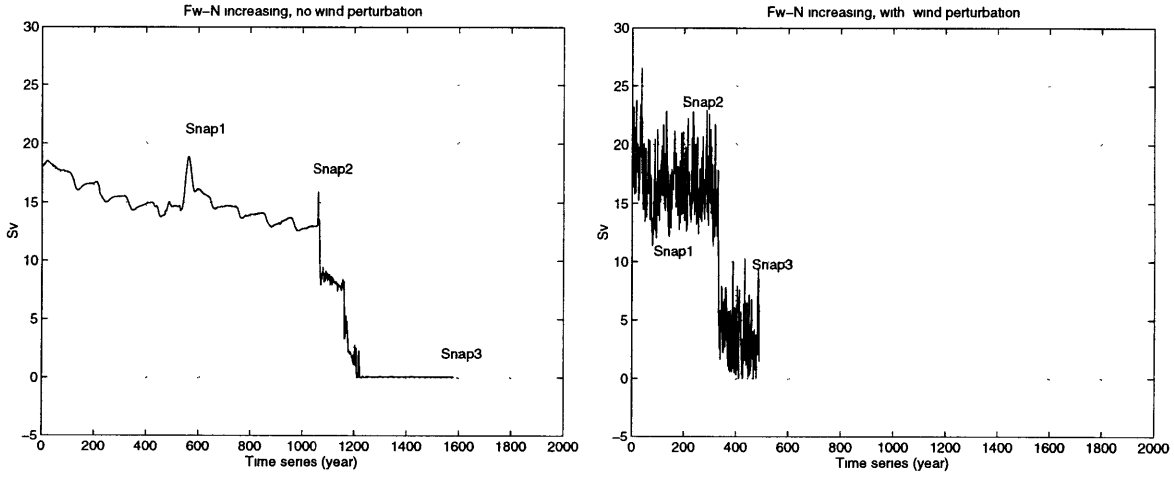

Figure 4-1: The time series of the North Atlantic overturning strength (unit of Sv), as Fw-N is increased at 0.1% per year. The right panel is with the random wind variation, while the left one without.

Two perturbation experiments are performed, one with random wind variation, the other without. Fig. 4-1 shows the time series of the North Atlantic overturning strength, which is defined as the maximum value of the overturning below 960m depth (to exclude the Ekman layer) in the North Atlantic. The freshwater flux in the northern hemisphere (Fw-N) is perturbed to increase by 0.1% per year. The random

wind variation greatly accelerates the collapse of the overturning (The reason for the collapse will be explained in Section 4.4). Fig.4-2 displays the vertical cross sections of salinity at 62° N. The time snapshots of the two runs indicate that without the wind variations the deep convection site can self-sustain even when the zonal freshwater flux is increased by 50% (upper panel of Fig. 4-2), whereas the convection is shut off much more rapidly in the presence of the wind variations (lower panel of Fig. 4-2).

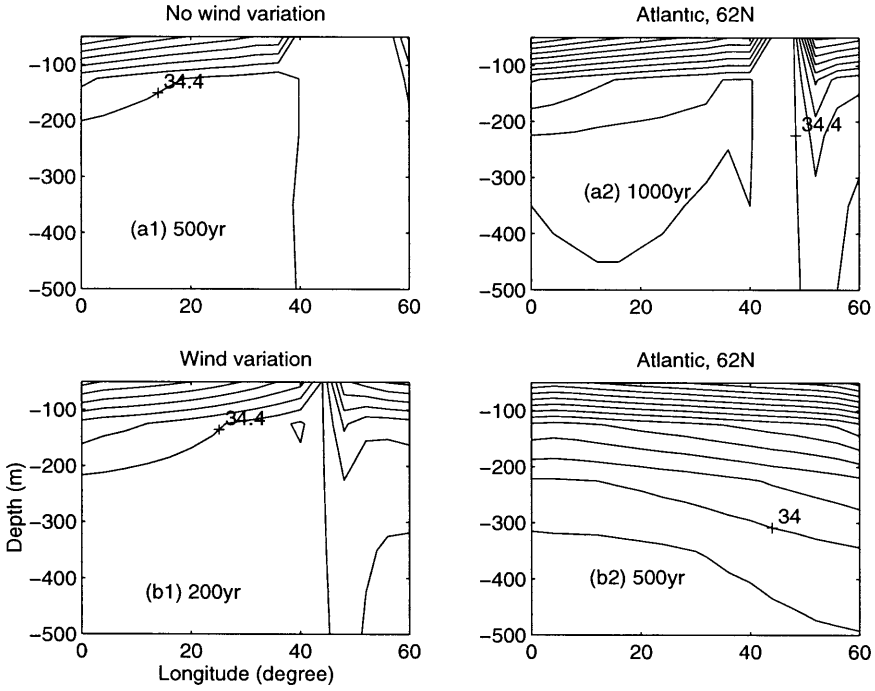

Figure 4-2: The time snapshots of the vertical sections of salinity on 62° N in the Fw-N increasing perturbations experiments. Upper panel is snapshots for the run without the wind variations, at 500 years (a1), and at 1000 years (a2). Lower panel is snapshots for the run with the wind variations, at 200 years (b1), and at 500 years (b2).

The self-sustained convection is associated with a positive feedback (e.g, Lenderink and Haarsma, 1994). Once the convection is triggered, it creates favorable conditions for further convection there. Convection mixes down cold and fresh water from the surface, and brings up warm and salty water from the deep ocean. In the coupled

model, SST relaxation to prescribed T^* leads to a rapid loss of the additional heat in the surface layer which thus becomes denser, meanwhile the surface salinity remains higher than before the onset of convection. As Fig.4-2 shows, this positive feedback is so powerful that the convection does not shut off until the freshening is virtually doubled at the convection site (around year 1000).

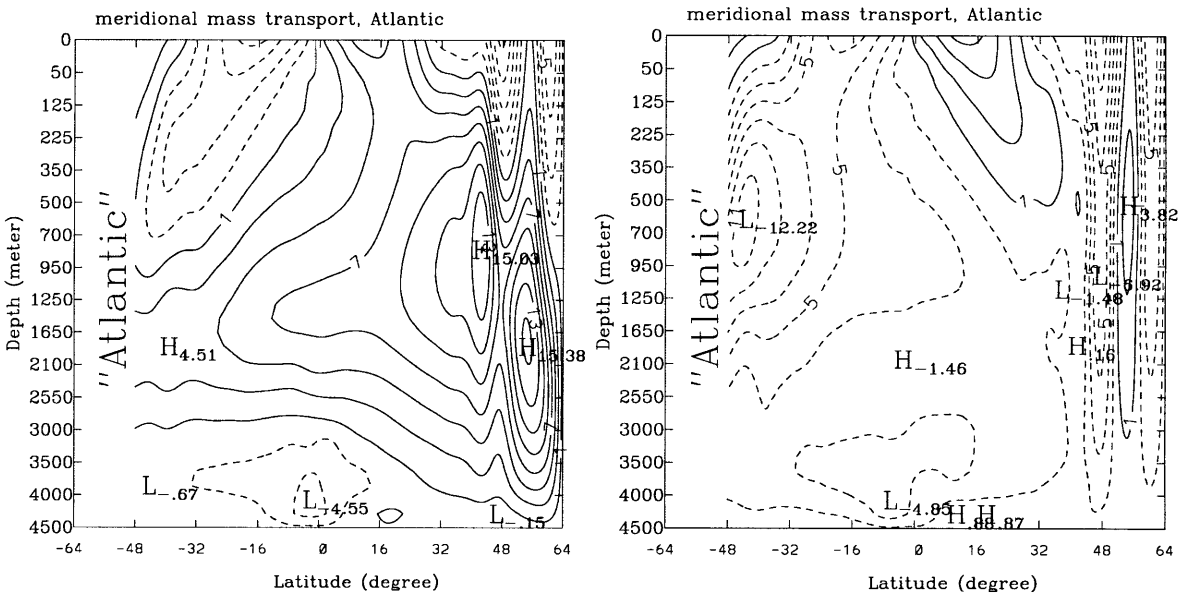

Figure 4-3: The snapshots of the North Atlantic overturning (unit of Sv) at year 200(left), and year 400(right), while the Fw-N increases 0.1% per year.

This positive feedback is apparently weakened by the random zonal wind variations. The random wind variations generate perturbations in the Ekman currents, and the noises are propagated downward to the deep layers. As Fig. 4-3 illustrates, the random wind variations cause oscillation in the overturning strength, and even when no deep water is formed in the North Atlantic (e.g, at year 400), there are still oscillations in the deep North Atlantic. That is why the North Atlantic overturning strength in the time series with the wind variations (Fig. 4-1) does not settle down to zero after the state is switched to the southern sinking. On a whole, the random

wind variation technique accelerates the changes in the convection sites, and therefore speeds up the model response to the external perturbation. [1]

To assess the possible effect of the random wind variation technique on the character of the model, we compare the perturbation runs with the wind variations to those without the wind variations (Fig.4-4). Note that the time scales of the two panels are not the same. Although the transitions are speeded up by the technique, the character of the model is not fundamentally altered by the random wind variations.

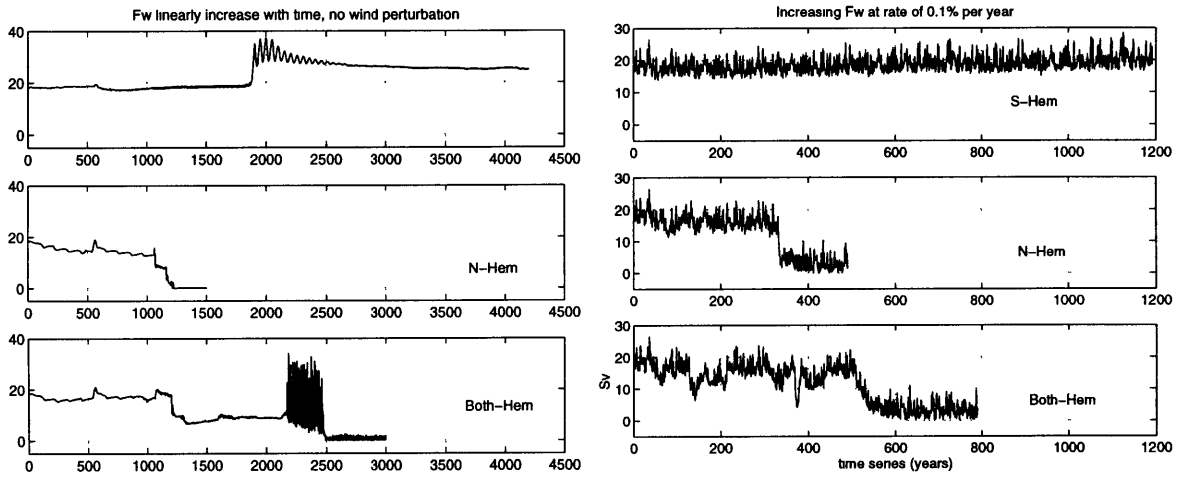

Figure 4-4: The time series of the North Atlantic overturning strength (unit of Sv), as the Fw-S (top panel), Fw-N (middle panel) and Fw-NS (bottom panel) increase 0.1% per year. The left panel is without wind variations, and the right panel with wind variations.

Although the fundamental character of the overturning is not changed by the random wind variations, it is worth finding out whether the overturning is sensitive to choices of random seeds in the wind variation calculations. Since different random variations represent transient weather-type perturbations to the overturning,

[1] Incidentally, the locking of the convection sites has also been a problem for modeling the ocean carbon cycle, because these convection areas have far too high biological productivity due to the large nutrients supply (Sarmiento, personal communication). The random wind variation technique developed in this study may have its application in the biological model too.

the question is in fact pertinent to the predictability of the overturning. Three runs with different random seeds are performed, as the Fw-N increases 0.1% per year. To objectively compare the collapse times of the North Atlantic overturning, we apply the 10-year averaged, zero-phase forward and reverse filter to the time series of the North Atlantic overturning strength. The criterion for the collapse time is defined as the time when the North Atlantic overturning strength falls below 6 Sv. As Fig. 4-5 shows, the collapse times of the three runs are year 270, year 340, and year 440 respectively. The sensitivity of the overturning to the random seeds suggests that the predictability of the overturning is surprisingly limited, and the weather-type, transient random noises have the capability of influencing the overturning temporal evolution paths in phase space. To exclude the effect of the random seeds, all the experiments in the following use the *identical random seed* to calculate the wind variation.

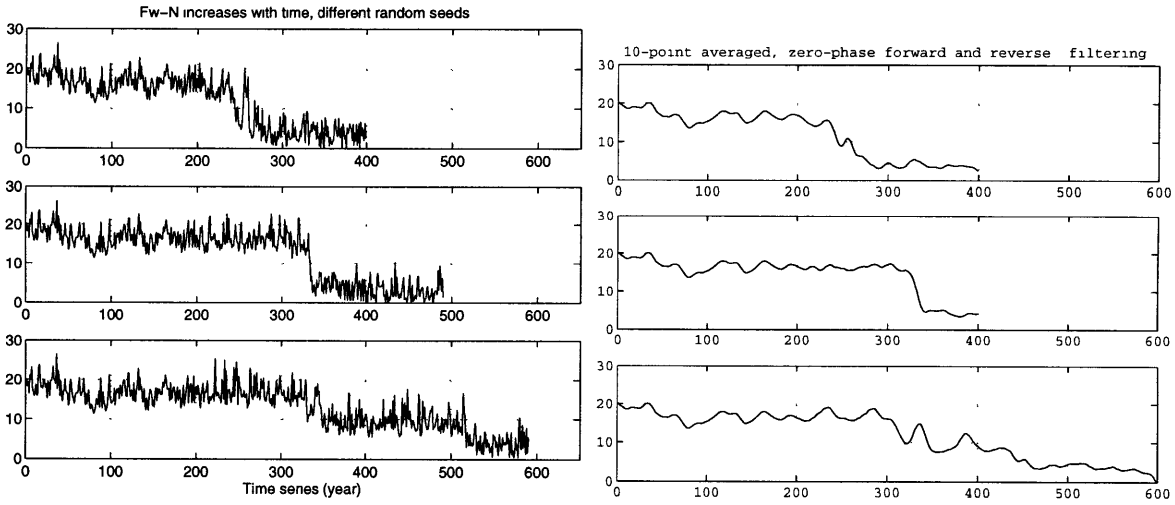

Figure 4-5: The time series of the maximum North Atlantic overturning (unit of Sv), as the wind variations are calculated with three random seeds. The Fw-N increases 0.1% per year. The left panel is the original time series, and the right one is the filtered time series. The filter is 10-year averaged, zero-phase forward and reverse digital filtering.

4.4 Internal perturbation experiments

First, we report some results from internal perturbation experiments. An initial salinity anomaly is applied to the Atlantic surface between 60° N and 64° N of the steady state (1.5Fw) in the coupled model. The salinity perturbation mimics meltwater input in the North Atlantic during deglaciation. The purpose of the salinity perturbation is to identify the relative stability of the equilibria in phase space.

Three different salinity anomalies (0.01ppt, 1ppt, and 10ppt) are applied to the initial field of the steady state (1.5Fw). Fig. 4-6 shows the time evolutions of the North Atlantic maximum overturning strength under the three salinity perturbations. We found two intermediate equilibria that are qualitatively similar to the control steady state, but have different overturning strengths (11 Sv and 15 Sv respectively). Such intermediate equilibrium states were also found in Hughes and Weaver (1994). The corresponding perturbation experiments with random wind variation are also shown in Fig. 4-6, where the technique does not alter the pattern qualitatively. The existence of multiple intermediate states of the conveyor belt circulation is attributed to the existence of multiple steady convection patterns under a given surface forcing but different initial states (Rahmstorf, 1995).

It is worth mentioning that such multiple convection patterns so far have not been observed in fully coupled GCMs (e.g, Manabe and Stouffer, 1995). We speculate that the convection sites in the GCMs may be locked to particular locations when realistic topography and stochastic atmospheric forcings are present. With our idealized model configuration, there is no topography or coastline to constraint the convection sites, and it is easy for the convection to flip-flop. Thus it becomes difficult to track the stability characteristics in phase space by using internal perturbations.

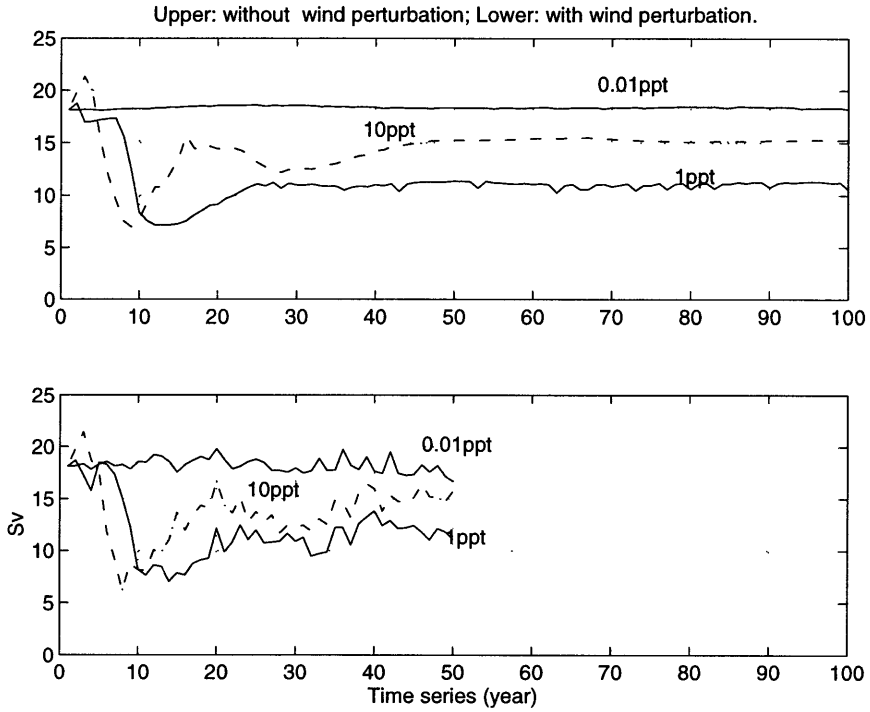

Figure 4-6: Temporal variations of the North Atlantic overturning obtained from three salinity perturbation runs.

4.5 External perturbation experiments

We first investigate the model transient responses to changes in hydrological cycles. The random wind variations are applied in the following perturbation experiments. The perturbation is applied separately in each hemisphere, in order to identify the possible asymmetric role of the hydrological cycle in the two hemispheres. Then, in a similar way, the hydrological cycle is decreased. Implications for climate changes are discussed at the end.

4.5.1 Increasing hydrological cycles

The freshwater flux of each hemisphere is increased linearly with time, first separately and then jointly. The strength of the North Atlantic overturning is defined as the

maximum value of the zonal mean mass transport streamfunction below 950m depth in the North Atlantic. The temporal variations of the North Atlantic overturning strength are described in order of the experiments when the hydrological cycles of the southern hemisphere, northern hemisphere, and both hemispheres increase.

Southern Hemisphere

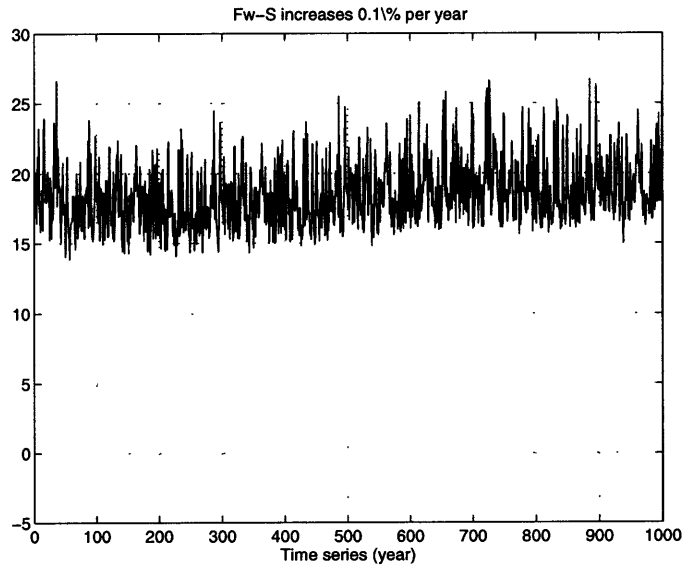

Figure 4-7: The time series of the North Atlantic overturning strength(unit of Sv), as the Fw-S increases 0.1% per year.

Fw in the southern hemisphere (Fw-S) is increasing linearly with time at 0.1% per year. In response to the perturbation, the North Atlantic overturning increases gradually with time, at quite a small rate (Fig. 4-7). It indicates a significant response delay of the North Atlantic overturning to changes in the southern hemisphere, consistent with the advection time scale from the South Ocean to the North Atlantic sinking region being more than several hundreds years. The state at the end of the perturbation (year 1,000) has not reached equilibrium. To demonstrate this, the forcing after 1000 year is held fixed, i.e, Fw-S at 3Fw, and Fw-N at 1.5Fw. Another

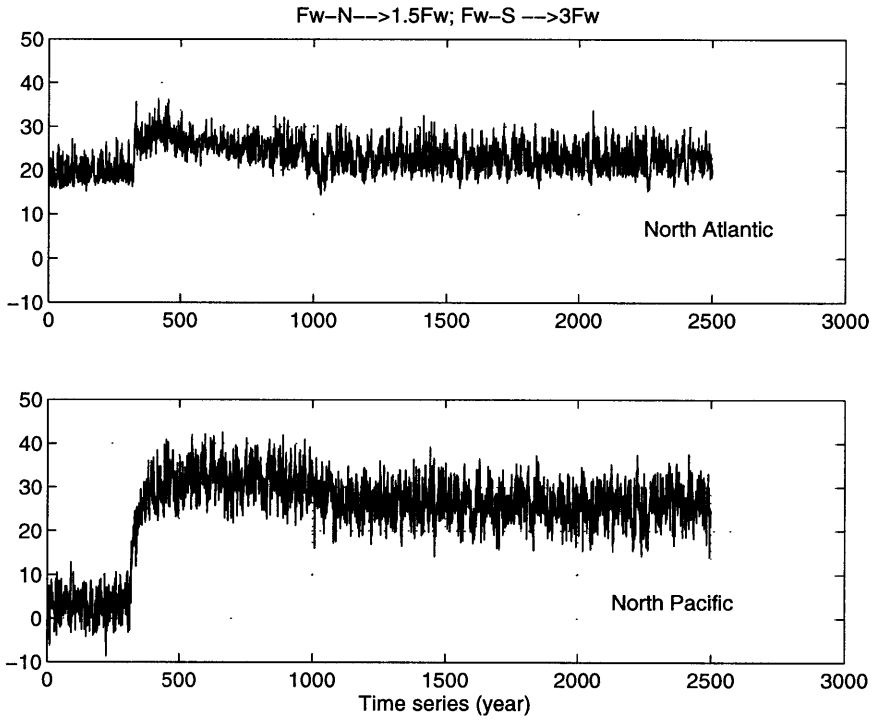

Figure 4-8: The time series of the overturning strength (unit of Sv) in the North Atlantic (upper panel), and in the North Pacific (lower panel), under the fixed forcing of Fw-S at 3Fw, and Fw-N at 1.5Fw.

2,500 years integration is carried out, until the equilibrium state is reached. The final steady state has northern sinking in both basins, rather than the conveyor belt equilibrium state. Fig. 4-8 displays the time series of the overturnings in the North Atlantic and North Pacific under the fixed forcing. Within 400 year of integration, the conveyor belt state is switched to the northern sinking in the both basins. The steady sinking strengths of the two basins are close to each other, and are about 24 Sv in each basin.

Northern Hemisphere

As the freshwater flux in the northern hemisphere (Fw-N) increases linearly at 0.1% per year, the GCM shows the overturning remains essentially unchanged until it

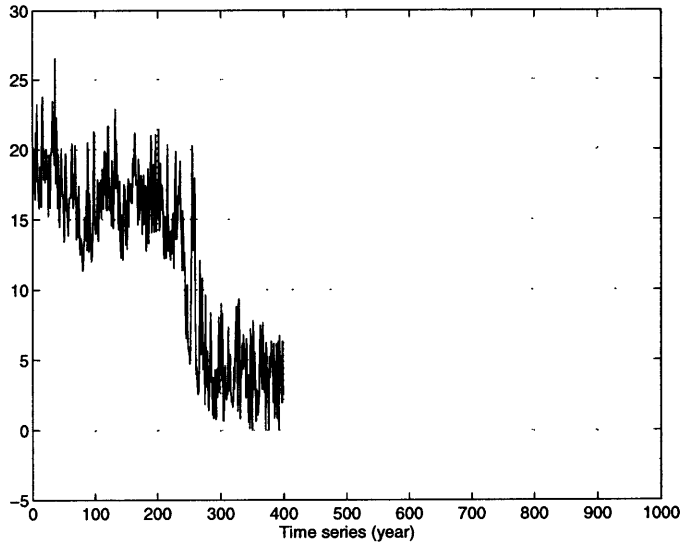

Figure 4-9: The time series of the North Atlantic overturning strength (unit of Sv), as Fw-N increases 0.1% per year.

suddenly collapses to sinking in the Southern Ocean (Fig. 4-9). The collapse time is year 270, when Fw-N has increased about 27%.

Two possible mechanisms can be cited to explain the collapse of the overturning. The first is the fine-scale convection mechanism. The convection can be wiped out by excessive fresh water capping over the convection sites. This collapsing mechanism is used to explain the weakening of the thermohaline circulation caused by atmospheric CO_2 increase (Manabe and Stouffer, 1994). As CO_2 increases, the atmospheric moisture transport becomes stronger due to warming, and the enhanced freshening shuts off the deep convection, resulting in the weakening of the thermohaline circulation .

The second possible mechanism, recognized by SMS96, is related to the large-scale processes. Their analysis indicated that the stable equilibrium state will move towards an unstable regime as the ratio of Fw between the two hemispheres (Fw_N/Fw_S) increases beyond a critical value. Here, the ratio is indeed increased, as Fw-N increases with time. To examine whether there is indeed a transition from the stable regime

to the unstable one, we perturb the freshwater flux of the collapsed state (around year 370) to re-establish the conveyor belt state. The new conveyor belt state reaches about 19 Sv of NADW formation under the fixed Fw-N of 2Fw, and Fw-S of 1.5FW. Furthermore, the state is stable (Fig. 4-10).

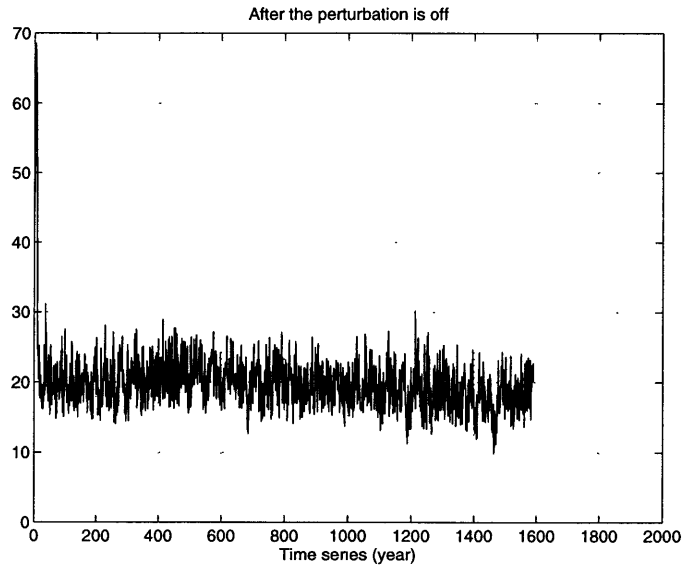

Figure 4-10: The time series of the maximum overturning strength (unit of Sv) in the North Atlantic, under the fixed forcing of Fw-S at 1.5Fw and Fw-N at 2Fw.

The fact that the re-established conveyor belt state is stable indicates that the collapse of the overturning is not a transition towards an unstable regime, rather the collapse depends on the perturbation procedure. This is consistent with the finding in Section 4.3 where the overturning is sensitive to the random seeds choice in the wind variations.

Both hemispheres

In the next experiment, Fw increases in both hemispheres with time. As Fig.4-11 illustrates, the collapse time of the Fw-NS run is year 500, delayed by about 230 years, compared to the Fw-N run with the same random seed. Using a different

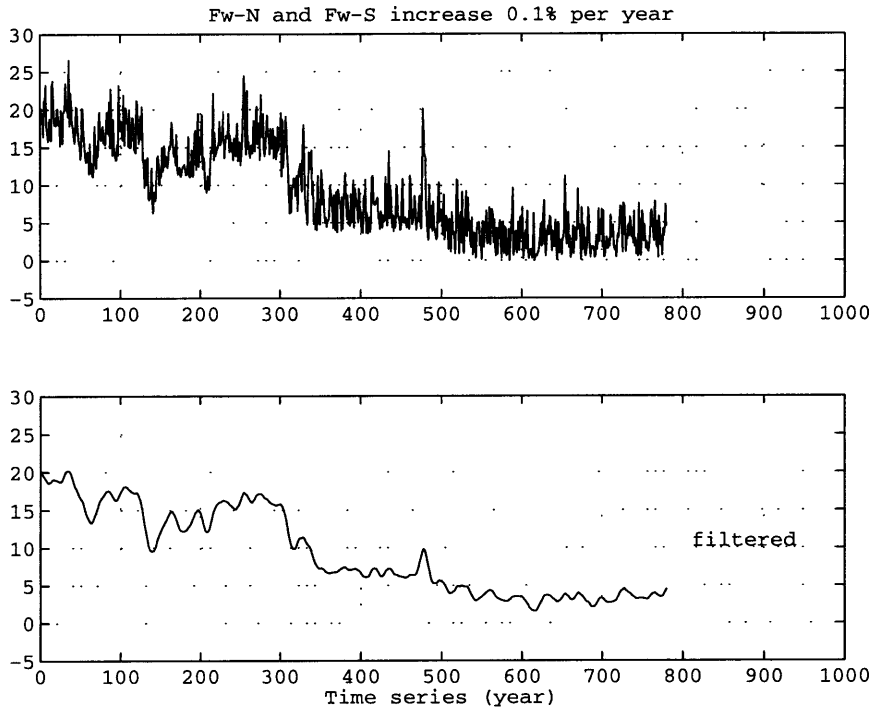

Figure 4-11: The time series of the North Atlantic overturning strength (unit of Sv), as Fw-N and Fw-S increase 0.1% per year. The upper panel is without the filter, and the lower one with the filter.

random seed, the two runs are repeated, and the collapse time in the Fw-NS run is again about 200 years later than that in the Fw-N run (Fig. 4-12). The collapse time differences between the two runs illustrate that the Fw ratio influences the thermohaline circulation stability. This demonstrates the importance of the large-scale processes. To predict the thermohaline circulation stability, the results here indicate that we need to improve simulations of the surface forcing not only in the northern hemisphere, but also in the southern hemisphere.

4.5.2 Decreasing hydrological cycles

The natural step to test further the above conclusion is to reverse the perturbation sign. We decrease Fw at 0.1% per year for each hemisphere (Fig.4-13). The North

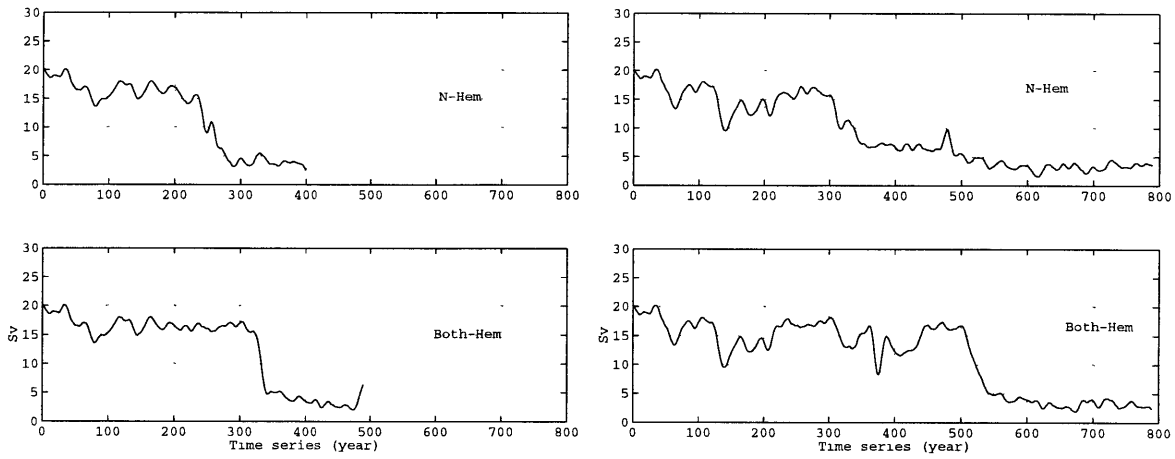

Figure 4-12: The time series of the North Atlantic overturning strength (unit of Sv). The difference from the left panel to the right panel is the random seeds of the wind variations. The difference from the upper panel to the lower panel is the perturbation method, Fw-N increasing in the upper panel, while both Fw-N and Fw-S increasing in the lower panel.

Atlantic overturning decreases as Fw-S decreases, which is consistent with the notion that the thermohaline circulation is controlled by the Fw-S.

For the case of Fw-N decreasing, the overturning rapidly increases. At the end of the perturbation (year 1000), the state has not equilibrated. A continued integration with fixed Fw (Fw-S=1.5Fw; Fw-N=0) shows that the additional convection sites triggered by decreasing of freshening gradually die out. The overturning reaches a steady state after 2,500 years, and settles down to 21 Sv, from the starting value of 30 Sv (fig.4-14). It is also shown that the deep water is formed in the North Pacific, as well as in the North Atlantic.

Another interesting case is both Fw-N and Fw-S decreasing to zero, i.e, there is no freshwater forcing in the model. Fig. 4-15 shows the time evolution of the North Atlantic overturning, as the global freshwater flux reduces to zero, and remains zero thereafter. The equilibrium strength of the North Atlantic overturning settles down to about 15 Sv. Note, however, that the circulation has changed to a northern

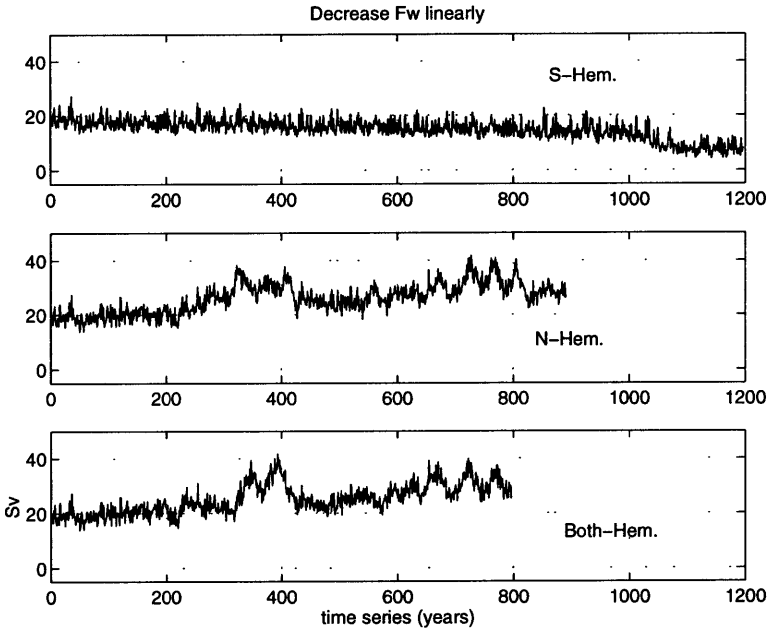

Figure 4-13: The time series of the North Atlantic maximum overturning (unit of Sv), as the Fw-S (top panel), Fw-N (middle panel), and Fw-NS (bottom panel) decrease 0.1% per year.

sinking equilibrium state. On the other hand, the overturning strength in the box model would reduce to zero, if the freshwater flux decreases to zero, as long as the temperature difference between the two high latitude boxes is zero. Thus, this result illustrates the break-down of the applicability of the box model, noted in Section 3.4.

In general, the results from all the perturbation experiments, with either increasing or decreasing freshwater fluxes in each hemisphere, are apparently not in conflict with the major conclusions from the pole-to-pole three-box model (SMS96). Some results agree reasonably well, for example, the overturning strength increases as the freshwater flux strength increases. In addition, the Fw ratio is important in both the box model and the GCM. However, the difference between the GCM and the box model is also provocative. It can be attributed primarily to the fact that there is no convection adjustment process in the box model. This suggests that the dynamics of

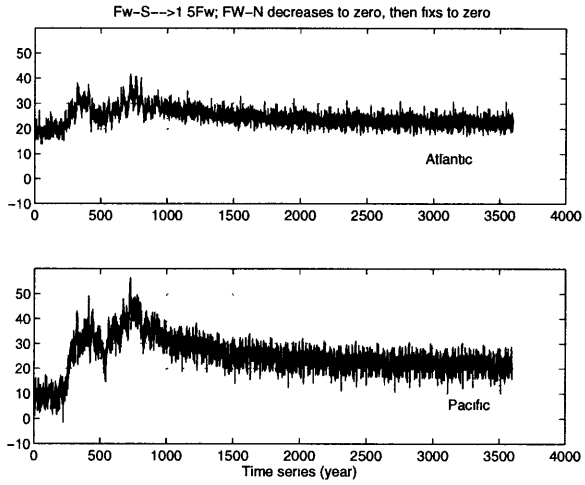

Figure 4-14: The time series of the overturning strength (unit of Sv) in the North Atlantic (upper panel), and in the North Pacific (lower panel), as the Fw-N decreases to zero (in year 1000), and then remains zero, while Fw-S is 1.5Fw.

the thermohaline circulation in the GCM can be essentially explained by the interplays between the fine-scale convection adjustment processes and the large-scale horizontal pole-to-pole processes.

4.6 Applications to the global change scenario

In the light of the above results, the roles of the hydrological cycles in the two hemispheres are highly asymmetric. While the hydrological cycle in the southern hemisphere controls the steady states of the thermohaline circulation , the northern hemisphere hydrological cycle has a direct impact on the transient behavior of the thermohaline circulation . Furthermore, the stability of the overturning is governed by the interplay between the convection processes and the large-scale processes. The fine-scale convection adjustment represents a major element in the deep water formation process, which in turn, is an integral part of the large-scale thermohaline circulation process. Since the large-scale and fine-scale processes are operating on

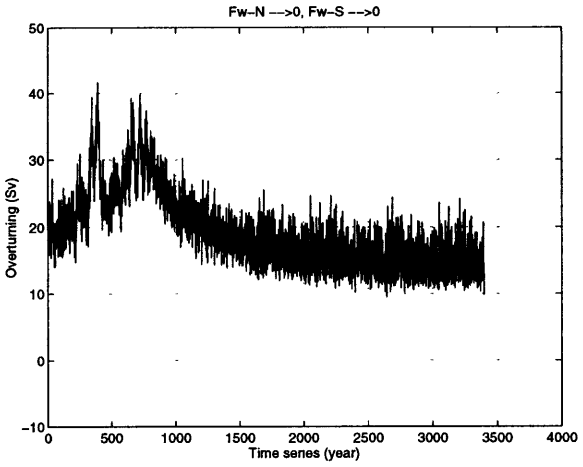

Figure 4-15: The time series of the overturning strength (unit of Sv) in the North Atlantic, as the global freshwater flux reduces to zero, and remains zero.

different time scales, it is still appropriate to consider them separately in the context of time scales. Over a few years, the convection variations can dominate the transient behavior of the deep water formation, without affecting the global climate. If the anomalies persist for sufficiently long time, the large-scale dynamics are capable of making the transition permanent.

One example of such interplay is the thermohaline circulation responses to CO_2 increasing in the fully coupled GCMs (MS94). It was found that the North Atlantic overturning became weaker or almost disappeared during the first 150 years of the CO_2 increasing experiments (Fig.4-16). This was mainly due to the freshwater capping of the high latitude convection sites, where the excess of precipitation over evaporation increased markedly due to the enhanced poleward moisture transport in the warmer model troposphere. In our idealized model, a similar perturbation has been simulated by increasing Fw-N slowly with time.

However, MS94 further found that the North Atlantic overturning almost recovered its original intensity by the 500th year for CO_2-doubling integration. According

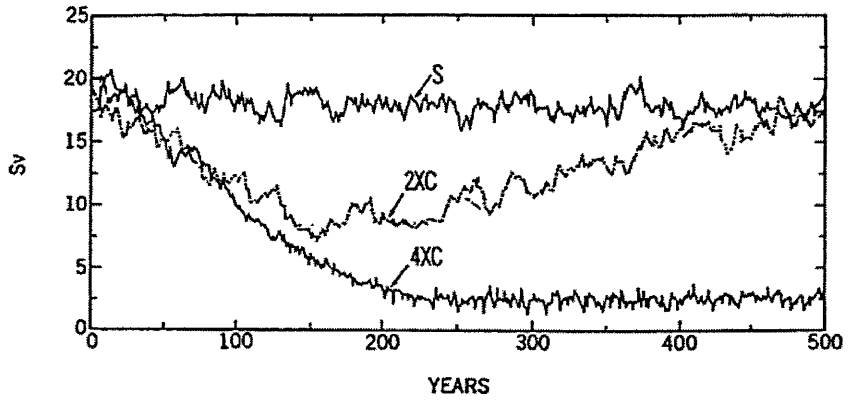

Figure 4-16: Temporal variation of the intensity of the thermohaline circulation in the North Atlantic from the 4XC, 2XC, and S integrations. Here the intensity is defined as the maximum value of the streamfunction representing the meridional circulation in the North Atlantic Ocean. Units are in Sverdrups. (from Manabe and Stouffer, 1994)

to MS94, the recovery of the overturning was associated with the development and intensification of a subsurface positive temperature anomaly in low and middle latitude of the North Atlantic, which resulted in increased density contrast between the high and low latitudes in the North Atlantic.

Here, based on our perturbation results, we provide a different possible reason for the recovery in MS94. A close look up of MS94's maps of temperature change in the CO_2 increasing experiments indicates highly asymmetric responses in the two hemispheres, with dramatic warming and increased salinity (not shown here) in the northern hemisphere (Fig.4-17), but relatively minor changes in the high latitudes of the southern hemisphere. We thus suggest that the pole-to-pole forcing gradient of the overturning experienced minor changes in the doubling of CO_2 experiment; therefore, the overturning recovered to its original strength after the initial weakening. The initial weakening of the overturning reveals the role of the fast convection processes. While the recovery of the overturning indicates the unchanged large-scale dynamical

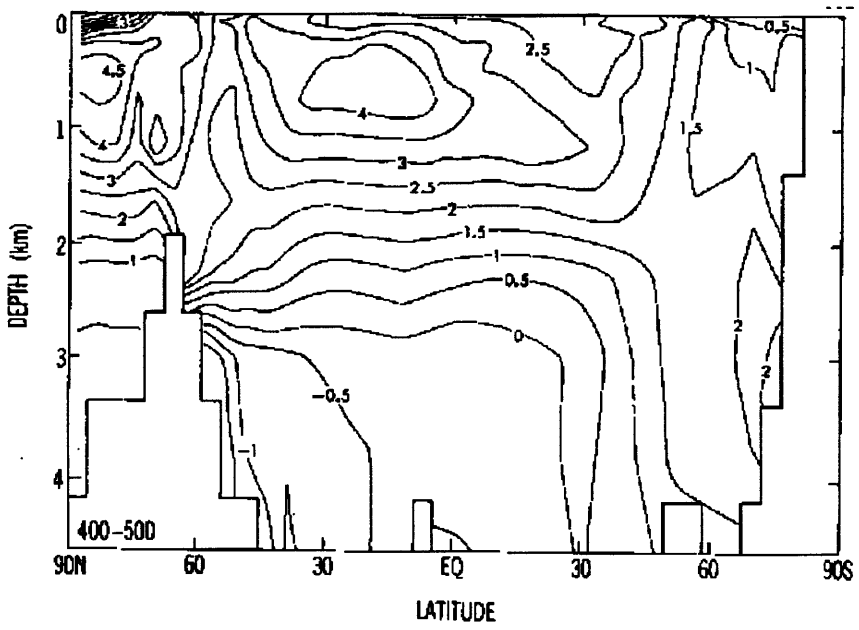

Figure 4-17: The Atlantic latitude-depth distribution of zonal mean difference in temperature (° C) between the 2XC and standard run for the 400th-500th-year period (taken from MS94).

constrain in the model. On the other hand, the permanent collapse of the overturning in the quadrupling of CO_2 experiment indicates that the large-scale dynamics has been fundamentally altered.

Another possible application of our experiments is related to the predictability of the thermohaline circulation . The sensitivity experiments of different random wind variations suggest that the overturning is sensitive to the details of the perturbation procedure. This implies that the responses of the thermohaline circulation to CO_2 increasing will depend not only on how much CO_2 is increased, but also on how fast the CO_2 increases with time. Furthermore, it may be well possible that the transient variations of the atmospheric state can influence the thermohaline circulation responses to the CO_2 changes. It thus presents a great challenge to the current climate model's ability to predict the global change.

Chapter 5

Feedbacks affecting the thermohaline circulation

5.1 Introduction

In the previous two chapters, the annual mean atmospheric meridional transports of heat and freshwater are prescribed from the observations, and thus are not allowed to interact with the ocean model. The longwave radiative term is the only interactive coupling between the atmospheric model and the ocean GCM. This version of the coupled model is defined as the 'non-interactive' model, and corresponds to the preliminary stage of ocean-atmosphere coupling.

Here, we are going to construct a series of coupled models with different couplings to the atmospheric transports, of which the highest stage is the coupled model with fully interactive atmospheric transports. The purpose is to understand feedbacks associated with the meridional transports in the atmosphere and the thermohaline circulation . The proceeding here closely follows the conceptual framework of NSM94, Marotzke and Stone (1995), and Marotzke (1996). We will emphasize the feedback in-

tercomparisons between the GCM version coupled model and the coupled box model, in particular, since some new feedbacks arise from the more complex coupled model.

Since flux adjustments are applied in our fully interactive model, another goal in this chapter is to investigate how different flux adjustment methods affect the strengths of the feedbacks, and therefore the climate sensitivity and stability of the thermohaline circulation . The flux adjustment scheme used in this study is discussed in Section 5.2. Then external perturbations are applied to the different versions of the coupled models, and the feedbacks are examined in a systematic way in Section 5.3. Two different flux adjustment methods are compared and assessed in Section 5.4.

5.2 Why flux adjustment is needed

In the fully interactive model, the meridional transports of heat and freshwater in the atmosphere are no longer held fixed, but are determined interactively by the parameterizations described in Section 2.4. We use the conveyor belt state of the 'non-interactive' coupled model (1.5Fw) as the initial state for the fully interactive model. Upon coupling, the fully interactive model immediately drifts away, and settles down to a new state without deep water formations in either basin (Fig.5-1).

The drift of the fully interactive model is not surprising, when we compare the atmospheric northward heat transport and the zonal mean surface heat flux from the non-interactive model, with those from the fully interactive model (fig.5-2). The surface forcings from the two models are apparently incompatible, and the discrepancy mainly results from the difference between the modeled SST and the observed SST (Levitus, 1982). As Fig. 5-3 shows, the meridional gradient of the zonal mean modeled SST is stronger than that of the observed SST. Therefore, the modeled at-

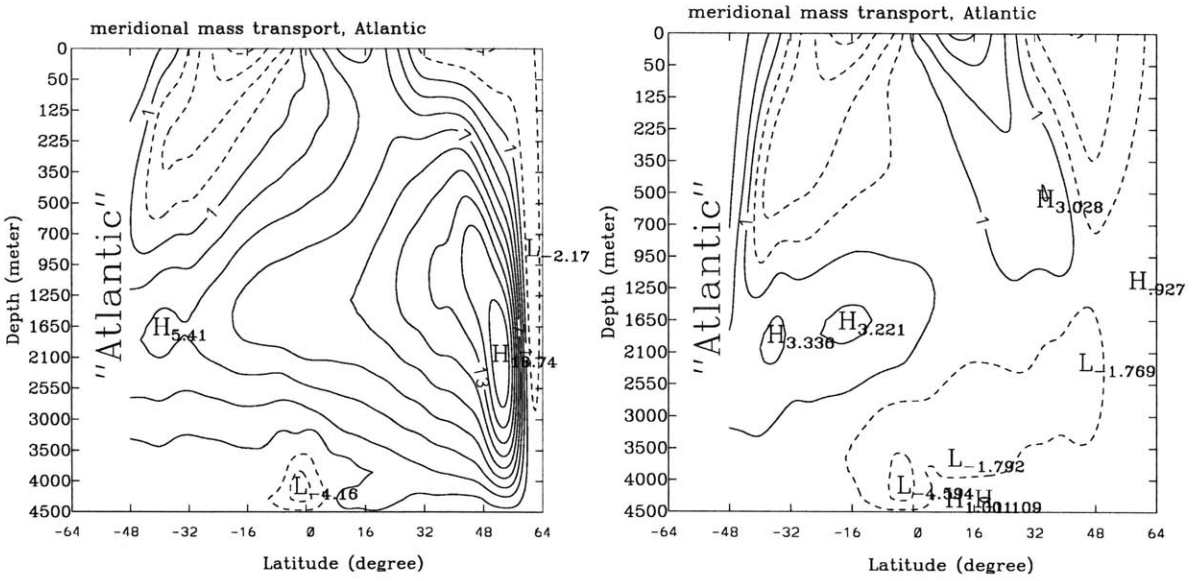

Figure 5-1: The Atlantic meridional mass streamfunction (Sv), at the initial state (left), and at the drifted state (right) of the fully interactive model.

mospheric eddy transports, which are proportional to the 2.5th power of the modeled temperature gradient (Eq. 2.10), are too strong, compared to the observed values (fig. 5-2). As a result of that, the fully interactive model drifts away under the excessive oceanic heat/freshwater fluxes.

The strong meridional gradient of the modeled SST arises because of the weak oceanic heat transport in the model, which is about half of the observed value, as shown in Section 3.3. When the ocean GCM is forced with the observed atmospheric heat transport, if the longwave radiation is also fixed from observations, the GCM would have transported the observed amount of heat in the ocean. However, since the longwave radiation is not fixed, but parameterized as a linear function of the modeled SST, the model can compensate its low oceanic heat transport by obtaining a much stronger meridional gradient of SST, and hence a stronger differential longwave radiative forcing.

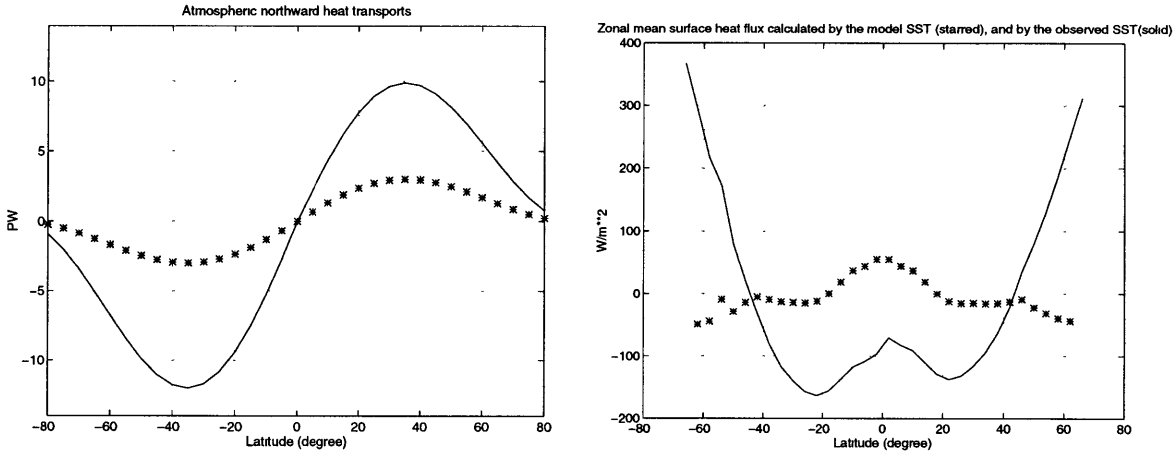

Figure 5-2: The atmospheric northward heat transports (left, unit of PW) and the zonal mean oceanic surface heat fluxes (right, unit of W/m^2), at the initial state (starred), and at the drifted state (solid) of the fully interactive model.

Fundamentally, the drift of the fully interactive model results from the incompatibility between the atmospheric model and the ocean model in poleward heat transports. The weak oceanic heat transport in the model can be attributed to several defects of the GCM, among them are the coarse horizontal resolution, the low North Atlantic Deep Water formation, the diffusive mixing scheme in the western boundary, to name a few. Improvements (e.g, the Gent and McWilliams (1990) scheme) were not available for the GCM (MOM1 version) until half way into this study. Also it still underestimates the oceanic heat transport (Boning et al. 1995). To maintain the consistency of the work, we decided not to modify the model in the middle of the study, but to continue to apply flux adjustment to prevent the drift of the fully interactive model.

The flux adjustment developed here is based on the observation that the atmosphere and the ocean actually are comparable in their heat transport efficiencies (Trenberth and Solomon, 1994). To preserve this character, we adjust the atmospheric heat transport efficiency to match the oceanic one, so that the two models

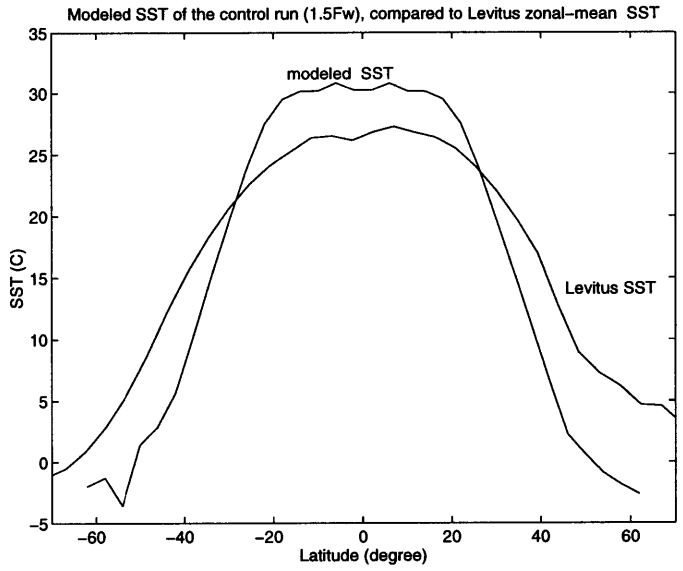

Figure 5-3: The zonal mean modeled SST and the observed SST (unit of C), as a function of latitudes.

can have comparable heat transport efficiencies. This approach is different from the conventional flux adjustment (e.g, Sausen et al., 1988; Manabe and Stouffer, 1988; Murphy and Mitchell, 1995), in which the fluxes are adjusted by constants. We believe that the efficiency adjustment serves better for the purpose of this work, because to preserve the relative efficiency of the two models may help recover the original characteristics of the interaction between the atmosphere and the thermohaline circulation . A further assessment for the two flux adjustment schemes will be discussed in a later section of this chapter.

To adjust the heat transport efficiency of the atmospheric model, we tune the coefficients in the parameterization (Eq. 2.10), to give the same atmospheric heat and freshwater transports as the observed values,

$$C_L'(\frac{\partial q_s}{\partial T})(\frac{dT_{model}}{dy})^{2.5} = C_L(\frac{\partial q_s}{\partial T})(\frac{dT_{observ}}{dy})^{2.5}, \tag{5.1}$$

$$[C'_S + C'_L(\frac{\partial q_s}{\partial T})](\frac{dT_{model}}{dy})^{2.5} = [C_S + C_L(\frac{\partial q_s}{\partial T})](\frac{dT_{observ}}{dy})^{2.5} \quad (5.2)$$

The two adjusted coefficients (C'_L and C'_S) are about 30% of the original ones. After the adjustments, the surface forcings from the fully interactive model are the same as those from the non-interactive model, and therefore, the initial state of the model remains the same upon fully coupling. The same flux adjustment is applied in all the following feedback experiments.

5.3 Feedbacks in the coupled models

5.3.1 Experimental strategy

In the following, there are a total of nine different versions of the coupled models, which are listed in Table 5.1. Models H1-3 have the atmospheric heat transport interactive in the northern, southern and both hemispheres respectively. Models F1-3 are similar to the models H1-3, except that the atmospheric freshwater transport is interactive, instead of the heat transport. Both transports become interactive in the models HF1-3. A negative (positive) feedback is present when a perturbation weakens (enhances) itself through the changes it causes. To elucidate feedbacks in the coupled models, all the nine coupled models are subjected to the external perturbation of increasing the global hydrological cycle 0.1% per year. That is, the moisture transport coefficient increases 0.1% per year, but the latent heat transport as well as the total heat transport remains unchanged. As shown in Fig. 4-11, with the non-interactive model, the North Atlantic overturning collapses to the South Ocean sinking state after several hundred years of such external perturbation. There, we have defined the collapse time as the time when the maximum value of the North Atlantic meridional

Table 5.1: Definition of the coupled models. Hd and Fw indicate the atmospheric heat and freshwater transports respectively.

Model #	Hd interactive	Fw interactive	Hd and Fw interactive
N-Hem. interactive	H1	F1	HF1
S-Hem. interactive	H2	F2	HF2
Both Hem. interactive	H3	F3	HF3

mass streamfunction is less than 6 Sv below 960m deep, after a certain filter is applied. Here, the goal is to examine how feedbacks modify the collapse time of each model, and to assess relative importance of each feedback. The shorter the collapse time, the less stable is the model. Furthermore, identical random wind variations are used in all the experiments to exclude the possible effects of the random wind variations.

5.3.2 Thermohaline feedbacks

Following the notation in Marotzke (1996), we first review some feedbacks that are associated with only the oceanic processes.

Feedback #1: Oceanic Heat Transport

decreased overturning $\longrightarrow$ reduced advection of warm water to high latitudes $\longrightarrow$ increased surface density in high latitudes $\longrightarrow$ increased deep sinking $\longrightarrow$ increased overturning.

This is a negative feedback, and is present in all versions of the coupled models

(including the non-interactive model).

Feedback #2: Oceanic Salinity Transport

> decreased overturning $\longrightarrow$ reduced advection of salty water to high latitudes $\longrightarrow$ reduced surface density in high latitudes $\longrightarrow$ reduced deep sinking $\longrightarrow$ further decreased overturning.

This is a positive feedback, and is fundamental to the existence of the multiple equilibrium states under mixed boundary conditions (Walin, 1985; Marotzke, 1990). Notice that the surface heat flux is conceptually assumed fixed in feedback #1, whereas fixed surface freshwater flux is assumed in feedback #2. Both feedbacks are purely oceanic.

However, the focus of this work is on the coupled feedbacks that involve changes in the atmospheric meridional transports, and hence changes in the surface heat and freshwater fluxes. These coupled feedbacks have been studied using the box models (NSM94, Marotzke and Stone, 1995; Marotzke, 1996), as well as more complex models (e.g, Saravanan and McWilliams, 1995; Lohmann et al. 1996). This work has mainly two new features. First, our applied perturbation is of large-scale as well as long time scale, while the previous studies used only the local perturbation with a short time duration (Saravanan and McWilliams, 1995; Lohmann et al. 1996). We believe that the coupled feedbacks associated with the large-scale processes can only be elucidated under the appropriate perturbation method. The perturbation of local scale (e.g, a few certain gridpoints) with short time scale may not allow the coupled feedbacks to respond before it is smoothed out by the local advection process. Second, our model geometry is of two basins, whereas only single basin was used in the previous works (Lohmann et al. 1996).

In spite of these new features, our coupled model approach follows that of the box

model (NSM94), since we want to assess how robust the feedbacks in the simple box model are in the frame of a complex ocean GCM.

Feedback #3: Atmospheric Heat Transport

> decreased overturning $\longrightarrow$ increased SST gradient $\longrightarrow$ increased atmospheric heat transport $\longrightarrow$ smaller SST gradient $\longrightarrow$ decreased further overturning

As discussed in Marotzke (1996), this is a positive, coupled atmosphere-ocean feedback. It involves the fundamental negative feedback in the *atmosphere* between the meridional temperature gradient and eddy activity and hence heat transport in the atmosphere. The anomalous atmospheric heat transport tends to damp out the change of SST meridional gradient, which limits the power of the negative oceanic feedback #1; therefore, it acts as a positive feedback for the thermohaline circulation

.

To examine this feedback in the GCM, the perturbations are applied to two types of coupled models, those with feedback #3 (Models H1-3) and the other without (non-interactive model). The time series of these models are plotted in Figure 5-4, which shows that the collapse times of the models with feedback #3 are, on the average, about 200 years shorter than that of the model without the feedback. This demonstrates that the atmospheric heat transport feedback identified in the box model acts in a similar fashion in the GCM. In addition, we find that the feedback #3 loop is not complete, it works only in the northern hemisphere. In the southern hemisphere, a new feedback loop is identified, which differs from the feedback #3 loop in two places, and works as follows,

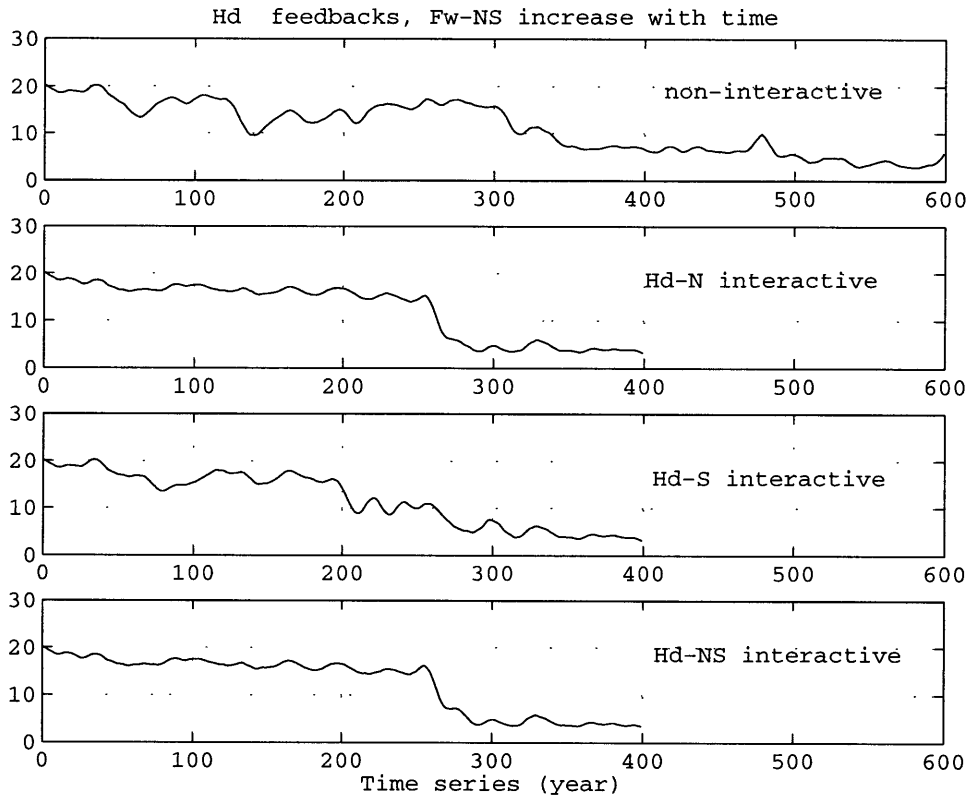

Figure 5-4: The filtered time series of the North Atlantic overturning strength, Top: non-interactive model; Upper-middle: Hd interactive in the northern hemisphere; Lower-middle: Hd interactive in the southern hemisphere; Bottom: Hd interactive in both hemispheres.

> decreased overturning $\longrightarrow$ reduced *equatorward* oceanic heat transport $\longrightarrow$ reduced SST meridional gradient $\longrightarrow$ reduced atmospheric heat transport $\longrightarrow$ increased SST meridional gradient $\longrightarrow$ increased surface density in high latitudes $\longrightarrow$ reduced *upwelling* in high latitudes $\longrightarrow$ further decreased overturning

The first difference between the two feedback loops is that the overturning upwells in the southern hemisphere. Second, the oceanic heat transport of the overturning is equatorward in the southern hemisphere. Due to these two signs changes, the atmospheric heat transport feedback still counteracts the negative oceanic temperature

Table 5.2: Collapse times (unit of year) in the models with/out the atmospheric heat transport, when the global freshwater fluxes increase 0.1% per year.

Collapse time	Hd interactive
Non-interactive	490
N-Hem. interactive	270
S-Hem. interactive	280
Both Hem. interactive	280

feedback in the southern hemisphere, therefore, it is positive. We call it feedback #3′. The existence of feedback #3′ is consistent with the pole-to-pole dynamical picture of the thermohaline circulation , as discussed in Chapter 4.

Table 5.2 summarizes the relative strength of the atmospheric heat transport feedback in each hemisphere. From the criteria of the collapse time, the feedback strength in each hemisphere is qualitatively similar. However, the temporal variations of the overturning are not the same in each model. For example, the model with feedback #3′ hovers near 10 Sv (the intermediate equilibrium) for about 80 years before collapsing, while other models (Models H1, and H3) maintain the original state of 20 Sv, then collapse within 20 years (Fig. 5-4).

It is worth mentioning that the model with two positive feedbacks combined does not become less stable than the model with one positive feedback. One possible explanation is associated with the low latitudes, which serves as a link between the

feedbacks in the two hemispheres. If this is the case, it is possible that the feedback in the southern hemisphere can set back the feedback strength in the northern hemisphere. For instance, as the overturning decreases, SST meridional gradient in the southern hemisphere reduces, while the gradient of SST in the northern hemisphere increases. Since mixing between the two hemispheres happens through the low latitudes, the opposite changes of the SST gradient counteract each other, therefore, the positive feedback in each hemisphere can be set back. Note that further diagnoses are needed to validate the above speculation.

As a whole, the feedback #3 found in the box model is also identifiable in the GCM. Additionally, we find a new positive feedback (feedback #3′) operating in the southern hemisphere, which is not addressed in the box model of one hemisphere.

Another interesting feedback studied in the box model involves the response of the atmospheric moisture transport to changes in the SST meridional gradient:

Feedback #4: Atmospheric Moisture Transport

> decreased overturning $\longrightarrow$ reduced northward oceanic heat transport $\longrightarrow$ increased SST meridional gradient $\longrightarrow$ increased atmospheric moisture transport $\longrightarrow$ reduced surface salinity in high latitudes $\longrightarrow$ reduced surface density in high latitudes $\longrightarrow$ further decreased overturning.

This is also a positive coupled atmosphere-ocean feedback, named EMT feedback in NSM94. With a similar argument, this feedback destabilizes the thermohaline circulation by enhancing the oceanic positive salinity feedback #2. Figure 5-5 displays the temporal variations of the North Atlantic overturning in the models with the atmospheric moisture transport feedback, and the one without. On average, the collapse time of those with the feedback is about 250 years shorter than that without

the feedback.

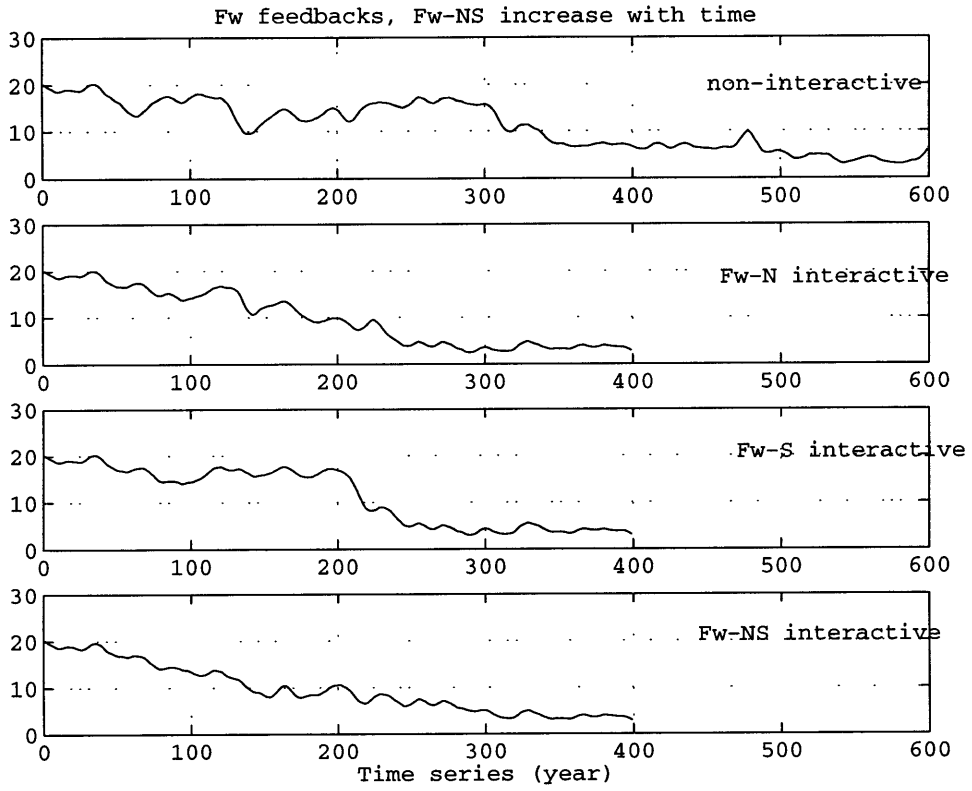

Figure 5-5: The filtered time series of the North Atlantic overturning strength, Top: non-interactive model; Upper-middle: Fw interactive in the northern hemisphere; Lower-middle: Fw interactive in the southern hemisphere; Bottom: Fw interactive in both hemispheres.

The equivalent feedback in the southern hemisphere is also found to be positive,

decreased overturning $\longrightarrow$ reduced equatorward oceanic heat transport $\longrightarrow$ reduced SST meridional gradient $\longrightarrow$ reduced atmospheric moisture transport $\longrightarrow$ increased surface salinity in high latitudes $\longrightarrow$ reduced upwelling in high latitudes $\longrightarrow$ further decreased overturning.

Here, the two sign changes are similar to that of feedback #3′. We call this new positive feedback of the atmospheric moisture transport in the southern hemisphere as feedback #4′.

Table 5.3: Collapse times (unit of year) in the models with/out the atmospheric moisture transport, when the global freshwater fluxes increase 0.1% per year

Collapse time	Fw interactive
Non-interactive	490
N-Hem. interactive	240
S-Hem. interactive	240
Both Hem. interactive	240

Table 5.3 gives the relative strengths of the atmospheric heat transport feedback in each hemisphere. From the criteria of the collapse time, the feedback strength in each hemisphere is qualitatively similar, but with different collapsing paths. Again, the agreement between the box model and the GCM concerning the atmospheric moisture transport feedback is reasonably good.

Since the latitudinal profile of the moisture transport is prescribed in this study, small scale changes on the moisture transport in high latitudes are not captured. Lohmann et al. (1996) found that, when local temperature effects are included, the moisture transport feedback is weaker than that in NSM94. However, studies with coupled atmospheric GCMs (e.g, Schiller et al, 1996) have indeed observed moisture transport changes due to large-scale changes in the temperature gradient, thus confirming the feedback #4 in the coupled system.

The combined atmospheric transports feedbacks are illustrated in Figure 5-6. One

interesting feature of this set of perturbation is the significantly different responses between the model with feedbacks in the northern hemisphere and that in the southern hemisphere. It cannot be explained by the results from the previous studies and the current work.

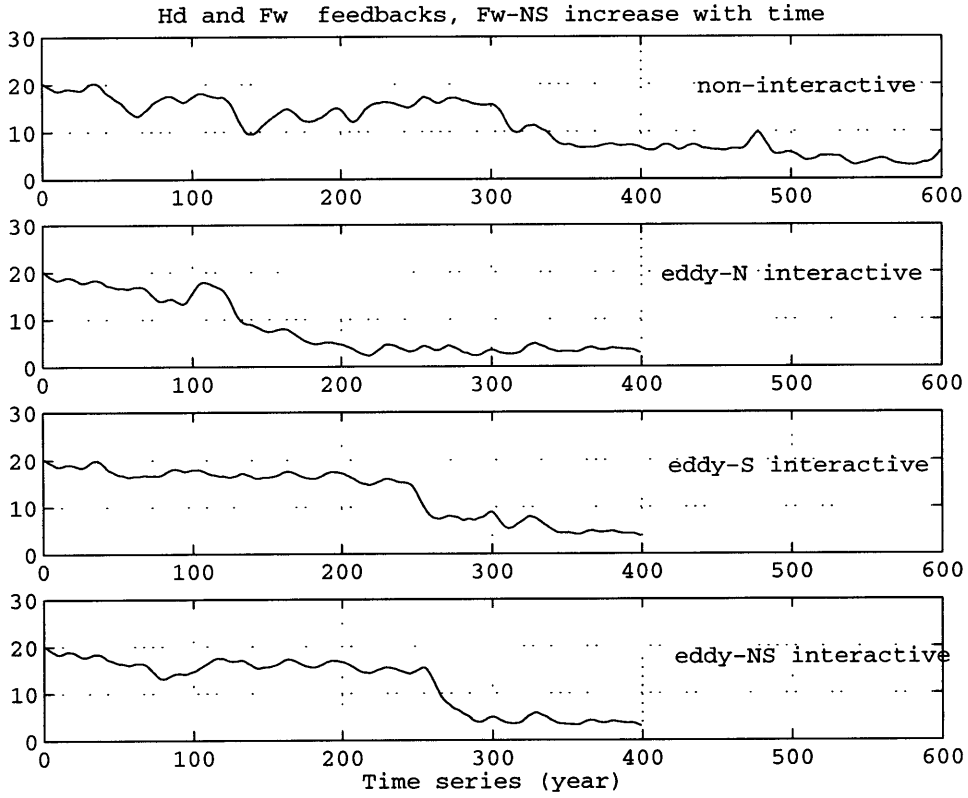

Figure 5-6: The filtered time series of the North Atlantic overturning strength, Top: non-interactive model; Upper-middle: Hd and Fw interactive in the northern hemisphere; Lower-middle: Hd and Fw interactive in the southern hemisphere; Bottom: Hd and Fw interactive in both hemispheres.

A summary of the coupled feedbacks is presented in Table 5.4. The coupled feedbacks in both hemispheres are found to destablize the thermohaline circulation . Notice that there is one exception, the Model HF2 (with feedback #3′ and #4′) is actually more stable than the Model F2 (with only feedback #4′). The stabilizing effect is associated with the atmospheric heat transport feedback. If it is strong, the

Table 5.4: The collapse times in the coupled models. Hd and Fw indicate the atmospheric heat and freshwater transports respectively.

Collapse time	Hd interactive	Fw interactive	Hd and Fw interactive
Non-interactive	490	490	490
N-Hem. interactive	270	240	170
S-Hem. interactive	280	240	310
Both Hem. interactive	280	240	280

temperature gradient is tightly confined, so is the atmospheric moisture transport, and the feedback #4′ is less powerful, as previously noted by NSM94, Marotzke and Stone (1995), and Marotzke (1996). Recently, Krasovskij and Stone (1996, submitted) have found an analytical solution including the nonlinearity in the atmospheric transports feedbacks with a box model.

5.4 Flux adjustment revisited

The insight gained about the feedbacks between the oceanic and atmospheric transports can directly guide us in assessing the validity of flux adjustments. Flux adjustments are performed to correct for incompatible transports in model ocean and model atmosphere. If a transport is in error, so is the associated feedback. For example, too strong an atmospheric moisture transport leads to artificial destabilization of the

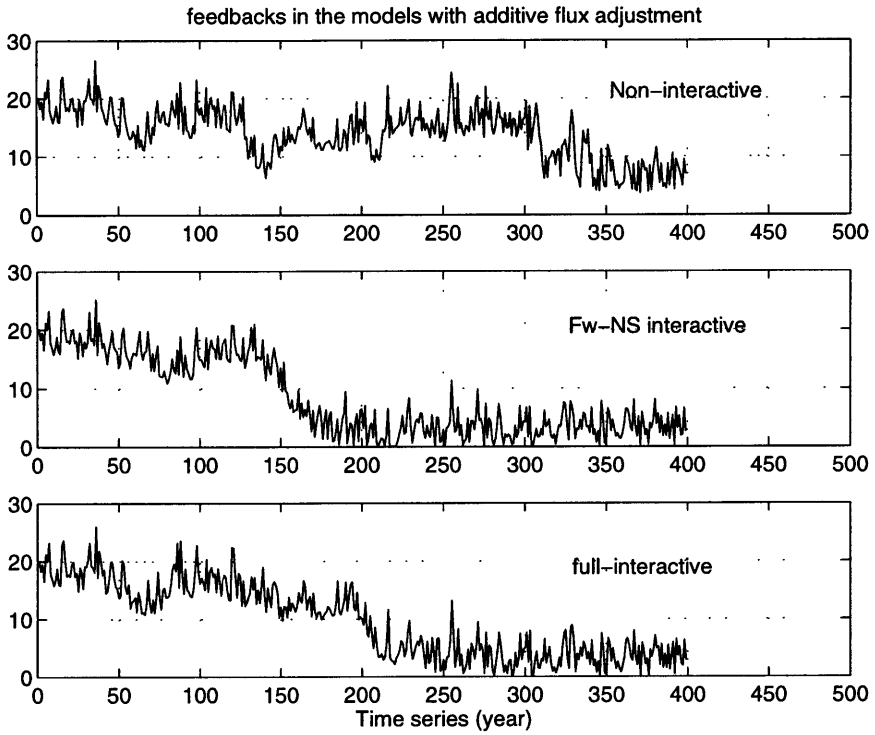

Figure 5-7: The time series of the North Atlantic overturning (unit of Sv) in the coupled models that use additive flux adjustment. Top: non-interactive model; Middle: model with the atmospheric moisture transport feedback; Bottom: fully interactive model

thermohaline circulation . The flux adjustment developed in this study is to adjust the atmospheric transports efficiencies to match the oceanic ones, even though the oceanic transports are in error.

To evaluate the effects of our flux adjustment, we construct a different flux adjustment scheme, in that the fluxes are adjusted by constants. We call it an *additive* flux adjustment. The additive flux adjustment does not change the observed atmospheric transports efficiencies, but subtracts constant fluxes to match the observed atmospheric fluxes,

$$H_{obs} = [C_S + C_L(\frac{\partial q_s}{\partial T})](\frac{dTs}{dy})^n - Constant \tag{5.3}$$

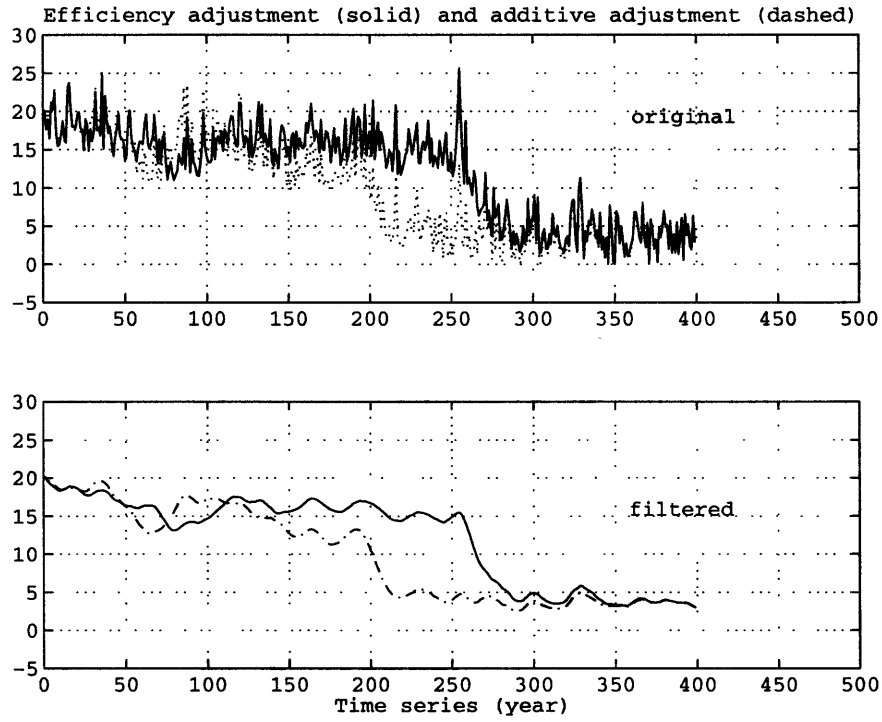

Figure 5-8: The time series of the North Atlantic overturning strength (unit of Sv) in the fully interactive models, with the additive flux adjustment (dashed), and the efficiency adjustment (solid), when the global freshwater fluxes increase 0.1% per year.

This is in contrast to the scheme constructed in Section 5.2, in which,

$$H_{obs} = [C'_S + C'_L(\frac{\partial q_s}{\partial T})](\frac{dTs}{dy})^n \tag{5.4}$$

Since in the latter scheme, the atmospheric transports efficiencies are multiplied by constants, we call it an *efficiency adjustment.* Notice that the scheme used here is different from the multiplicative flux adjustment proposed by Marotzke and Stone (1995), which was designed to conserve the original stability of their box model. The scheme used here does not necessarily have such a property.

With the two different adjustment schemes, the primary concern is whether the

conclusions of the previous section will be altered if the additive scheme is used. We selectively repeat two perturbation runs using the additive scheme, and the results are shown in Fig. 5-7. Both feedback #3 and #4 remain positive, the same as that with the other adjustment scheme. However, the feedback strengths are sensitive to the adjustment schemes. Under the two adjustment schemes, the fully interactive model has different collapse times of the North Atlantic overturning when the global freshwater fluxes increase linearly with time, as shown by Figure 5-8. The model with the additive flux adjustment is less stable than that with the efficiency adjustment, for the latter reduces the atmospheric transports efficiencies, and therefore reduces the positive atmospheric transports feedbacks.

Chapter 6

Conclusion and Outlook

6.1 Conclusion

This thesis has developed a hybrid coupled model which is simpler than coupled GCMs, and yet can capture the salient features of the thermohaline circulation and the large-scale coupling processes between the thermohaline circulation and the extratropical atmospheric dynamics. The coupled model is composed of an idealized global ocean GCM and an energy balance model with nonlinear parameterizations of atmospheric transports of heat and moisture. Two fundamentally important climate issues have been systematically investigated: (i) the large-scale dynamics of the thermohaline circulation , and (ii) the coupled feedbacks between the thermohaline circulation and the atmospheric mid-latitude eddy activities.

Though its limits of applicability to the real climate are as yet unclear, a prime virtue of the coupled model is that it allows a self-consistent representation of extratropical, large-scale ocean-atmosphere coupling. In addition, the ocean model, in major aspects, resembles that of the coupled GCMs (e.g, Manabe and Stouffer, 1988). The insight gained from this hybrid coupled model can carry over directly to

the analyses of a coupled GCM, and provide useful guidelines to the improvement of climate prediction.

If the thermohaline circulation behaves as in the model, the model results suggest answers to the two questions about the thermohaline circulation which were posed earlier.

I. How does the global thermohaline circulation respond to changes in hydrological cycle?

The sensitivity experiments of Chapter 3 have systematically explored the equilibrium responses of the conveyor belt circulation to the global freshwater fluxes with different strengthes. There, the coupled model has been simplified with fixed observed atmospheric transports of heat and moisture, and the only coupling is the longwave radiative flux dependence on surface temperature. Surprisingly, it is found that the North Atlantic overturning equilibrium strength generally increases with the strength of the global freshwater fluxes. Following the reasoning of Manabe and Stouffer (1994), who argued that the collapse of the North Atlantic overturning in their global warming experiment with a coupled GCM was caused by the increase of atmospheric moisture transport in the warmer climate, we had expected the stronger freshwater flux to lead to a weaker overturning. In fact, Manabe and Stouffer's reasoning only applied to the northern hemisphere, where the increased freshwater flux tends to reduce the sinking that forms the deep water, thus to reduce the overturning strength. In the southern hemisphere where the overturning is rising rather than sinking, the effect is the opposite, and in our model this effect dominates. This result illustrates that changes in the thermohaline circulation can only be predicted correctly in models that simulate the hemispheric asymmetries accurately. The conventional freshwater flux adjustment used in coupled GCMs are generally highly asymmetric,

and are in danger of possibly distorting the original character of the climate system.

Another implication is the different sensitivity of the overturning depicted by hemispheric models and by global models. With a hemispheric model, Winton and Sarachik (1993) found that, as the freshwater flux becomes stronger, the overturning began to oscillate with periods of no deep water formation followed by sudden flushing. Apparently, the overturning sensitivity changes significantly in our model of global configuration. When the global freshwater flux exceeds a certain threshold, and the surface becomes too fresh to sustain the deep water formation (e.g, the $4\times CO_2$ case in Manabe and Stouffer, 1994), the global model may exhibit similar oscillations to those found in the single hemispheric model. Our results indicate that the oscillation regime is not present in the global model within reasonable parameter choices.

One drawback of the global model is that the Antarctic Bottom Water formation is very weak or even absent, and the dynamics in ACC is highly simplified. As a result of that, there is little sinking in the southern high-latitude, and the GCM is in fact a model for the North Atlantic Deep Water formation, with sinking and rising in the high-latitudes of each hemisphere respectively. That's why the box model (Rooth, 1982), which assumes the flow linearly proportional to the density difference between the two high-latitude boxes, gives an analytical solution of the square root law, if the temperature in the two high-latitude boxes are held identical. This, in turn, confirms that the North Atlantic overturning is overwhelmed by the interhemispheric, pole-to-pole dynamics.

To further substantiate the above hypothesis, a series of perturbation experiments were performed using a special perturbation method, in which the freshwater flux strength is varied 0.1% per year at each hemisphere separately and jointly. This perturbation strategy allows us to probe the large-scale dynamics of the overturning

in each hemisphere separately. The results suggest that, for realistic parameter values, the equilibrated responses of the overturning is governed primarily by the freshwater flux in the southern hemisphere. The freshwater flux in the northern hemisphere has, surprisingly, little control on the equilibrium state of the overturning, simply because of the compensation between the stronger freshwater flux and stronger salt advection. Such asymmetric role of the two hemispheres freshwater fluxes is also found with the Rooth's box model (Rahmstorf, 1996; Scott et al., 1996). Rahmstorf (1996) tested the box model results in an ocean GCM, through the freshwater perturbation to certain gridpoints. Although the perturbation strategies are different in Rahmstorf (1996) and ours, the pole-to-pole dynamics of the overturning is found robust in these two studies.

One feature which was not studied by Rahmstorf (1996) is the transient behavior of the overturning. Here, our perturbation experiments illustrate that the change of the freshwater flux in the northern hemisphere has major impact on the overturning transient response, which is governed by the local convection dynamics. The convection process represents a major element in the deep water formation process, which in turn, is an integral part of the large-scale thermohaline circulation process. Although the large-scale and the local convection processes are operating on different time scales, the interplay between the two processes is evident.

The experiments illustrate interesting behaviors of the overturning when a random component is added to the zonal wind stress of the northern high latitudes. First, the random wind perturbation accelerates the transient responses of the overturning to changes in the hydrological cycle, but the fundamental character of the overturning is not altered by the random wind variation. Second, the exact path of the overturning evolution is sensitive to the choices of random seeds in the wind stress field, which

implies that the weather-type random noise is remembered and sustained long enough by the model to lead to changes in the overturning temporal paths. This suggests that the long term prediction of the overturning may be very limited, if possible.

The interplay between the two different scales processes is also found affecting the overturning stability. The results suggest two different modulations on the overturning stability. The first involves the freshwater capping over the high latitude convection sites. This is a local destabilizing mechanism, and is used to explain the collapse of the North Atlantic overturning in the global warming experiments (Manabe and Stouffer, 1994). The second modulation is associated with the large-scale process. It was first identified in the box model (Scott et al., 1996) that increasing the ratio of the freshwater fluxes between the two hemispheres (north vs. south) destabilizes the flow state. Our results found that the Fw ratio affects the stability of the global model as well.

II. How do the coupled feedbacks operate in the global model?

This question was the major focus of Chapter 5, where a series of coupled models were developed, with different assumptions about the atmospheric transports, which are shown to correspond to different stages of ocean-atmosphere coupling. When the atmospheric transports were made interactive, the coupled model drifted away from the conveyor belt circulation. The basic cause of the collapse is the ocean model's underestimate of the poleward heat transport. The weak oceanic heat transport in the model are attributed to several factors, among them are the weak North Atlantic Deep Water formation rate, the coarse horizontal resolution of the model, the diffusive mixing scheme, to name a few. Because of the underestimate, the temperature meridional gradients are too strong. Thus when the atmospheric transports are made interactive, the too strong gradients produce the atmospheric transports which are

also too strong, so strong that surface waters in the high-latitudes of the North Atlantic are now warmed by the atmospheric heat fluxes, rather than cooled, and the deep water formation there is completely turned off. This is in fact a possible explanation of why the overturning collapses in some coupled GCMs if no flux adjustments are used (e.g, Manabe and Stouffer, 1988).

In order to prevent the drift of the coupled model, the atmospheric transports parameterization were tuned, so that the the parameterizations produced the observed atmospheric transports when the temperature structure of the coupled model was used to calculate the transports, rather than when the observed temperature structure was used. In effect, this introduces errors in the efficiencies of the atmospheric transports which are matched to the errors in the efficiencies of the oceanic transports, and thereby preserves a realistic balance between the atmospheric and oceanic processes. This efficiency adjustment is quite different from the conventional additive adjustment used in coupled GCMs, where specified latitudinal dependent constants are added to the surface fluxes and held fixed. In light of Marotzke and Stone's (1995) discussion, both adjustment schemes can not preserve the original stability of the thermohaline circulation . But the efficiency adjustment is a more rational choice concerning the relative efficiencies of heat transports in the two systems. Furthermore, the results suggest that the coupled feedbacks are robust with either of the adjustment schemes.

The coupled feedbacks associated with the meridional transports in the atmosphere that were identified in the box models (Nakamura et al., 1994; Marotzke and Stone, 1995), are found operating in a similar fashion in the ocean GCM. The perturbation used in this study is of large-scale as well as long time scale, while the previous studies used the local perturbation with a short time duration (Saravanan and McWilliams, 1995; Lohmann et al. 1996). We believe that the coupled feedbacks

associated with the large-scale processes are more effectively and correctly elucidated under our perturbation method.

In addition, a series of new feedbacks are found operating in the southern hemisphere, with the same signs as those in the northern hemisphere, but different feedback loops. The differences arises from the upwelling of the overturning in the southern hemisphere, as well as the equatorward oceanic heat transport by the overturning there.

The feedback loop in the Southern Hemisphere acts as follows:

> decreased the overturning $\longrightarrow$ reduced *equatorward* oceanic heat transport $\longrightarrow$ reduced SST meridional gradient $\longrightarrow$ reduced atmospheric heat and moisture transports $\longrightarrow$ reduced buoyancy in high latitude $\longrightarrow$ reduced *upwelling* in high latitude $\longrightarrow$ further decreased the overturning

The results also suggest that the different adjustment schemes lead to the coupled feedbacks with different amplitudes. Because of it, the stability of the thermohaline circulation is in fact sensitive to how the flux adjustment is applied.

6.2 Outlook

On the basis of our numerical results with a global ocean GCM coupled to an energy balance atmospheric model, certain dynamical processes have been shown to be essential in predicting the variability and stability of the thermohaline circulation . These include,

- large-scale dynamical processes;
- fine-scale vertical convection processes;

- coupled feedbacks associated with the atmospheric eddy transports.

Some features of the model behavior have been explained only tentatively. This is particularly true with regard to the fine-scale convection process. It is very likely that the idealized lateral and bottom topography and coarse resolution may not represent the convection well, or possibly distort it.

Although the model is successful in reproducing the conveyor belt circulation, systematic discrepancies are also evident. In particular, the oceanic heat transport was seriously underestimated in the model. One promising improvement is the inclusion of the isopycnal mixing scheme (Gent and McWilliams, 1990), which was found increasing the oceanic heat transport (Boning et al, 1995).

The conjecture that upwelling of the overturning is concentrated in the South Ocean points strongly to the necessity of including more sophisticated dynamics in that region. Meanwhile, since the wind stress was held fixed in this study, any possible interactions between the wind-driven circulation and the thermohaline circulation are not investigated. In particular, the upwelling may be well correlated to the wind stress.

Another model improvement involves the prescribed latitudinal distributions of the atmospheric transports. A more consistent formulation would allow the latitudinal profiles internally determined, so that the local temperature effect on the moisture transport could be included.

These modifications will likely allow an even better simulation of the thermohaline circulation . If so, yet further progress can be made in answering the many questions surrounding the thermohaline circulation .

Reference

Baumgartner, A., and E. Reichel, 1975: The world water balance. *Verlag, Germany.*

Birchfield, G. E., 1989: A coupled ocean-atmosphere climate model: temperature vs. salinity effects on the thermohaline circulation. *Clim. Dyn.*, **4** , 57-71.

Boning, C.W., W.R. Holland, F.O. Bryan, G. Danabasoglu, and J.C. McWilliams, 1995: An overlooked problem in model simulations of the thermohaline circulation and heat transport in the Atlantic Ocean. *J. Climate*, **8** , 515-523.

Boning, C.W., F.O. Bryan, W.R. Holland, R. Doscher, 1996: Deep-Water formation and meridional overturning in a high-resolution model of the North Atlantic. *J. Phys. Ocean.*, **26** , 1142-1164.

Boyle, E.A., and L.D. Keigwin, 1987: North Atlantic thermohaline circulation during the past 20,000 years linked to high-latitude surface temperature. *Nature*, **330**, 35-40.

Brass, G. W., J. R. Southam and W. H. Peterson, 1982: Warm saline bottom water in the ancient ocean. *Nature* , **296** , 620-623.

Branscome, L. E., 1983: A parameterization of transient eddy heat flux on a beta-plane. *J. Atmos. Sci.*, **40**, 2508-2521.

Bretherton, F. P., 1982: Ocean climate modeling. *Progr. Oceanogr.*, **11**, 93-129.

Broecker, W. S., D. M. Peteet, and D. Rind, 1985: Does the ocean-atmosphere system have more than one stable mode of operation? *Nature* , **315**, 21-26.

Broecker, W.S.,and T.H. Peng, 1992: Interhemispheric transport of carbon dioxide by ocean circulation. *Nature*, **356**, 587-589.

Bryan, F., 1986: High-latitude salinity effects and interhemispheric thermohaline circulation. *Nature* , **323**, 301-304.

Bryan, F., 1987: Parameter sensitivity of primitive equation ocean general circulation models. *J. Phys. Oceanogr.* , **17**, 970-985.

Bryan, K., 1969: A numerical method for the study of the circulation of the world ocean. *J. Comput. Phys.*, **3**, 347-376.

Bryan, K., S. Manabe, and R. Pacanowski, 1975: A global ocean-atmosphere climate model. Part II: The oceanic circulation. *J. Phys. Oceanogr.*, **5**, 30-46.

Bryan, K., 1984: Accelerating the convergence to equilibrium of ocean-climate models. *J. Phys. Oceanogr.*, **2**, 510-514.

Bryden, H., D.H. Roemmich, and J.A. Church, 1991: Ocean heat transport across 24° N in the Pacific. *Deep-Sea Res.*, **38**, 297–324.

Budyko, M.I., 1969: The effect of solar radiation variations on the climate of the earth. *Tellus*, **21**, 611-619.

Carissimo, B. C., A. H. Oort, and T. H. Vonder Haar, 1985: Estimating the meridional energy transports in the atmosphere and ocean. *J. Phys. Ocean.*, **15**, 82-91.

Cox, M. D., 1984: A primitive equation, 3-dimensional model of the ocean. *GFDL Ocean Group Tech. Rep.*, No.1, GFDL/Princeton University.

Cubasch, U., K. Hasselmann, H. Hock, E. Maier-Reimer, U. Mikolajewicz, B. Santer, and R. Sausen, 1991: Time-dependent greenhouse warming computations with a coupled ocean-atmosphere model. *Clim. Dyn.*, **8**, 55-69.

Dansgaard, W., S. J. Johnsen, 1993: Evidence for general instability of past climate from a 250-Kyr ice-core record. *Nature* , **364**, 218-220.

Fiadeiro, 1983: Physical-chemical processes in the open ocean. In: The major biogeochemical cycles and their interactions. Eds. Bolin and Cook. Wiley and Sons, 461-476.

Gent, R.P. and J.C. McWilliams, 1990: Isopycnal mixing in ocean circulation models. *J. Phys. Ocean.* , **20**, 150-155.

Gleckler, P., D. Randall, G.Boer, R. Colman, M. Dix, V. Galin, M. Helfand, J. Kiehl, A. Kitoh, W. Lau, X. Liang, V. Lykossov, B. McAvaney, Miyakoda, S. Planton, and W. Stern, 1995: Cloud-radiative effects on implied oceanic energy transports as simulated by atmospheric general circulation models. *Geophys. Res. Letter*, **22**, 791-794.

Gordon, A.L., 1986: Interocean exchange of thermocline water. *J. Geophys. Res.*, **91**, 5037-5046.

GRIP Project Members, 1993: Climate instability during the last interglacial period recorded in the GRIP ice core. *Nature* , **364** , 203-208.

Hall, M. M. and H. Bryden, 1982: Direct estimates and mechanisms of ocean heat transport. *Deep-Sea Res.*, **29**, 339–359.

Haney, R. L., 1971: Surface thermal boundary condition for ocean circulation models. *J. Phys. Oceanogr.*, **1**, 241–248.

Held, I. M., 1978: The vertical scale of an unstable baroclinic wave and its importance for eddy heat flux parameterizations. *J. Atmos. Sci.* , **35** , 572-576.

Hughes, T. and A.J. Weaver, 1994: Multiple equilibria of an asymmetric two-basin model. *J. Phys. Ocean.*, **24** , 619-637.

Keith, D., 1995: Meridional energy transport: uncertainty in zonal means. *Tellus,* **47A**, 30-44.

Krasovskiy, Y. and P.H. Stone, 1996: Destabilization of the thermohaline circulation by atmospheric transports: an analytic solution. *J. Climate submitted.*

Lenderink, G. and R. J. Haarsma, 1994: Variability and multiple equilibria of the thermohaline circulation, associated with deep water formation. *J. Phys. Ocean.*, **24** , 1480-1493.

Leovy, C. B., 1973: Exchange of water vapor between the atmosphere and surface of Mars. *Icarus*, **18**, 120-125.

Levitus, S., 1982: Climatological atlas of the world ocean. NOAA Professional Paper 13, U.S., Dept. of Commerce, NOAA, Washington, D.C.

Lohmann, G., R. Gerdes, and D. Chen, 1996: Sensitivity of the thermohaline circulation in coupled oceanic GCM-atmospheric EBM experiments. *Clim. Dyn.,* **12**, 403-416.

Macdonald, A., C. Wunsch, 1996: An estimate of global ocean circulation and heat fluxes. *Nature.* , **382**, 436-439.

Maier-Reimer, E. and U. Mikolajewicz, 1989: Experiments with an OGCM on the cause of the Younger Dryas. Report No. 39. Max-Plank-Institute fur Meteorologie, Hamburg.

Manabe, S. and R. Stouffer, 1988: Two stable equilibria of a coupled ocean-atmosphere model. *J. Climate*, **1**, 841–866.

Manabe, S. and R. Stouffer, 1994: Multiple-century response of a coupled ocean-atmosphere model to an increase of atmospheric carbon dioxide. *J. Climate*, **7**, 5-23.

Manabe, S. and R. Stouffer, 1995: Simulation of abrupt climate change induced by freshwater input to the North Atlantic Ocean. *Nature*, **378**, 165-167.

Manabe, S., K. Bryan, and M.J. Spelman, 1990: Transient response of a global ocean-atmosphere model to a doubling of atmospheric carbon dioxide. *J. Phys. Oceanogr.*, **20**, 722-749.

Marotzke, J., 1990: Instabilities and multiple equilibria of the thermohaline circulation. Ph. D. thesis. *Ber. Inst. Meeresk, Kiel* .

Marotzke, J., 1994: Ocean models in climate problem. *Ocean Dynamics in Climate Processes*, P. Malanotte-Rizzoli and A. R. Robinson, eds., NATO ASI series.

Marotzke, J., 1996: Analysis of thermohaline feedbacks. *Decadal climate variability; dynamics and predictability.*, 333-378, L.T. Anderson and J. Willebrand, eds., NATO ASI series, Vol. I44.

Marotzke, J., P. Welander, and J. Willebrand, 1988: Instability and multiple steady states in a meridional-plane model of the thermohaline circulation. *Tellus*, **40A** , 162-172.

Marotzke, J. and J. Willebrand, 1991: Multiple equilibria of the global thermohaline circulation. *J. Phys. Oceanogr.* , **21** , 1372-1385.

Marotzke, J. and P.H. Stone, 1995: Atmospheric transports, the thermohaline circulation, and flux adjustments in a simple coupled model. *J. Phys. Oceanogr.*, **25** , 1350-1364.

Mikolajewicz, U. and Maier-Reimer, E., 1994: Mixed boundary conditions in ocean general circulation models and their influence on the stability of the model's conveyor belt. *J. Geophys. Res.*, **99** , 22,633-22,644.

Murphy, J.M., 1995: Transient response of the Hadley Center coupled ocean-atmosphere model to increasing carbon dioxide. Part I: Control climate and flux adjustment. *J. Climate*, **8**, 36-56.

Nakamura, M., P. H. Stone, and J. Marotzke, 1994: Destabilization of the thermohaline circulation by atmospheric eddy transports. *J. Climate.* , **7**, 1870-1882.

North, G.R., 1975: Theory of energy-balance climate models. *J. Atmos. Sci.* , **32**, 2033-2043.

Oort, A. H., 1983: Global atmospheric circulation statistics, 1958-73. NOAA Prof. Pap. No. 14, U.S. Dept. of Commerce, Washington, DC, 180pp.

Pacanowski, R. C., 1995: MOM 2 Documentation, User's Guide and Reference Manual, GFDL Ocean Group Tech. Rep. No.3.

Pacanowski, R. C., K. Dixon, and A. Rosati, 1990: The GFDL Modular Ocean Model Users Guide. Version 1.0, GFDL Ocean Group Tech. Rep. No.2.

Peixoto, J. P. and A. H. Oort, 1992: *Physics of Climate*, American Institute of Physics, New York.

Rahmstorf, S., 1994: Rapid climate transitions in a coupled ocean-atmosphere model. *Nature*, **372**, 82-85.

Rahmstorf, S., 1995: Multiple convection patterns and thermohaline flow in an idealized OGCM. *J. Climate.*, **8**, 3028-3039.

Rahmstorf, S., 1996: On the freshwater forcing and transport of the Atlantic thermohaline circulation. *Clim. Dyn.*, **12**, 799-811.

Rahmstorf, S. and J. Willebrand, 1995: The role of temperature feedback in stabilizing the thermohaline circulation. *J. Phys. Oceanogr.*, **25**, 787-805.

Rahmstorf, S., J. Marotzke, and J. Willebrand, 1996: Stability of the thermohaline circulation. *The warm water sphere of the North Atlantic Ocean.* W. Krauss, ed.,

Borntrager, Stuttgart. 129-157.

Rhines, P., 1993: Modelling oceanic climate interactions. *Ed.* Willebrand and Anderson, Springer-Verlag, 104-149.

Roemmich, D., and C. Wunsch, 1985: Two transatlantic sections: meridional circulation and heat flux in the subtropical North Atlantic Ocean. *Deep-Sea Res.*, **32**, 619-664.

Rooth, C., 1982: Hydrology and ocean circulation. *Progr. Oceanogr.*, **11**, 131-149.

Saravanan, R., and J.C. McWilliams, 1995: Multiple equilibria, natural variability, and climate transitions in an idealized ocean-atmosphere model. *J. Climate*, **8**, 2296-2323.

Sarnthein, M., K. Winn, S. Jung, C. Duplessy, L. Labeyrie, H. Erlenkeuser, G. Ganssen, 1994: Changes in East Atlantic deepwater circulation over the last 30,000 years; eight time slice reconstructions. *Paleoceanography*, **9**, 209-267.

Sausen, R., R.K. Barthels, and K. Hasselmann, 1988: Coupled ocean-atmosphere models with flux correction. *Clim. Dyn.*, **2**, 154-163.

Schiller, A., U. Mikolajewicz, and R. Voss, 1996: The stability of the thermohaline circulation in a coupled ocean-atmosphere general circulation model. *submitted.*

Schmitt, R., P. S. Bogden, and C. E. Dorman, 1989: Evaporation minus precipitation and density fluxes for the North Atlantic. *J. Phys. Oceanogr.*, **19**, 1208-1221.

Stephens, G.L., G.G. Campbell, and T.H. Vonder Haar, 1981: Earth radiation budgets. *J. Geophys. Res.*, **86**, 9739-9760.

Stocker, T. F., and D. G. Wright, 1991: A zonally-averaged ocean model for the thermohaline circulation. Part II. Interocean circulation in the Pacific-Atlantic basin system. *J. Phys. Oceanogr.*, **21**, 1725-1739.

Stocker, T. F., D. G. Wright and L. A. Mysak, 1992: A zonally averaged coupled ocean-atmosphere model for paleoclimatic studies. *J. Climate.*, **5** , 773-797.

Stommel, H., 1961: Thermohaline convection with two stable regimes of flow. *Tellus* , **13** , 224-230.

Stommel, H., and A. B. Arons, 1960: On the abyssal circulation of the world ocean-II. An idealized model of the circulation pattern and amplitude in oceanic basins. *Deep-Sea Res.*, **6** , 217-233.

Stone, P. H., 1984: Feedbacks between dynamical heat fluxes and temperature structure in the atmosphere. *Climate Processes and Climate Sensitivity*, Americal Geophysical Union, Geophysical Monograph, **29** , 6-17.

Stone, P. H. and D. A. Miller, 1980: Empirical relations between seasonal changes in meridional temperature gradients and meridional fluxes of heat. *J. Atmos. Sci.*, **37** , 1708-1721.

Stone, P. H. and J. Risbey, 1990: On the limitations of general circulation climate models. *Geophys. Res. Lett.*, **17** , 2173-2176.

Stone, P. H. and M. S. Yao, 1990: Development of a two-dimensional zonally averaged statistical-dynamical model. Part III: The parameterization of the eddy fluxes of heat and moisture. *J. Climate.*, **3** , 726-740.

Speer, K. and E. Tziperman, 1992: Rates of water mass formation in the North Atlantic Ocean. *J. Phys. Oceanogr.*, **22** , 93-104.

Tans, P. P., I. Y. Fung, and T. Takahashi, 1990: Observational constraints on the global atmospheric CO_2 budget. *Science*, **247**, 1431-1438.

Taylor, K., G. Lamorey, G. Doyle, R. Alley, P. Grootes, P. Mayewski, J. White, L. Barlow, 1993: The "flickering switch" of late Pleistocene climate change. *Nature*, **361**, 432-436.

Toggweiler, J.R, and B. Samuels, 1992: New radiocarbon constraints on the upwelling of abyssal water to the ocean's surface. *The global carbon cycle*, Heimann, eds., NATO ASI Series.

Toggweiler, J.R, and B. Samuels, 1992: Is the magnitude of the deep outflow from the Atlantic Ocean actually governed by Southern Hemisphere winds? *The global carbon cycle*, Heimann, eds., NATO ASI Series.

Trenberth, K. E., A. Solomon, 1994: The global heat balance: heat trnsports in the atmosphere and ocean. *Clim, Dyn.*, **10** , 107-134.

Veronis, G., 1975: The role of models in tracer studies. *Numerical Models of Ocean Circulation.*, National Academy of Science, Washington, D.C., 133-146.

Vonder Haar, T.H., and A. H. Oort, 1973: New estimate of annual poleward energy transport by northern hemisphere oceans. *J. Phys. Oceanogr.*, **3**, 169-172.

Walin, G., 1982: On the relation between sea-surface heat flow and thermal circulation in the ocean. *Tellus*, **34**, 187-195.

Wang, X., P. H. Stone, and J. Marotzke, 1995: Poleward heat transport in a barotropic ocean model. *J. Phys. Oceanogr.*, **25** , 256-265.

Warren., B.A., 1981: Deep circulation of the world ocean. In: Evolution of Physical Oceanography, Scientific Surveys in Honor of Henry Stommel. Eds. B.A. Warren and C. Wunsch, MIT Press, Cambridge, Mass. 42-69.

Warren., B., 1983: Why is no deep water formed in the North Pacific. *J. Mar. Res.*, **41**, 327–347.

Washington, W. M., and G. A., Meehl, 1989: Climate sensitivity due to increased CO_2: experiments with a coupled atmosphere and ocean general circulation model. *Clim. Dyn.*, **4**, 1-38.

Weaver, A. J., and E. S. Sarachik, 1990: On the importance of vertical resolution in certain ocean general circulation models. *J. Phys. Oceanogr.*, **20** , 600-609.

Weaver, A. J., E. S. Sarachik, and J. Marotzke, 1991: Internal low frequency variability of the ocean's thermohaline circulation. *nature*, **353** , 836-838.

Weaver, A. J., and E. S. Sarachik, 1991: The role of mixed boundary conditions in numerical models of the ocean's climate. *J. Phys. Oceanogr.*, **21** , 1470-1493.

Weaver, A. J., and T. M. C. Hughes, 1992: Stability and variability of the thermohaline circulation and its link to climate. *Trends in Phys. Oceanogr.*, **1**, 15-70.

Weaver, A. J., J. Marotzke, P. F. Cummins, and E. S. Sarachik, 1993: Stability and variability of the thermohaline circulation. *J. Phys. Oceanogr.*, **23** , 39-60.

Welander, P., 1986: Thermohaline effects in the ocean circulation and related simple models. *Large-scale Transport Processes in Oceans and Atmosphere*, J. Willebrand and D. L. T. Anderson, Eds., D. Reidel, 163-200.

Weyl, P.,1968: The role of the oceans in climatic change: a theory of the ice ages. *Meteorology Monographs*, **8**, 37-61.

Willebrand, J., 1993: Forcing the ocean with heat and freshwater fluxes. *Energy and Water Cycles in the Climate System*, E. Raschke, ed. Springer Verlag.

Winton, M. and E.S. Sarachik, 1993: Thermohaline oscillations induced by strong steady salinity forcing of ocean general circulation models. *J. Phys. Oceanogr.*, **23** , 1389-1409.

Yin, F.L. and E.S. Sarachik, 1994: An efficient convection adjustment scheme for ocean general circulation models. *J. Phys. Oceanogr.*, **24**, 1425-1430.

Zaucker, F., T. F. Stocker, and W. S. Broecker, 1994: Atmospheric freshwater fluxes and their effect on the global thermohaline circulation. *J. Geophys. Res.*, **99** , 12,443-12,457.

Appendix A

A.1 Conveyor belt circulation under different atmospheric heat transport

As a counterpart of the Fw variation on the thermohaline circulation , here we also perform the sensitivity study to the atmospheric heat transport. The motivation for this set of experiments comes from the study by Stone and Risbey (1990), where they pointed out that atmospheric GCMs for climate study tend to overestimate atmospheric heat transport by 50 to 100%. To assess the effect of stronger atmospheric heat transport on the thermohaline circulation , the atmospheric heat transport is increased by 30%, and is used for the runs of the 3.Fw and 1.Fw. Similar procedures are applied to the two runs, as described in section 3.3.1. For the 1.Fw, the final conveyor belt type circulation is 12 Sv (Fig.A-1), which is about 20% reduction, compared to the 1.Fw with the observed atmospheric heat transport Hd. It can be explained from the view of energy balance for the atmosphere and the ocean. Increasing of the Hd will decrease the oceanic heat transport, if assuming the sum of the two is approximately constant, this will result a weaker thermohaline circulation . On the other hand, increased Hd will reduce the temperature meridional gradient,

therefore, reduce the driving forcing for the thermohaline circulation (Fig.A-1). The

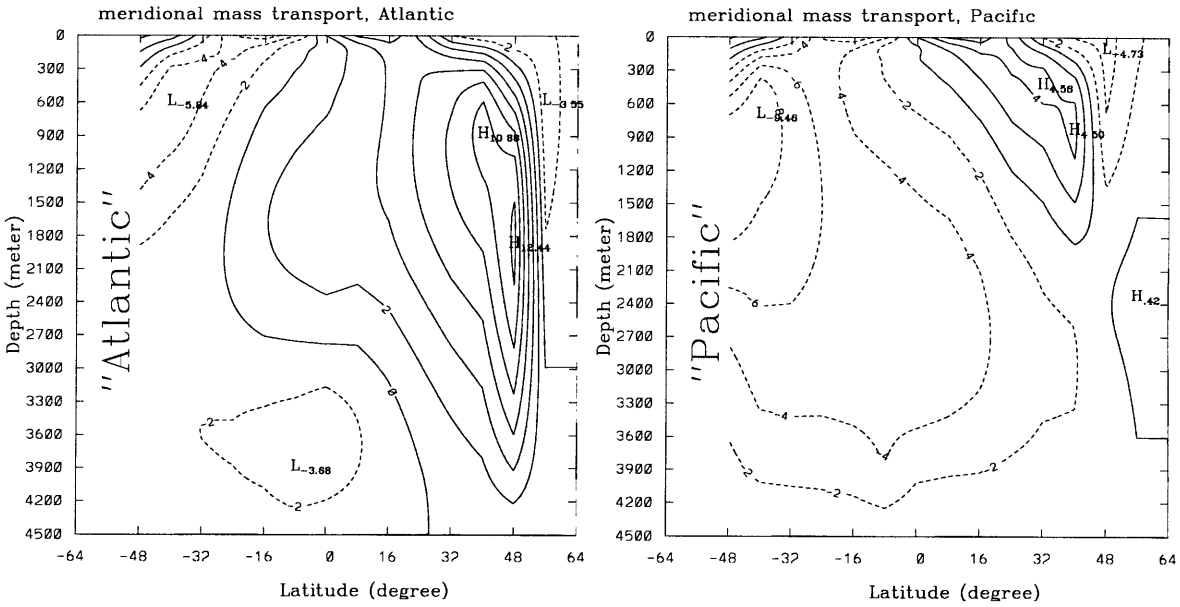

Figure A-1: 1.Fw and 1.3Hd, Atlantic (left), Pacific (right)

3.Fw run with increased Hd can not sustain the conveyor belt circulation, even though the initial state is perturbed to set up the conveyor belt type circulation, the final state is the sinking in the southern ocean. The collapsing of the conveyor belt circulation indicates that under the strong freshwater flux, the temperature increasing will cause the surface layer too fresh and warm to sink in the North Atlantic. The southern sinking becomes the only possible equilibrium state then.

2755-25